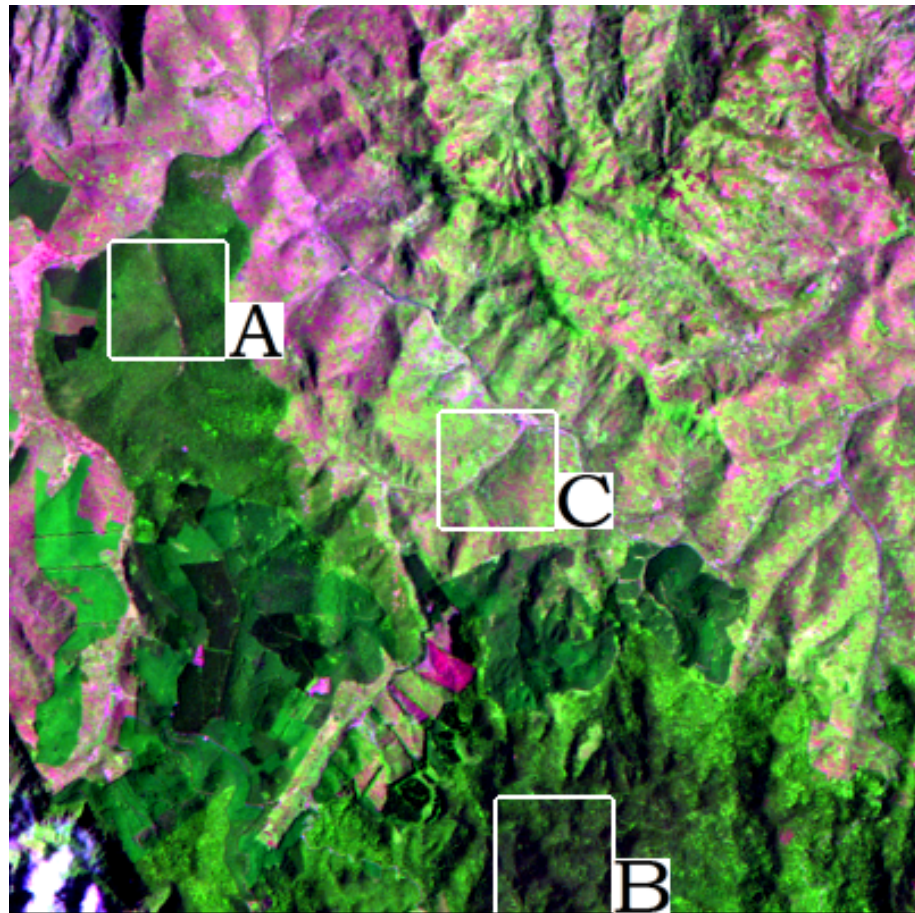


Evaluation of the Landsat surface reflectance estimated by LEDAPS



SAMBA/37/11
Maciel Zortea
Øivind Due Trier
Arnt-Børre Salberg

Note no
Authors

Date

18th October 2011

The authors

The authors are with the SAMBA/NR

Norwegian Computing Center

Norsk Regnesentral (Norwegian Computing Center, NR) is a private, independent, non-profit foundation established in 1952. NR carries out contract research and development projects in the areas of information and communication technology and applied statistical modelling. The clients are a broad range of industrial, commercial and public service organizations in the national as well as the international market. Our scientific and technical capabilities are further developed in co-operation with The Research Council of Norway and key customers. The results of our projects may take the form of reports, software, prototypes, and short courses. A proof of the confidence and appreciation our clients have for us is given by the fact that most of our new contracts are signed with previous customers.

Title Evaluation of the Landsat surface reflectance estimated by LEDAPS

Authors Maciel Zortea <Maciel.Zortea@nr.no>
Øivind Due Trier <Oivind.Due.Trier@nr.no>
Arnt-Børre Salberg <Arnt-Borre.Salberg@nr.no>

Date 18th October 2011

Publication number SAMBA/37/11

Abstract

The surface reflectance is one of the key parameters measured by space-borne sensors for use in environmental monitoring applications. The purpose of this report is to evaluate the surface reflectance generated by the Landsat Ecosystem Disturbance Adaptive Processing System (LEDAPS). Several different subregions from scenes acquired by Landsat 5 and 7 over Tanzania were selected for an intercomparison analysis. Short and long revisit time conditions are analyzed. The evaluation includes both a qualitative and quantitative assessment of the results.

Keywords Land surface reflectance, LEDAPS, Landsat, atmospheric correction, remote sensing.

Target group Remote sensing researchers

Availability Internal

Project GEO-FCT Hub

Project number 220 515

Research field Land surface reflectance

Number of pages 85

© Copyright Norwegian Computing Center

Contents

1	Introduction	5
2	The methodological approach	6
3	Data	7
4	Experimental evaluation	11
4.1	Long satellite revisit time: image set 1	11
4.1.1	Inter-image surface reflectance comparison, study area 1	11
4.1.2	Inter-image surface reflectance comparison, study area 2	16
4.2	Long satellite revisit time: image set 2	21
4.2.1	Inter-image surface reflectance comparison, study area 3	21
4.2.2	Inter-image surface reflectance comparison, study area 4	26
4.3	Summary tables of long revisit time for the study areas 1–4	31
4.4	Comparison of top of atmosphere (TOA) with surface reflectance	36
4.5	Surface reflectance on regions under cloud shadows	41
4.6	Surface reflectance on regions under thin clouds	42
4.7	Short satellite revisit time: image set 1	46
4.7.1	Inter-image surface reflectance comparison, study area 7	49
4.7.2	Inter-image surface reflectance comparison, study area 8	51
4.7.3	Inter-image surface reflectance comparison, study area 9	53
4.7.4	Inter-image surface reflectance comparison, study area 10	55
4.8	Short satellite revisit time: image set 2	57
4.8.1	Inter-image surface reflectance comparison, study area 11	57
4.8.2	Inter-image surface reflectance comparison, study area 12	59
4.8.3	Inter-image surface reflectance comparison, study area 13	61
4.8.4	Inter-image surface reflectance comparison, study area 14	63
4.9	Short satellite revisit time: image set 3	65
4.9.1	Inter-image surface reflectance comparison, study area 15	65
4.9.2	Inter-image surface reflectance comparison, study area 16	67
4.9.3	Inter-image surface reflectance comparison, study area 17	69
4.10	Summary tables of short revisit time for the study areas 7–17	71
4.11	An example of reflectance comparison on deforested areas	73
4.12	An example of reflectance comparison in adjacent Landsat images	77
5	Discussion and conclusions	83
	References	85

1 Introduction

The main purpose of this study is to evaluate if the LEDAPS preprocessing of Landsat images should be included in tropical forest monitoring in Tanzania and other tropical countries. Also, limitations and restrictions, if any, should be described. If the LEDAPS preprocessing tools are able to produce Landsat images with reliable surface reflectance values, then a major obstacle to reliable tropical forest monitoring has been removed.

As stated by [Vermote and Saleous \(2007\)](#) in the LEDAPS surface reflectance product description “the directional surface reflectance is defined as the ratio between the radiance measured in specific observation geometry (zenith and azimuth) and a direct source of illumination (zenith and azimuth) in an infinitely small solid angle. The directional surface reflectance is determined from satellite observations though the atmospheric correction process. When properly retrieved, the directional reflectance is fully decoupled from the atmospheric signal, and thus represents the value that would be measured by an ideal sensor held at the same sun-view geometry and located just above the Earth’s surface if there were no atmosphere.

Directional surface reflectance is the most basic remotely sensed surface parameter in the solar reflective wavelengths. It therefore provides the primary input for essentially all higher-level surface geophysical parameters, including Vegetation Indices, Albedo, Fraction-of-Photosynthetically Active Radiation (FPAR) and Leaf Area Index (LAI), Burned Area, Land Cover and Land Cover Change. Directional surface reflectance is also used in various “imagery” applications to detect and monitor changes on the Earth’s surface (e.g., anthropogenic impacts, red-green-blue images).”

The Landsat Ecosystem Disturbance Adaptive Processing System (LEDAPS)¹ processes Landsat data from L1B to surface reflectance using atmospheric correction routines similar to that developed for the MODIS instrument ([Masek et al. \(2006\)](#)). The LEDAPS package includes three basic modules (plus a parameter parser and an internal cloud detection program) to convert Landsat data from digital numbers (DN) to surface reflectance. The three steps include:

- Calibrate digital number (DN) to top-of-atmosphere (TOA) reflectance
- Detect cloud pixels based on the TOA reflectance
- Correct to surface reflectance from TOA reflectance and ancillary data sets

The above extracts, and additional information, can be found at the LEDAPS web site: <http://ledaps.nascom.nasa.gov/>

1. <http://ledaps.nascom.nasa.gov/>

2 The methodological approach

Validation of the surface reflectance product is a challenging task. Ideally one would like to compare estimated reflectance values with simultaneously acquired measurements at the ground. Simultaneous ground truth reflectance measurements for the area analyzed are not available, nor are reflectance products estimated by alternative sensors available for intercomparisons. Thus, we resort to an alternative approach to evaluate the Landsat surface reflectance estimated by LEDAPS. The main idea is to compare scenes acquired at different years, but at similar day of the year (similar phenological conditions), in selected areas where no significant change detection is visually observed. Images from both Landsat 5 and 7 are used in the study, and are listed in Tab. 1 and shown in Fig. 1.

In the second part of the report we compare scenes acquired with short revisit time. In short revisit time conditions, the expected phenological changes, if present, are expected to be smaller.

The images of surface reflectance were automatically calculated by LEDAPS using the parameters contained in the MTL files, that are stored together with the Landsat bands, and additional ancillary data. According to [Vermote and Saleous \(2007\)](#), "the ozone concentrations are derived from Total Ozone Mapping Spectrometer (TOMS) data aboard the Nimbus-7, Meteor-3, and Earth Probe platforms. The gridded TOMS ozone products are available at a resolution of 1.25 longitude and 1.00 latitude from the NASA GSFC Data Active Archive Center (DAAC). In cases where TOMS data are not available (e.g., 1994-1996), NOAA's Tiros Operational Vertical Sounder (TOVS) ozone data are used. Column water vapor is taken from NOAA National Centers for Environmental Prediction (NCEP) reanalysis data available at a resolution of 2.5 2.5 (<http://dss.ucar.edu/datasets/ds090.0/>). Digital topography (1 km GTopo30) and NCEP surface pressure data are used to adjust Rayleigh scattering to local conditions."

Subregions of interest were selected in the images, with focus on locations not strongly affected by cloud coverage to allow visual inspection of the surface reflectance. Reflectance composite images of bands RGB (5,4,3) were generated and used for qualitative analysis (visual inspection). For a fair and better visualization of the color composite reflectance images, linear stretching was applied. The thresholds needed for linear stretching were conveniently computed from each band to display the reflectance images in a 24bit color format, and kept identical for each set of three images compared in each study area.

Accurate registration is necessary for pixel-level comparisons. We resort to region-based instead of pixel-wise comparisons. For quantitative analysis, we compute the (a) median of each reflectance band and (b) the probability density estimate (pdf) of the reflectance pixels, using small image patches. The pdfs are computed using kernel density estimation. A Gaussian kernel is used, and the bandwidth of the kernel smoothing is automatically set as the optimal value for normal densities.

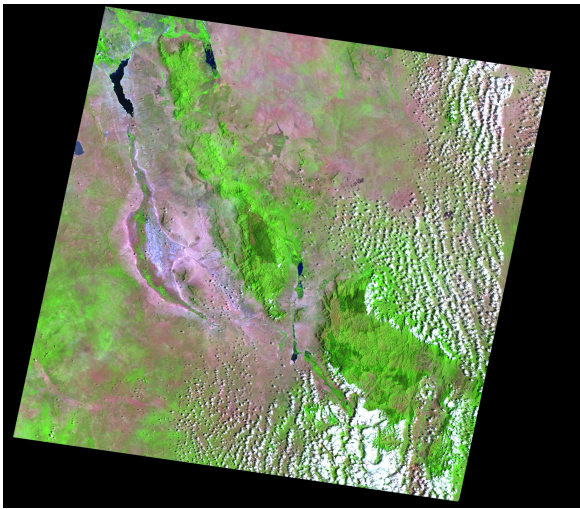
In addition, using the above comparison strategies, we evaluate the ability of LEDAPS to remove thin clouds, and also the estimated surface reflectance in regions under cloud shadows.

3 Data

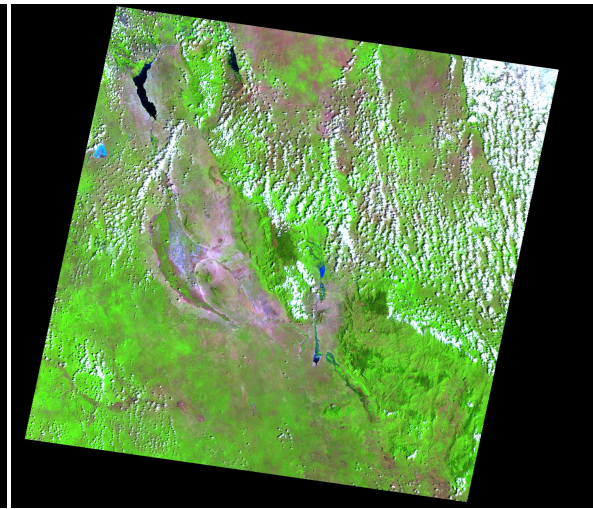
The LEDAPS processing code was tested with several images acquired by LandSat 5 and 7 on paths/row 166/063, 167/063, and 166/067, acquired between 1984 and 2009. A subset of these images, indicated in Tab 1, was used to assess qualitatively and quantitatively the estimated surface reflectance. The selected images are shown in Fig. 1.

Table 1. Landsat scenes selected for evaluation. We focus the analysis on 12×12 km study areas, selected for inter-image surface reflectance comparisons. Inside each study area, subwindow regions are selected to compare the reflectance at different time points.

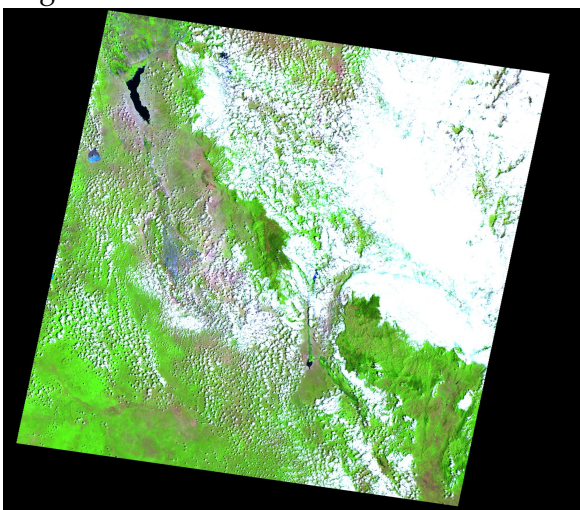
Image	Satellite	path	row	year	month	day	Study Areas
1	Landsat 5	167	063	1987	02	02	1,2,18
2	Landsat 7	167	063	2001	01	15	1,2,5,18
3	Landsat 7	167	063	2001	01	31	1,2,5,18
4	Landsat 5	167	063	1984	12	10	3,4,6
5	Landsat 5	167	063	1987	01	01	3,4
6	Landsat 7	167	063	2001	12	01	3,4
7	Landsat 5	166	063	2009	11	06	7,8,9,10
8	Landsat 5	166	063	2009	11	22	7,8,9,10,19
9	Landsat 5	166	063	2009	12	08	7,8,9,10,19
10	Landsat 5	166	067	2009	05	30	11,12,13,14
11	Landsat 5	166	067	2009	06	15	11,12,13,14
12	Landsat 5	166	067	2009	07	01	15,16,17
13	Landsat 5	166	067	2009	07	17	15,16,17
14	Landsat 5	167	063	2009	11	29	19



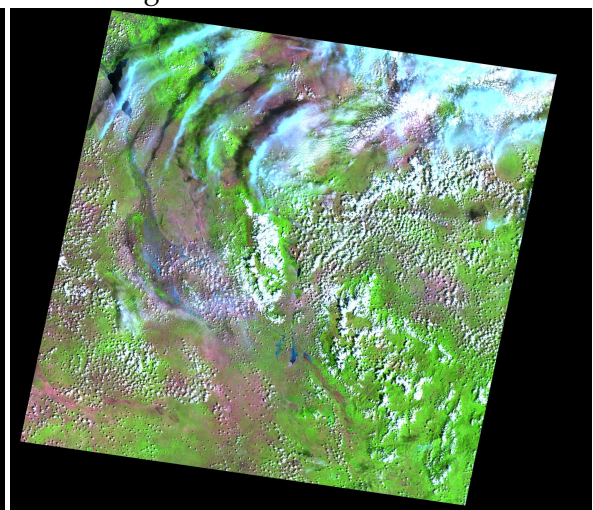
Img.01:L5167063-0631987-02-02



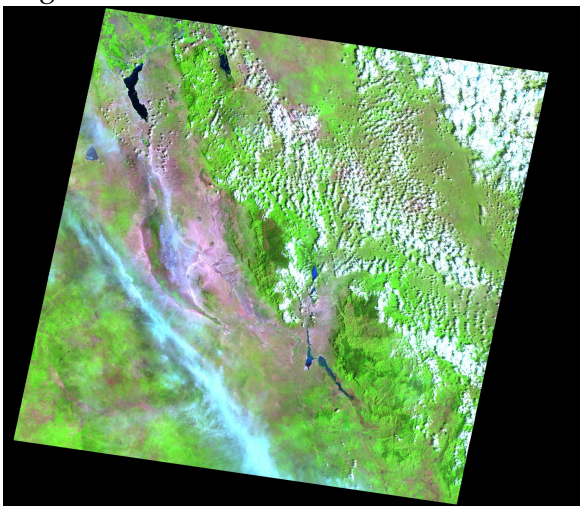
Img.02:L71167063-0632001-01-15



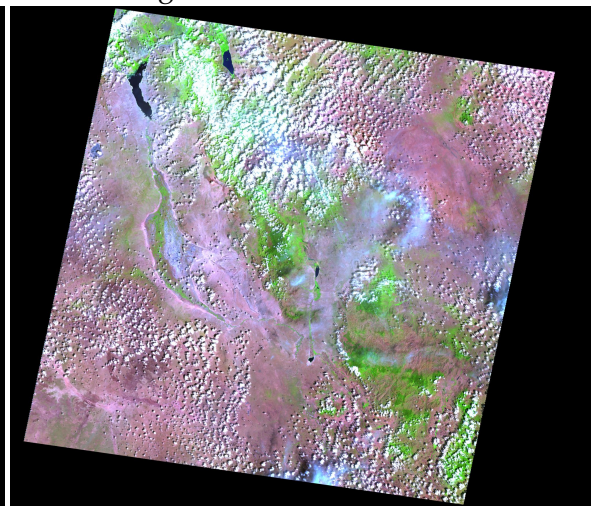
Img.03:L71167063-0632001-01-31



Img.04:L5167063-0631984-12-10

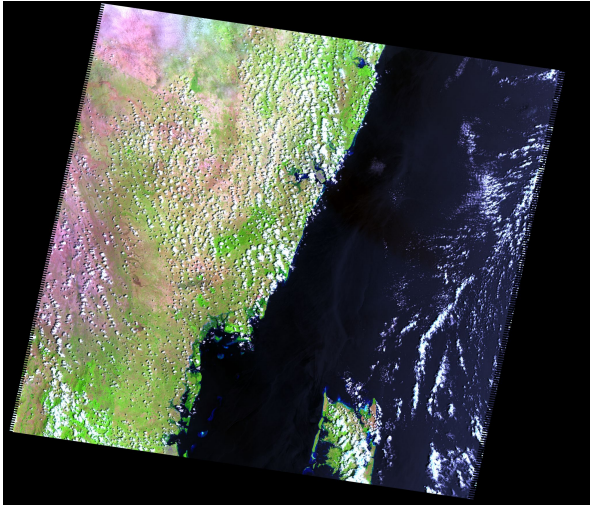


Img.05:L5167063-0631987-01-01

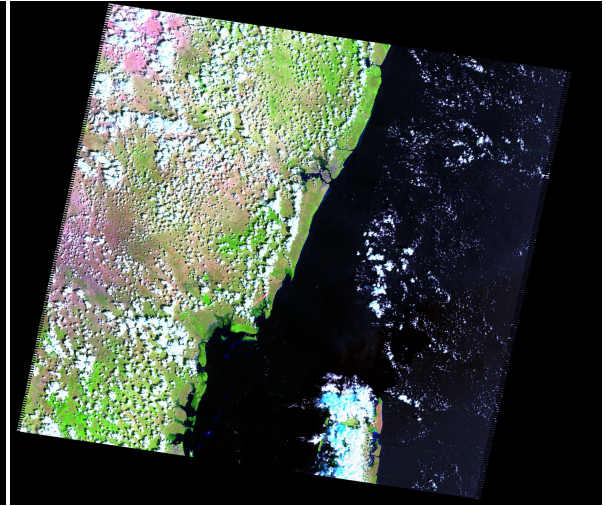


Img.06:L71167063-0632001-12-01

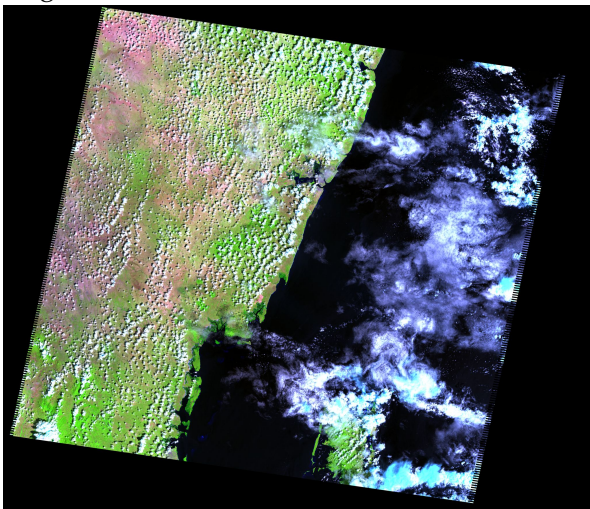
Figure 1. Color composition of the Landsat images used in this study. The RGB color composition is generated using the LEDAPS surface reflectance at bands (5,4,3). In this particular visualization, linear stretching with identical saturation thresholds were used in all the images. The surface reflectance thresholds used are: band5 [0–0.46], band 4 [0–0.44], and band 3 [0–0.23]. Subregions not affected by clouds were selected for the analysis.



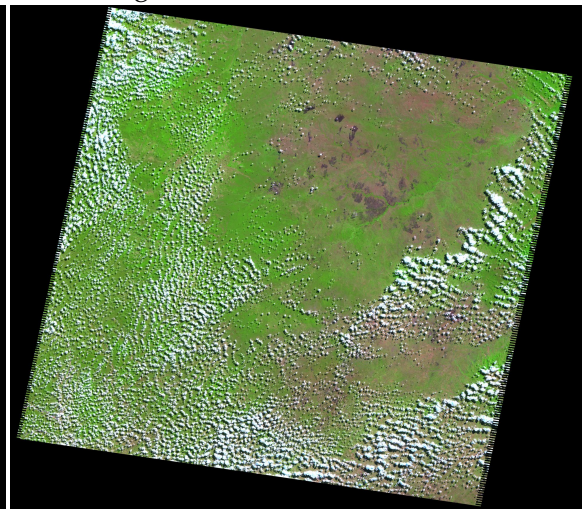
Img.07:L5166063-0632009-11-06



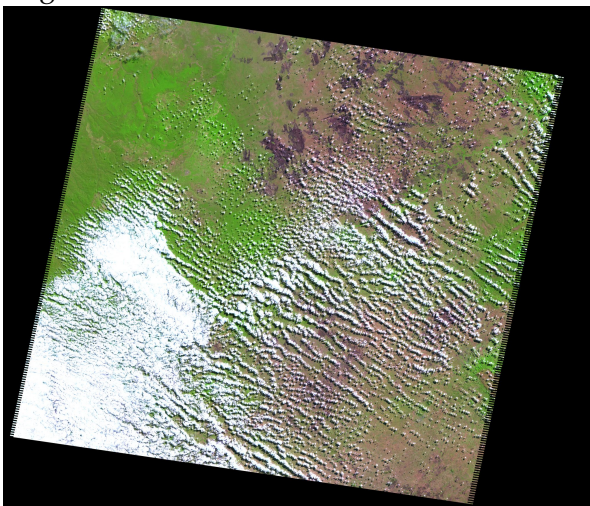
Img.08:L5166063-0632009-11-22



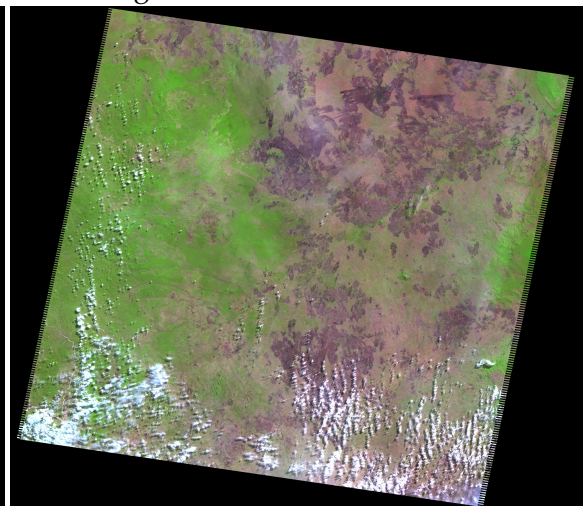
Img.09:L5166063-0632009-12-08



Img.10:L5166067-0672009-05-30

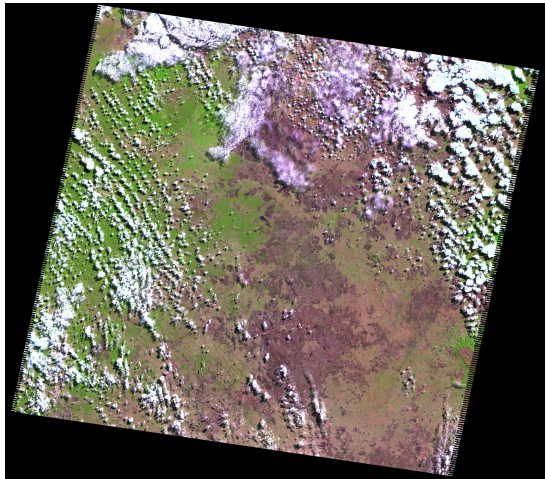


Img.11:L5166067-0672009-06-15

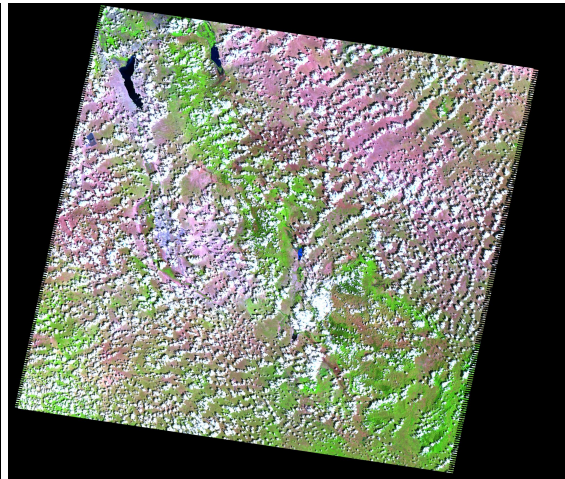


Img.12:L5166067-0672009-07-01

Figure 1 (continued)



Img.13:L5166067-0672009-07-17



Img.14:L5167063-0632009-11-29

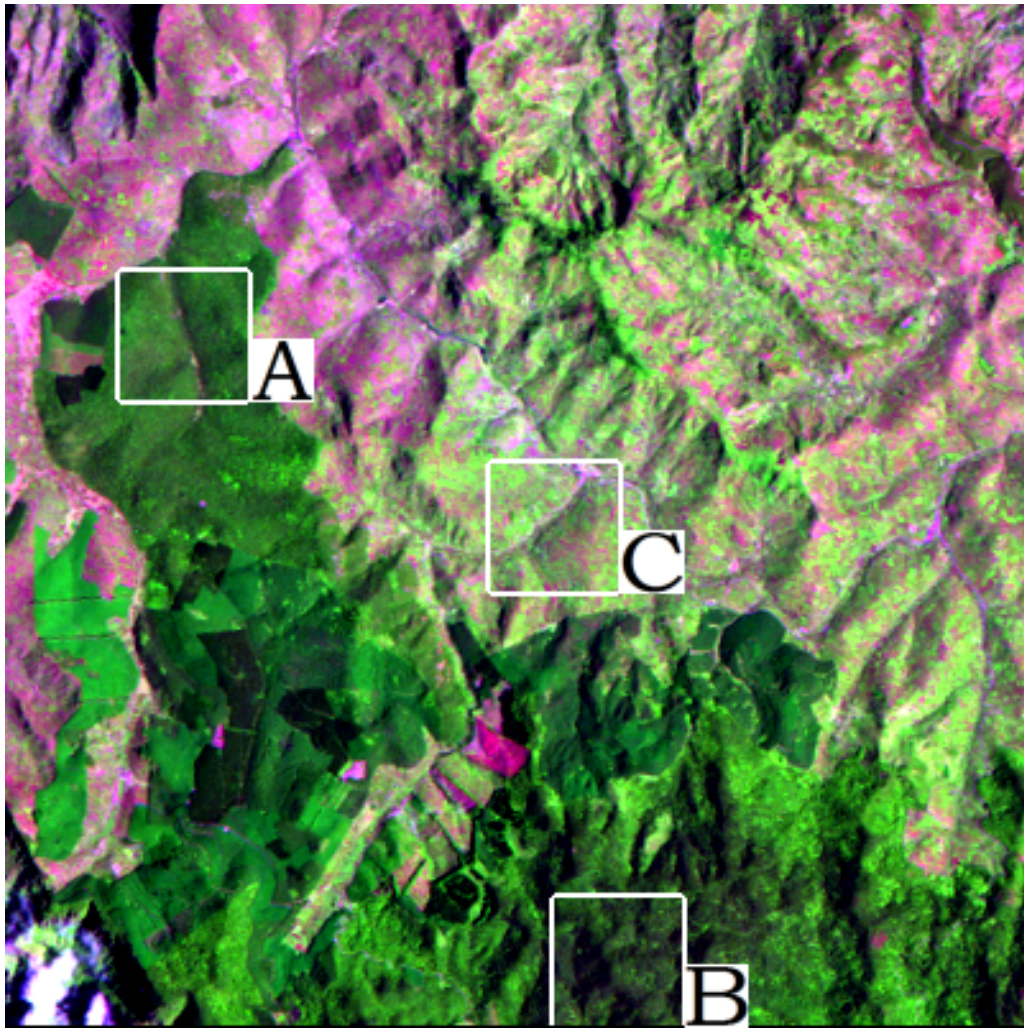
Figure 1 (continued)

4 Experimental evaluation

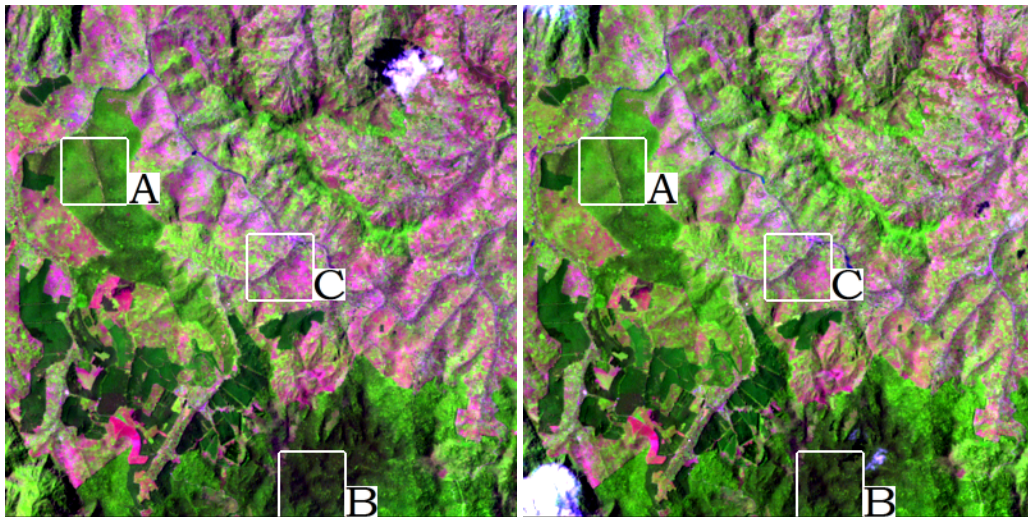
4.1 Long satellite revisit time: image set 1

4.1.1 Inter-image surface reflectance comparison, study area 1

The comparisons for the study 1 are shown in Fig. 2–5. These include color composite of the surface reflectance and the estimated probability function of the surface reflectance of the bands 1–5 and 7 for selected subregions.



L5167063-06319870202



L71167063-06320010115

L71167063-06320010131

Figure 2. Study area 1. Surface reflectance composite (RGB bands 5,4,3) of a 12×12 km area from the Landsat images L5167063-06319870202 (top), L71167063-06320010115 (left), and L71167063-06320010131 (right). To enhance visualization for a qualitative assessment, linear stretching with identical and conveniently chosen saturation thresholds were used in the three images. Three regions are used for the quantitative assessment of the surface reflectance, by computing the pdf, and the median, of the surface reflectance in each Landsat band.

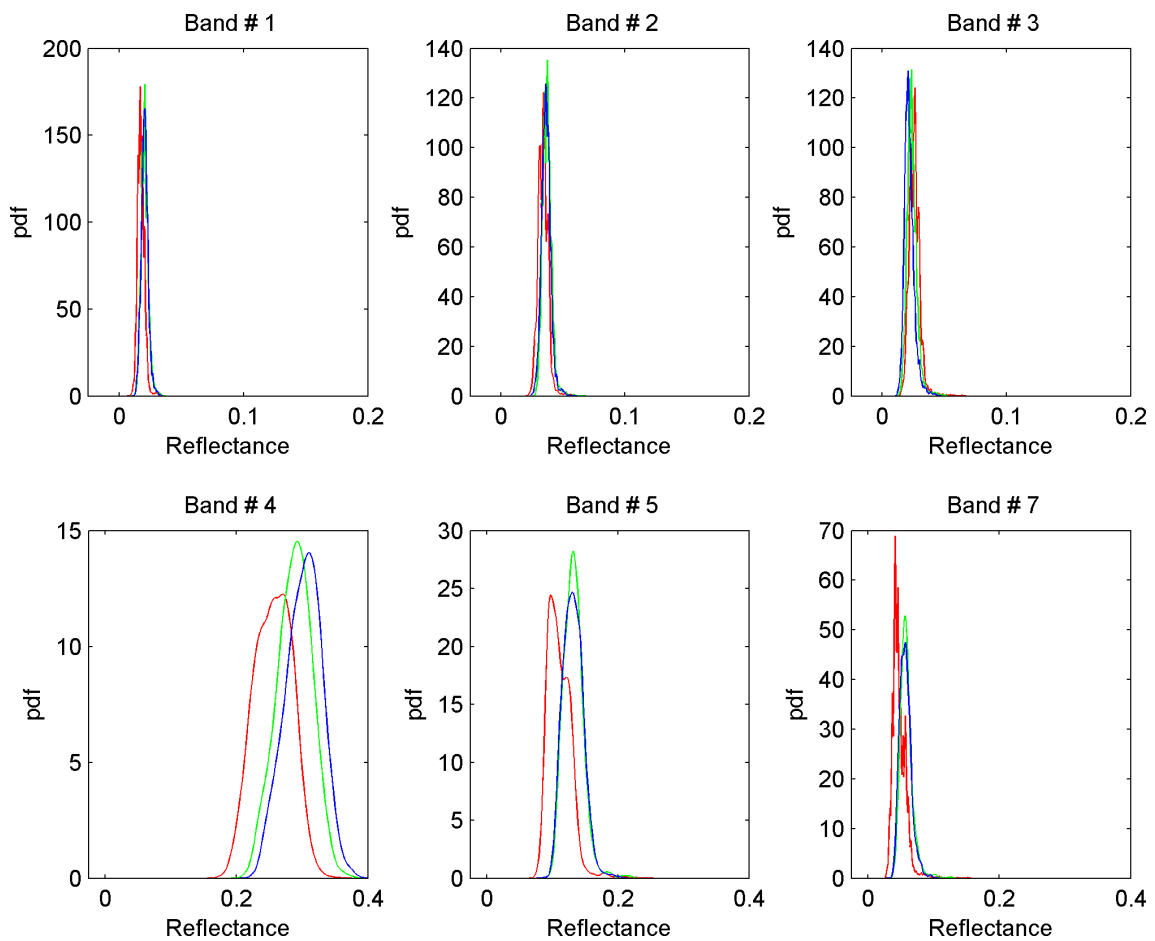
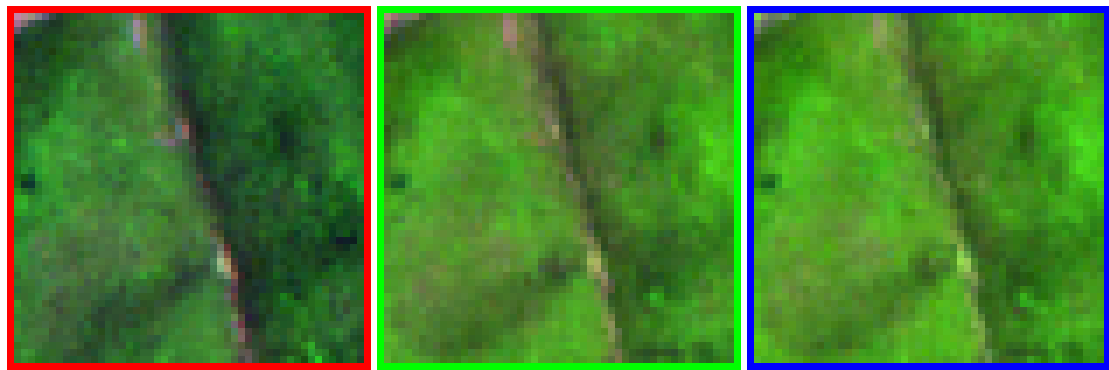


Figure 3. Study area 1. (Top) Closer look at the surface reflectance composite (RGB bands 5,4,3) of the 1500×1500 m subregion "A" in Fig. 2. The patches are from the Landsat images L5167063-06319870202 (red color), L71167063-06320010115 (green color), and L71167063-06320010131 (blue color). (Bottom) The correspondent probability density estimates of the surface reflectance for the bands 1–5 and 7 of Landsat are depicted. A total of 2500 reflectance samples (pixels) are available in each patch.

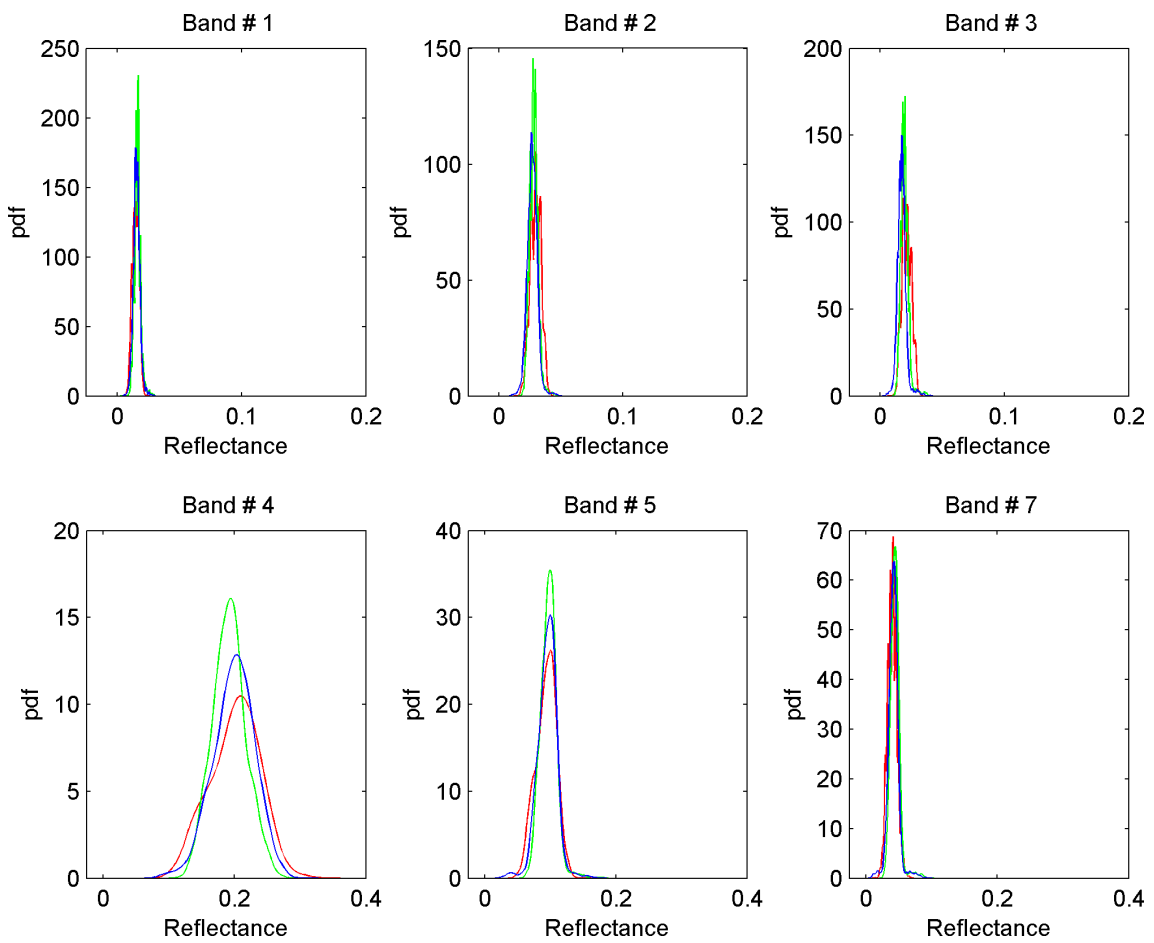
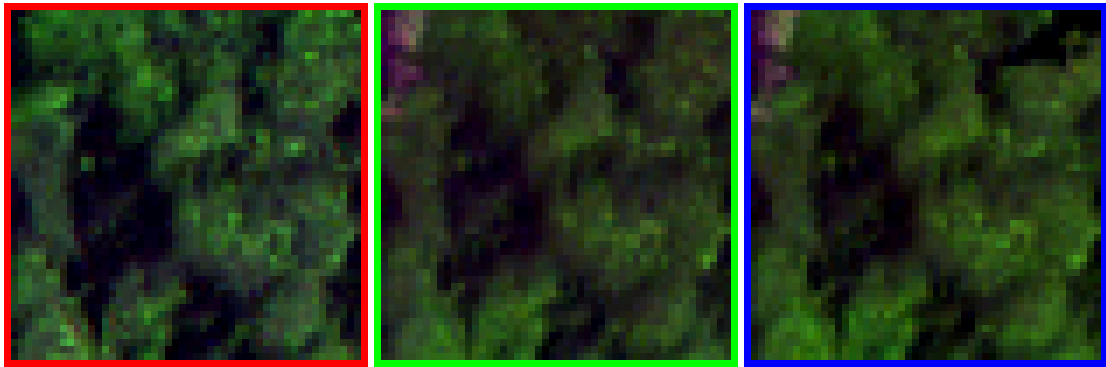


Figure 4. Study area 1. (Top) Closer look at the surface reflectance composite (RGB bands 5,4,3) of the 1500×1500 m subregion “B” in Fig. 2. The patches are from the Landsat images L5167063-06319870202 (red color), L71167063-06320010115 (green color), and L71167063-06320010131 (blue color). (Bottom) The correspondent probability density estimates of the surface reflectance for the bands 1–5 and 7 of Landsat are depicted. A total of 2500 reflectance samples (pixels) are available in each patch.

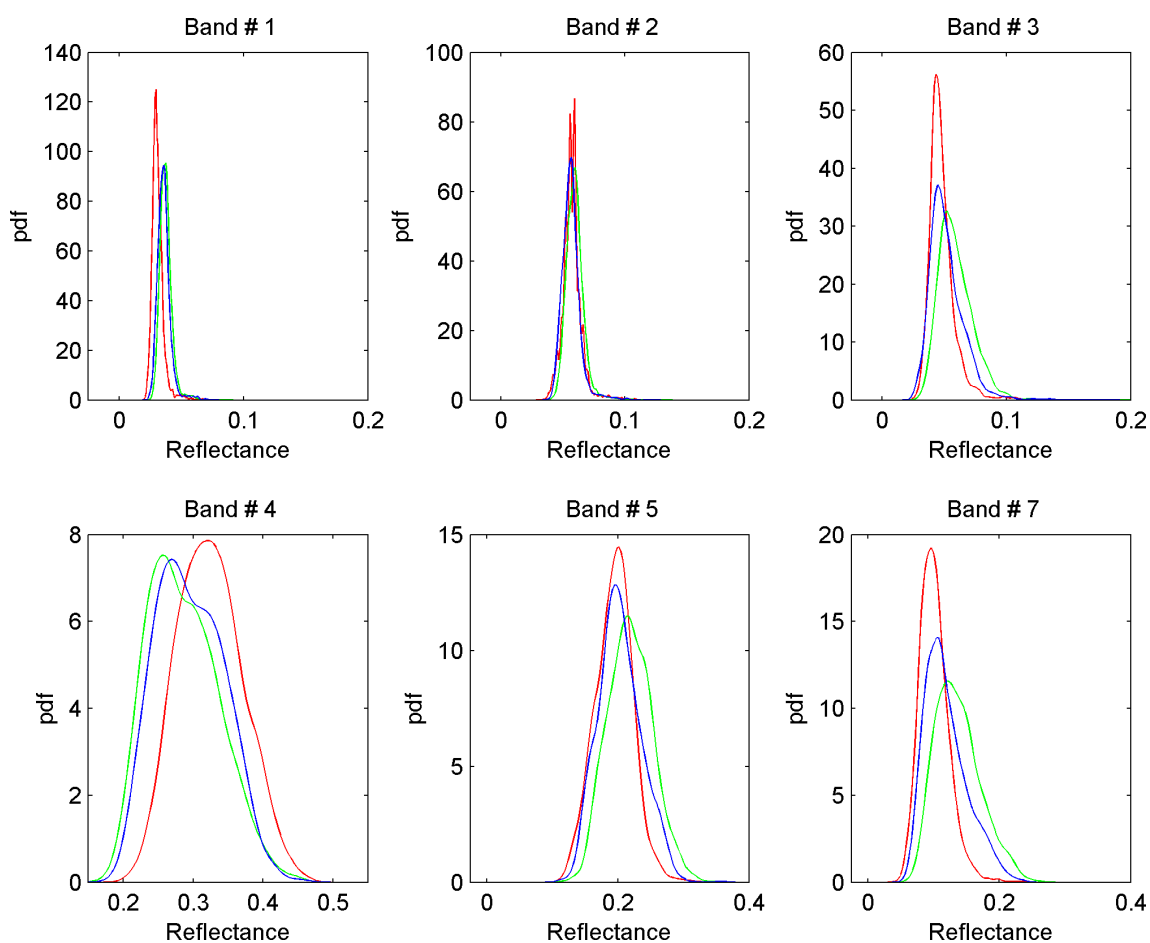
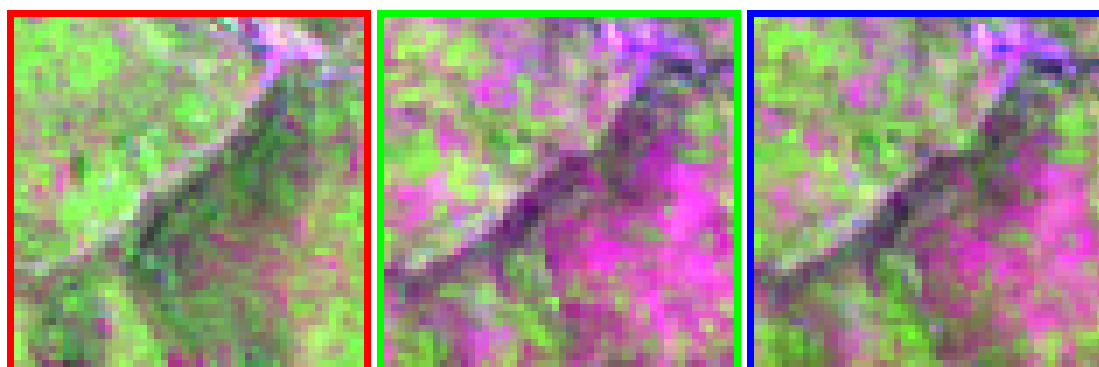


Figure 5. Study area 1. (Top) Closer look at the surface reflectance composite (RGB bands 5,4,3) of the 1500×1500 m subregion "C" in Fig. 2. The patches are from the Landsat images L5167063-06319870202 (red color), L71167063-06320010115 (green color), and L71167063-06320010131 (blue color). (Bottom) The correspondent probability density estimates of the surface reflectance for the bands 1–5 and 7 of Landsat are depicted. A total of 2500 reflectance samples (pixels) are available in each patch.

4.1.2 Inter-image surface reflectance comparison, study area 2

The comparisons for the study 2 are shown in Fig. 6–9. This include color composite of the surface reflectance and the estimated probability function of the surface reflectance of the bands 1–5 and 7 for selected subregions.

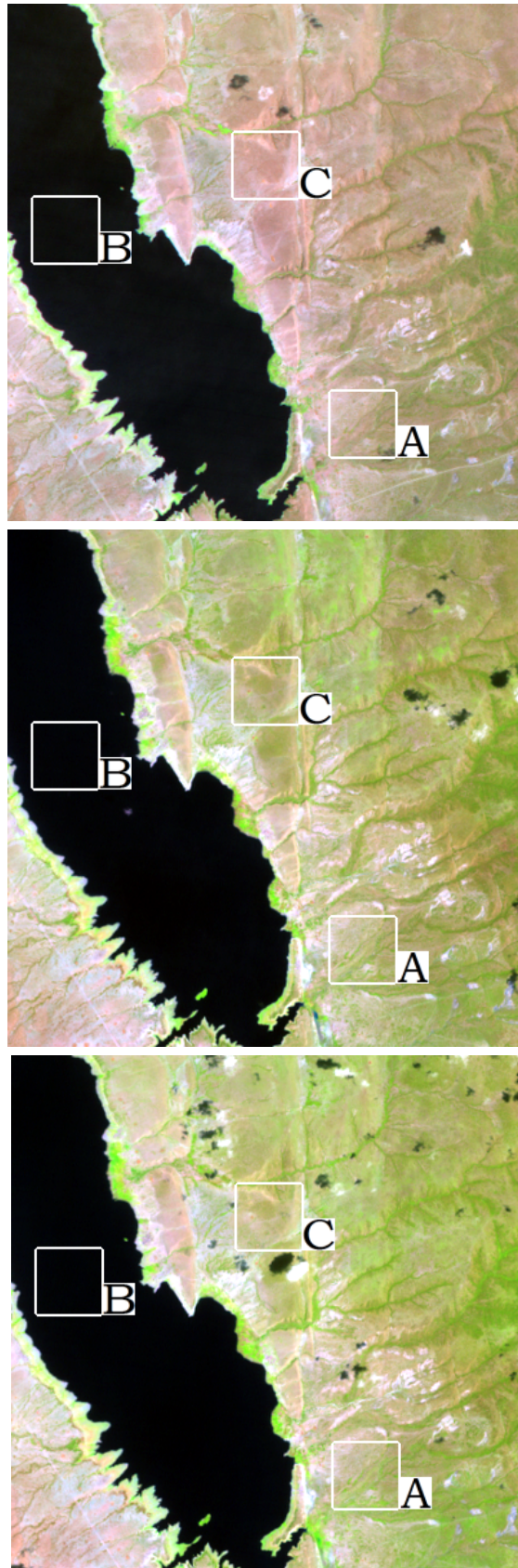


Figure 6. Study area 2. Surface reflectance composite (RGB bands 5,4,3) of a 12×12 km area from the Landsat images L5167063-06319870202 (top), L71167063-06320010115 (middle), and L71167063-06320010131 (bottom). To enhance visualization for a qualitative assessment, linear stretching with identical and conveniently chosen saturation thresholds were used in the three images. Three regions are used for the quantitative assessment of the surface reflectance, by computing the pdf, and the median, of the surface reflectance in each Landsat band.

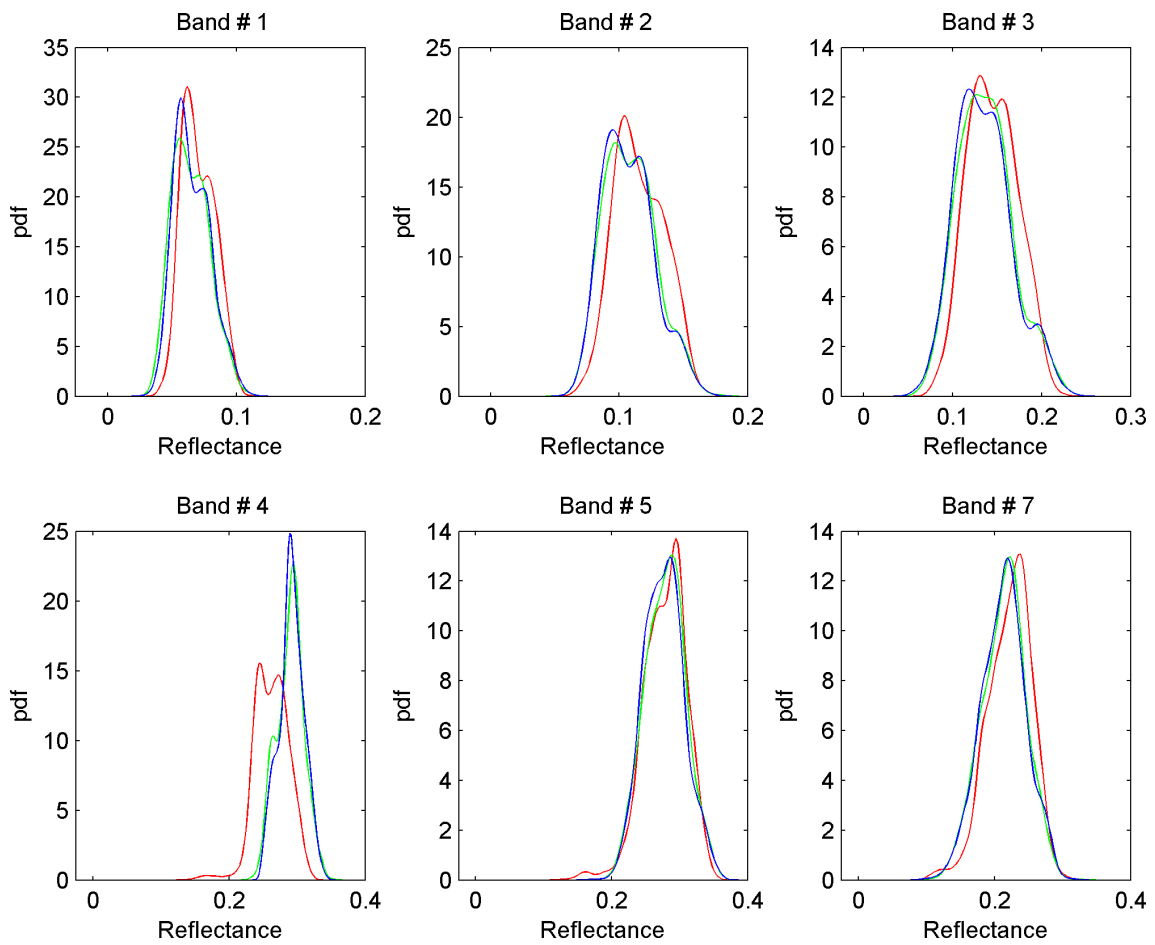


Figure 7. Study area 2. (Top) Closer look at the surface reflectance composite (RGB bands 5,4,3) of the 1500×1500 m subregion "A" in Fig. 6. The patches are from the Landsat images L5167063-06319870202 (red color), L71167063-06320010115 (green color), and L71167063-06320010131 (blue color). (Bottom) The correspondent probability density estimates of the surface reflectance for the bands 1–5 and 7 of Landsat are depicted. A total of 2500 reflectance samples (pixels) are available in each patch.

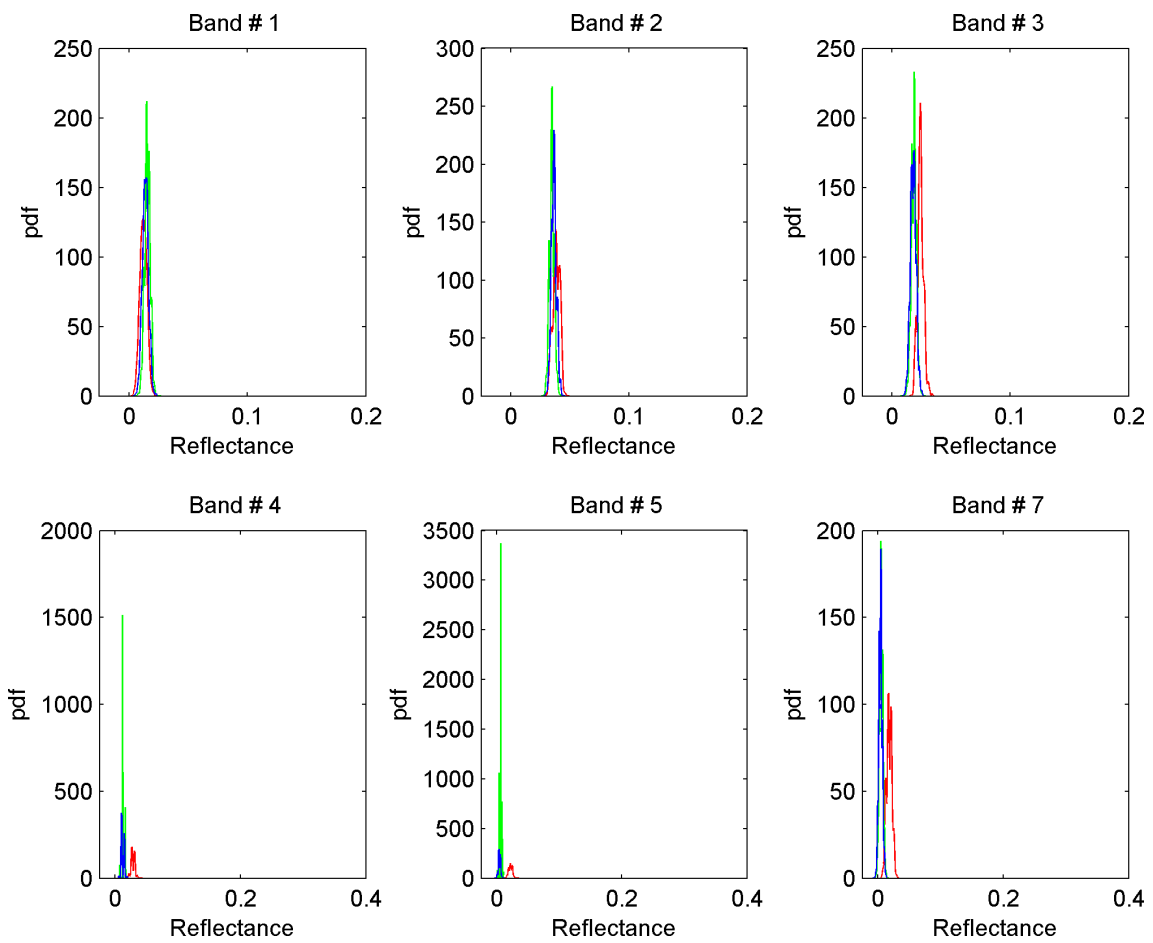
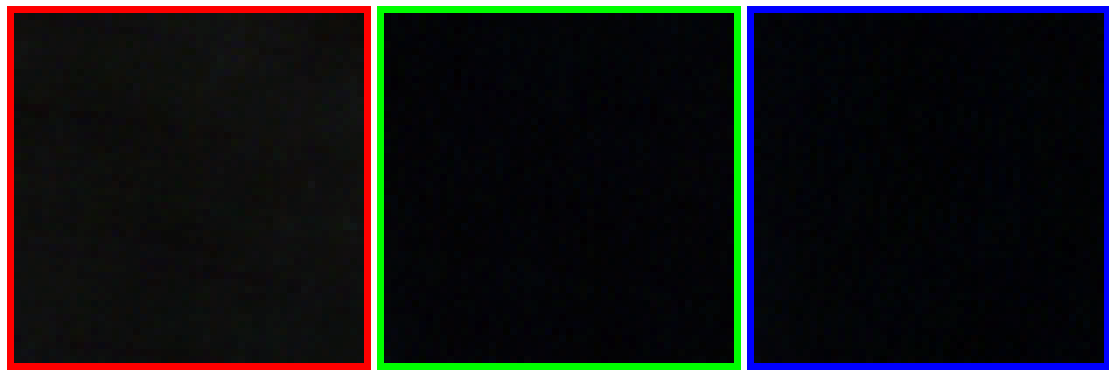


Figure 8. Study area 2. (Top) Closer look at the surface reflectance composite (RGB bands 5,4,3) of the 1500×1500 m subregion “B” in Fig. 6. The patches are from the Landsat images L5167063-06319870202 (red color), L71167063-06320010115 (green color), and L71167063-06320010131 (blue color). (Bottom) The correspondent probability density estimates of the surface reflectance for the bands 1–5 and 7 of Landsat are depicted. A total of 2500 reflectance samples (pixels) are available in each patch.

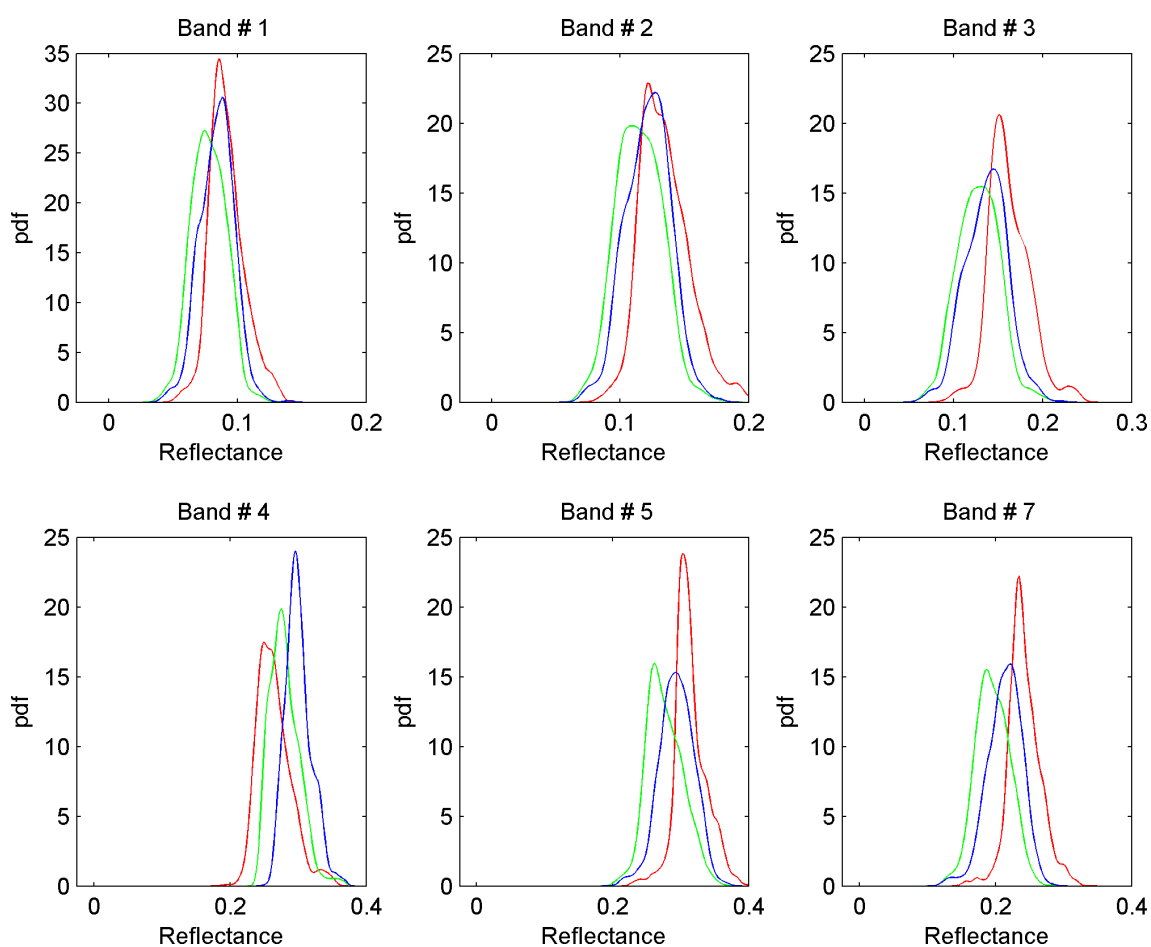
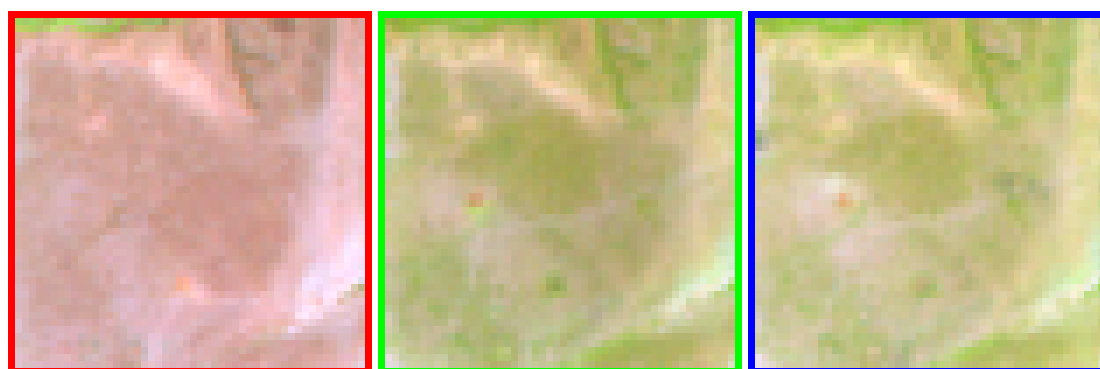
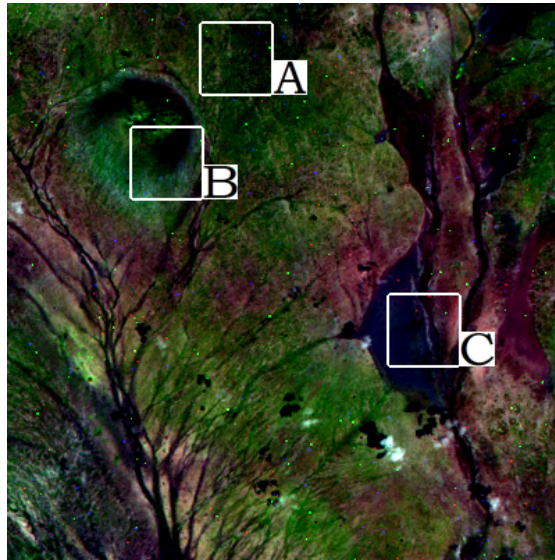


Figure 9. Study area 2. (Top) Closer look at the surface reflectance composite (RGB bands 5,4,3) of the 1500×1500 m subregion “C” in Fig. 6. The patches are from the Landsat images L5167063-06319870202 (red color), L71167063-06320010115 (green color), and L71167063-06320010131 (blue color). (Bottom) The correspondent probability density estimates of the surface reflectance for the bands 1–5 and 7 of Landsat are depicted. A total of 2500 reflectance samples (pixels) are available in each patch.

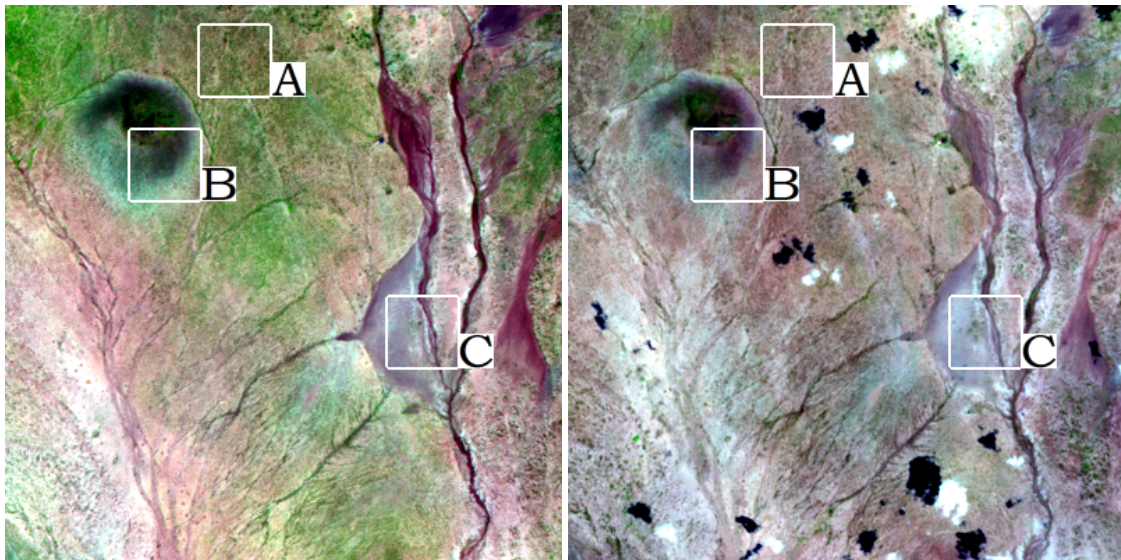
4.2 Long satellite revisit time: image set 2

4.2.1 Inter-image surface reflectance comparison, study area 3

The comparisons for the study 3 are shown in Fig. 10–13. This include color composite of the surface reflectance and the estimated probability function of the surface reflectance of the bands 1–5 and 7 for selected subregions.



L5167063-06319841210



L5167063-06319870101

L71167063-06320011201

Figure 10. Study area 3. Surface reflectance composite (RGB bands 5,4,3) of a 12×12 km area from the Landsat images L5167063-06319841210 (top), L5167063-06319870101 (middle), and L71167063-06320011201 (bottom). To enhance visualization for a qualitative assessment, linear stretching with identical and conveniently chosen saturation thresholds were used in the three images. Three regions are used for the quantitative assessment of the surface reflectance, by computing the pdf, and the median, of the surface reflectance in each Landsat band.

Note that some pixels of the image L5167063-06319841210 are corrupted by high levels of noise.

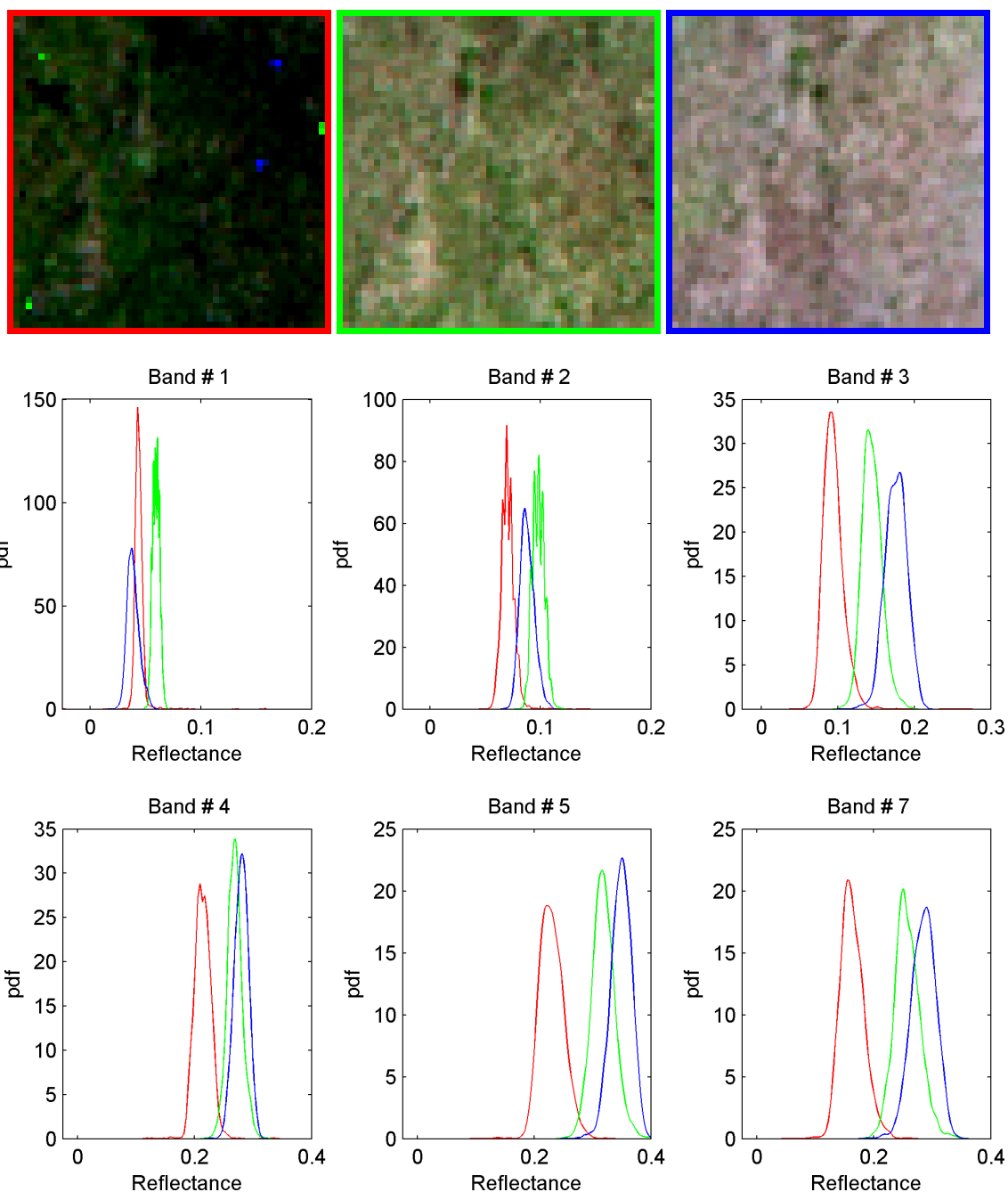


Figure 11. Study area 3. (Top) Closer look at the surface reflectance composite (RGB bands 5,4,3) of the 1500×1500 m subregion "A" in Fig. 10. The patches are from the Landsat images L5167063-06319841210 (red color), L5167063-06319870101 (green color), and L71167063-06320011201 (blue color). (Bottom) The correspondent probability density estimates of the surface reflectance for the bands 1–5 and 7 of Landsat are depicted. A total of 2500 reflectance samples (pixels) are available in each patch.

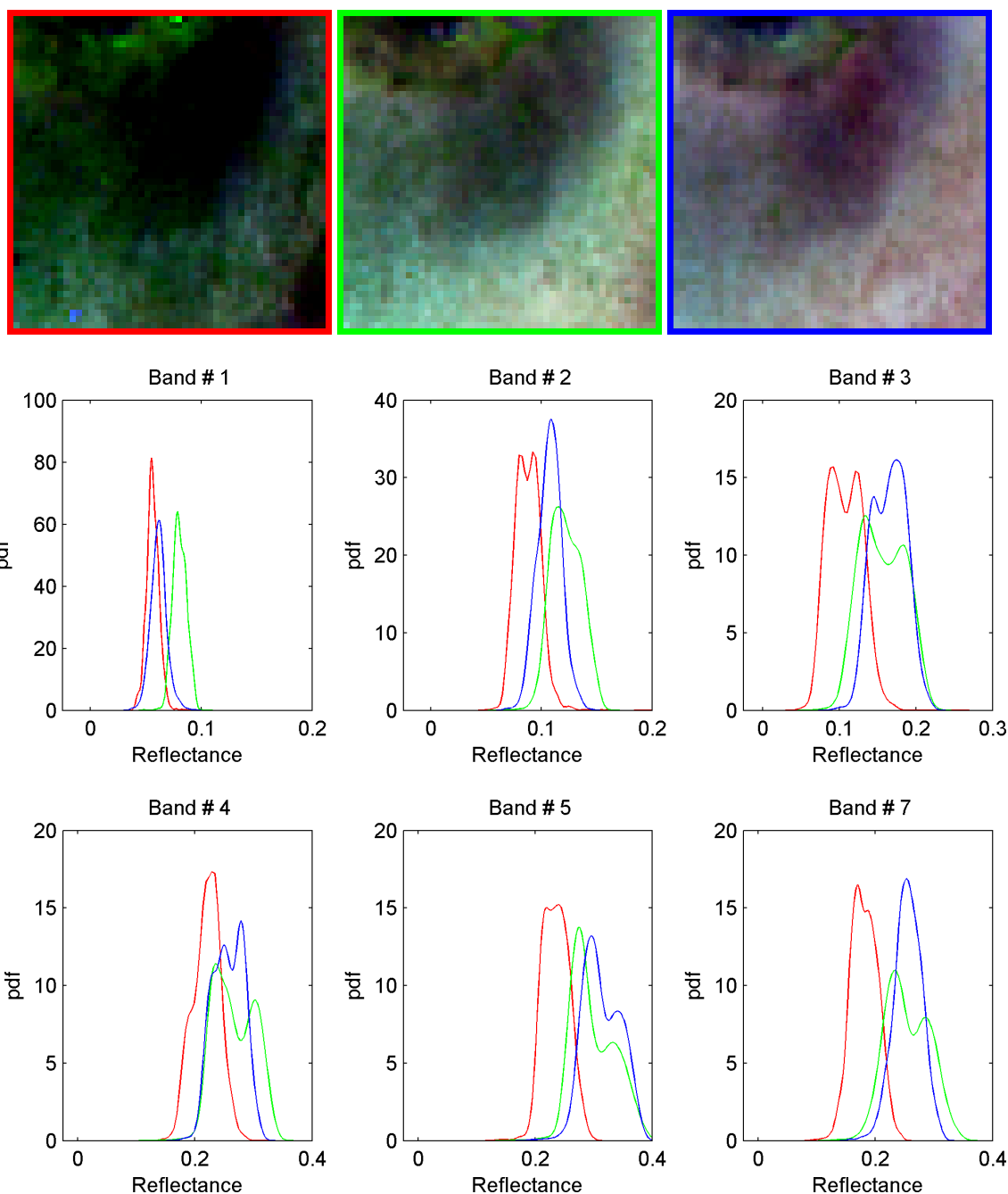


Figure 12. Study area 3. (Top) Closer look at the surface reflectance composite (RGB bands 5,4,3) of the 1500×1500 m subregion “B” in Fig. 10. The patches are from the Landsat images L5167063-06319841210 (red color), L5167063-06319870101 (green color), and L71167063-06320011201 (blue color). (Bottom) The correspondent probability density estimates of the surface reflectance for the bands 1–5 and 7 of Landsat are depicted. A total of 2500 reflectance samples (pixels) are available in each patch.

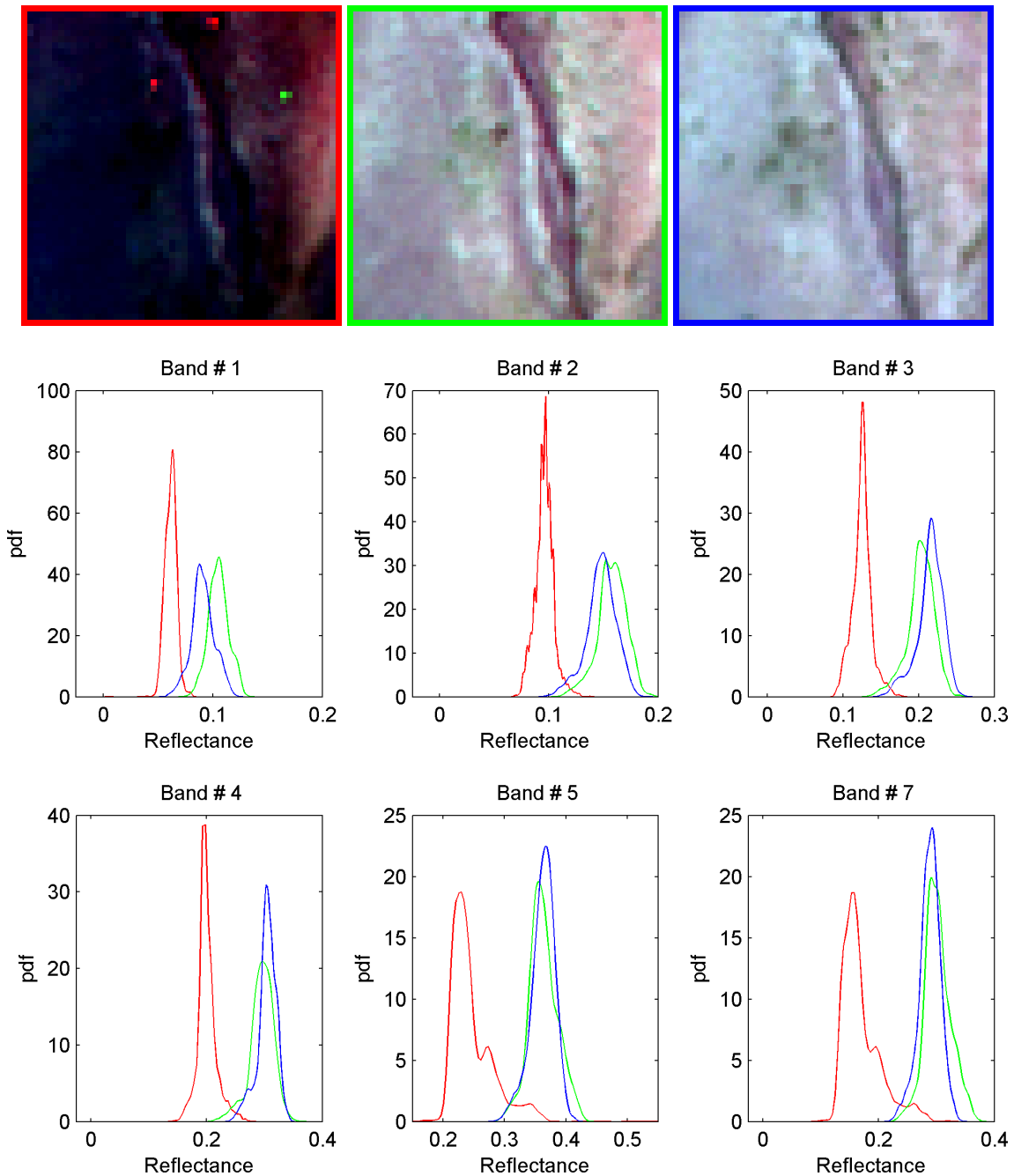
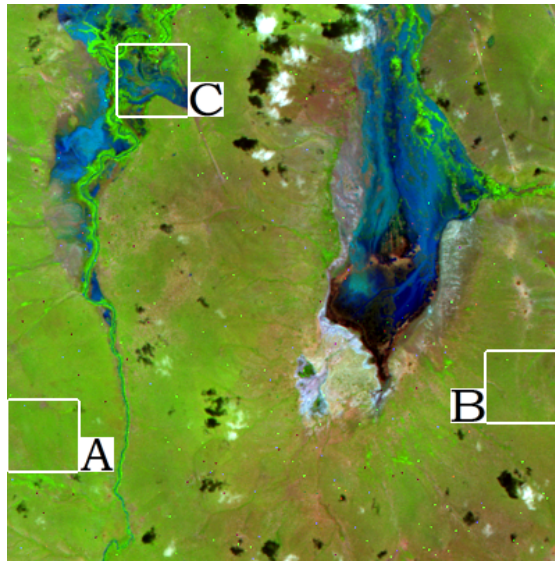


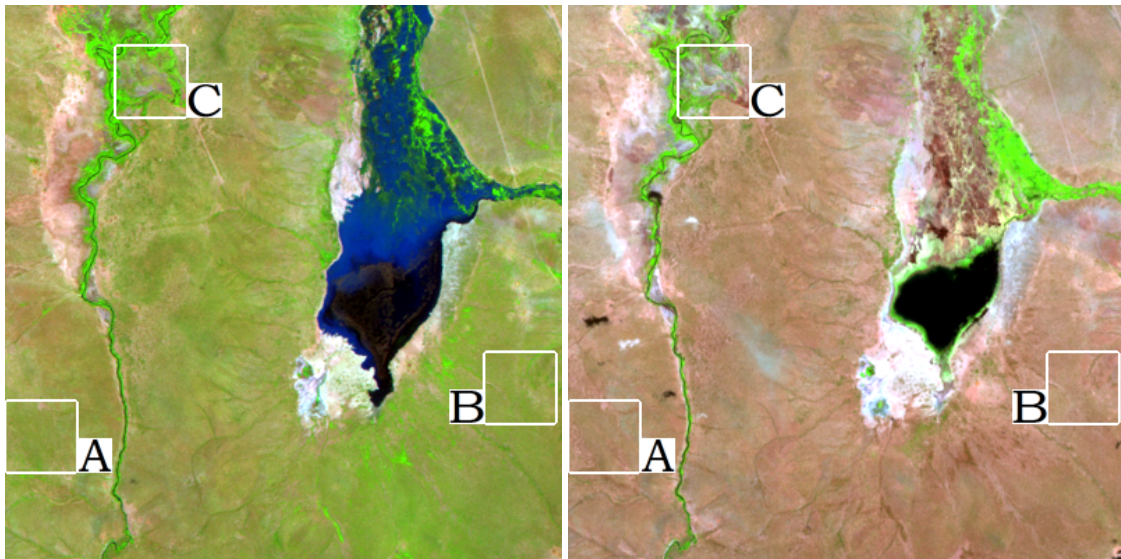
Figure 13. Study area 3. (Top) Closer look at the surface reflectance composite (RGB bands 5,4,3) of the 1500×1500 m subregion "C" in Fig. 10. The patches are from the Landsat images L5167063-06319841210 (red color), L5167063-06319870101 (green color), and L71167063-06320011201 (blue color). (Bottom) The correspondent probability density estimates of the surface reflectance for the bands 1–5 and 7 of Landsat are depicted. A total of 2500 reflectance samples (pixels) are available in each patch.

4.2.2 Inter-image surface reflectance comparison, study area 4

The comparisons for the study 4 are shown in Fig. 14–17. This include color composite of the surface reflectance and the estimated probability function of the surface reflectance of the bands 1–5 and 7 for selected subregions.



L5167063-06319841210



L5167063-06319870101

L71167063-06320011201

Figure 14. Study area 4. Surface reflectance composite (RGB bands 5,4,3) of a 12×12 km area from the Landsat images L5167063-06319841210 (top), L5167063-06319870101 (left), and L71167063-06320011201 (right). To enhance visualization for a qualitative assessment, linear stretching with identical and conveniently chosen saturation thresholds were used in the three images. Three regions are used for the quantitative assessment of the surface reflectance, by computing the pdf, and the median, of the surface reflectance in each Landsat band.

Note that some pixels of the image L5167063-06319841210 are corrupted by high levels of noise.

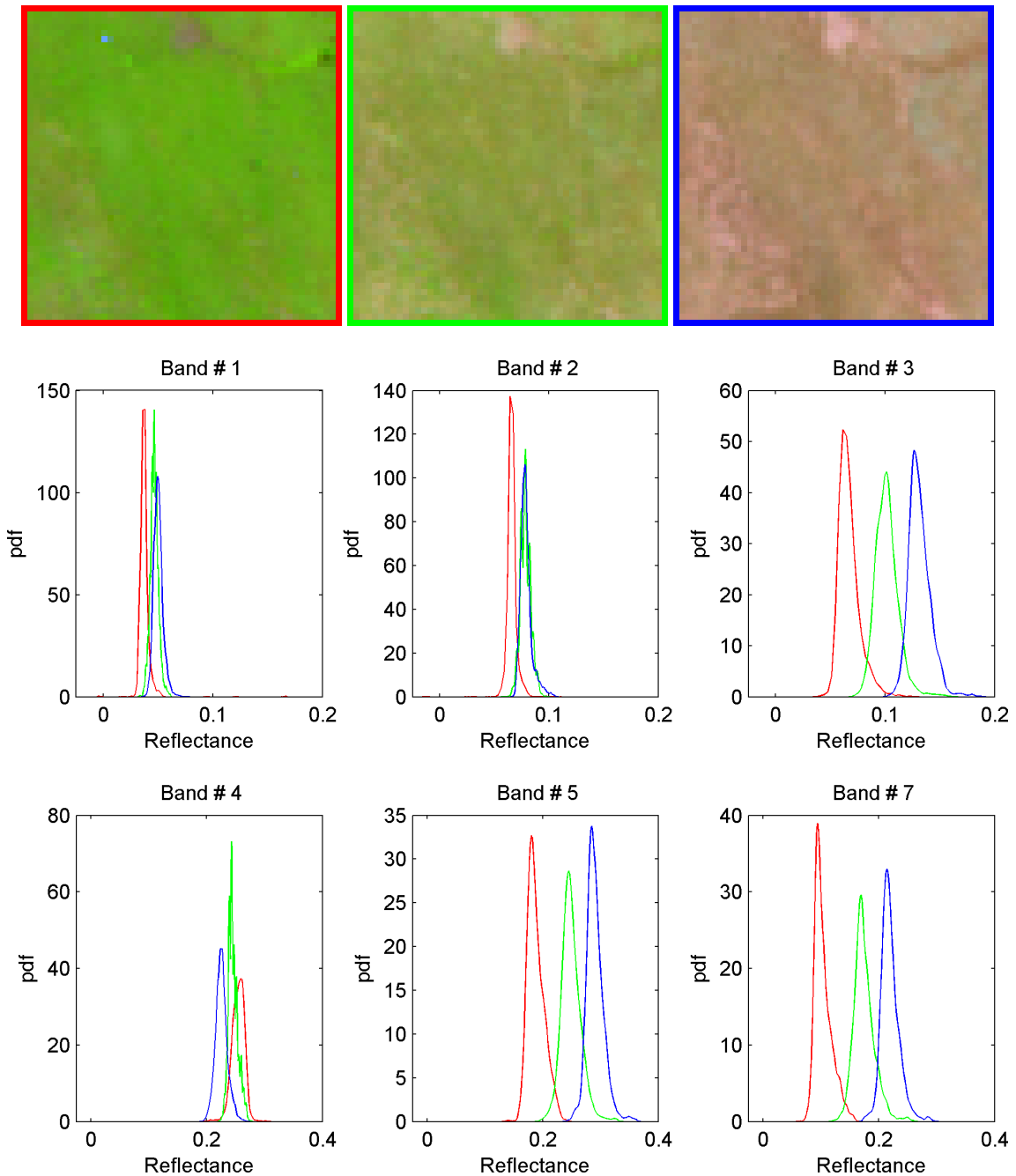


Figure 15. Study area 4. (Top) Closer look at the surface reflectance composite (RGB bands 5,4,3) of the 1500×1500 m subregion "A" in Fig. 14. The patches are from the Landsat images L5167063-06319841210 (red color), L5167063-06319870101 (green color), and L7167063-06320011201 (blue color). (Bottom) The correspondent probability density estimates of the surface reflectance for the bands 1–5 and 7 of Landsat are depicted. A total of 2500 reflectance samples (pixels) are available in each patch.

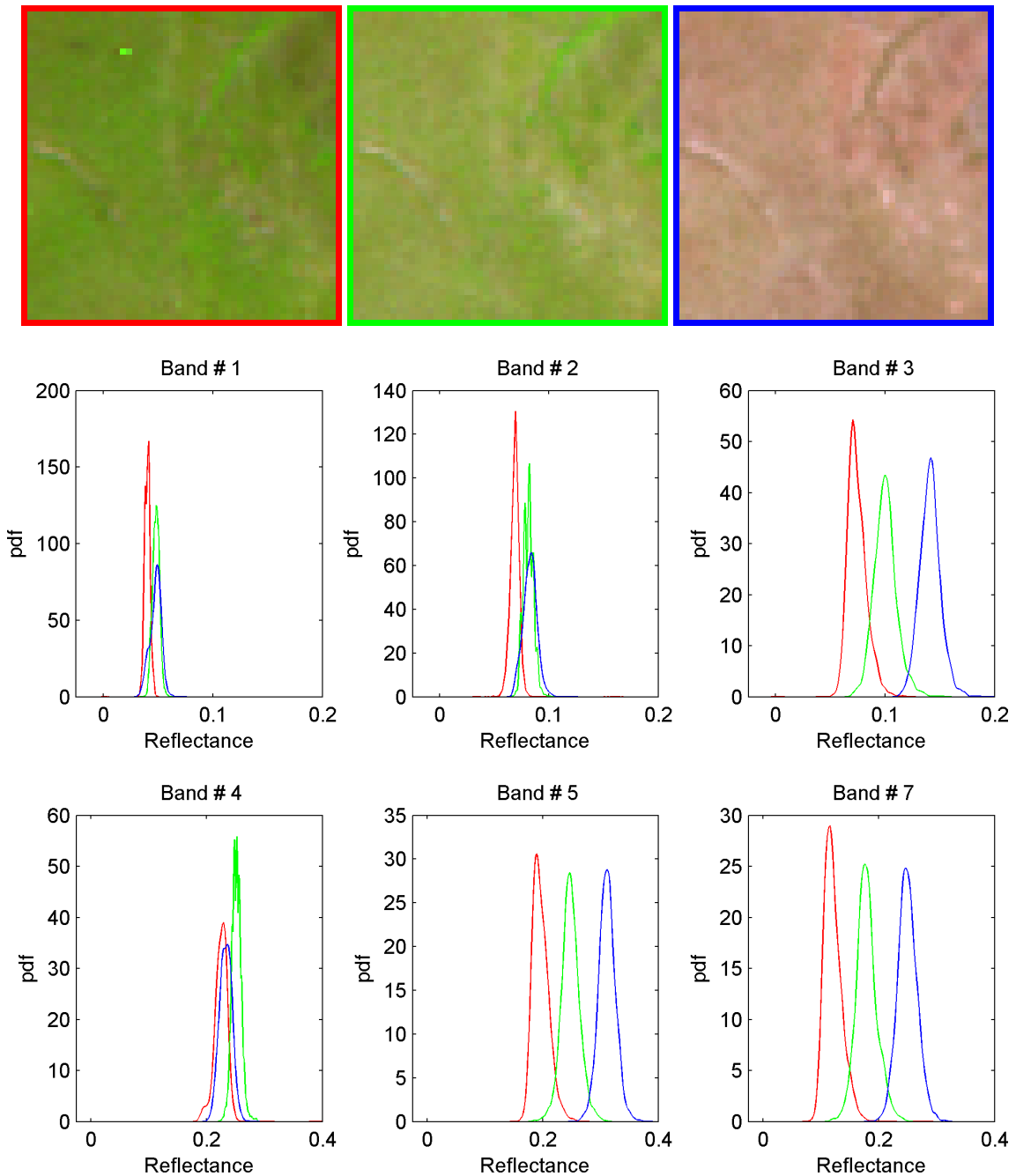


Figure 16. Study area 4. (Top) Closer look at the surface reflectance composite (RGB bands 5,4,3) of the 1500×1500 m subregion “B” in Fig. 14. The patches are from the Landsat images L5167063-06319841210 (red color), L5167063-06319870101 (green color), and L7167063-06320011201 (blue color). (Bottom) The correspondent probability density estimates of the surface reflectance for the bands 1–5 and 7 of Landsat are depicted. A total of 2500 reflectance samples (pixels) are available in each patch.

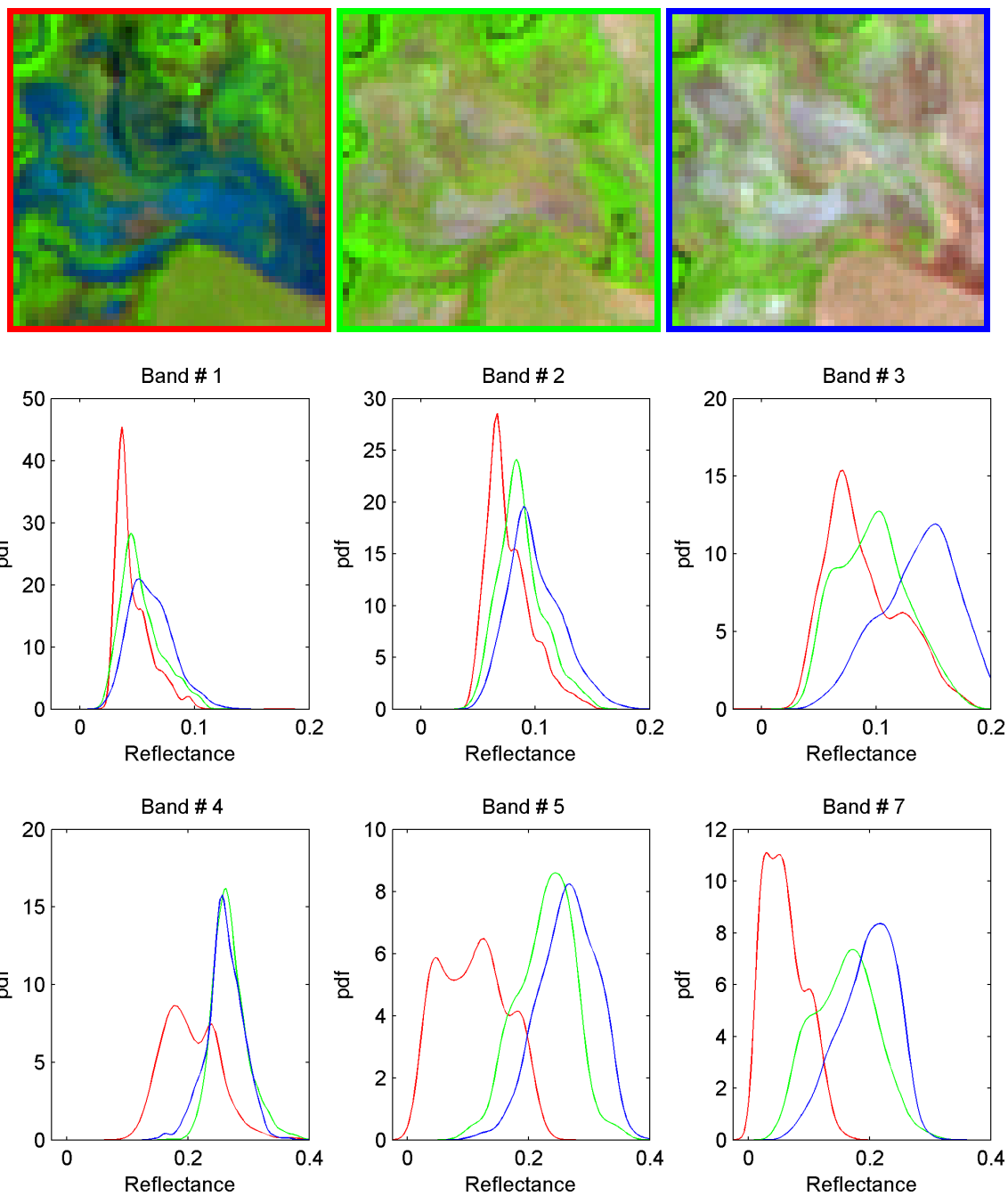


Figure 17. Study area 4. (Top) Closer look at the surface reflectance composite (RGB bands 5,4,3) of the 1500×1500 m subregion "C" in Fig. 14. The patches are from the Landsat images L5167063-06319841210 (red color), L5167063-06319870101 (green color), and L7167063-06320011201 (blue color). (Bottom) The correspondent probability density estimates of the surface reflectance for the bands 1–5 and 7 of Landsat are depicted. A total of 2500 reflectance samples (pixels) are available in each patch.

4.3 Summary tables of long revisit time for the study areas 1–4

Summary scores of the inter comparison of surface reflectance images generated by LEDAPS for the first four areas studied are shown in Tables 2–5. Scores are based on the median of the 50×50 pixel subregions previously shown. In addition to the median, the absolute difference (computed as the maximum minus the minimum value) and the relative (maximum divided by the minimum) of the median of the surface reflectance for each of the three images is included.

The agreement scores are not constant over all bands and image sets compared. Results from the study areas 1 and 2 were found to be more stable. The median of the absolute reflectance difference was 0.006 and 0.013 for the study areas 1 and 2, respectively. The relative difference for the study areas 1 and 2 was 17% and 15% of the estimated reflectance value, respectively. (Tab. 2–3). For the study areas 3 and 4, these median figures increase to a absolute difference of 0.070 and 0.063, and a relative difference of 54% and 51% of the estimated reflectance value, respectively (Tab. 4–5).

Note that the land cover and the phenology of the selected subregions to compute the above figures were assumed to be unchanged over the many years that passed between the acquisition of the images (Tab. 1). This may be not the case for all regions considered, contributing to an increase in the figures above indicated. It was also assumed that the images acquired by Landsat 5 and 7 were directly comparable on all bands.

Table 2. Study Area 1: Summary scores for the median of the surface reflectance (in %) computed by LEDAPS for Landsat bands 1–5 and 7. Statistics are computed in the 50 × 50 pixel subregions labeled A in red, B in green, and C in blue color.

Subregion	Landsat image	B1	B2	B3	B4	B5	B7
1A	L5167063-06319870202	1.68	3.43	2.60	25.62	10.72	4.55
1A	L71167063-06320010115	2.02	3.70	2.33	29.04	13.12	5.74
1A	L71167063-06320010131	2.01	3.62	2.09	30.40	13.14	5.72
1A	Δ absolute	0.34	0.27	0.51	4.79	2.42	1.19
1A	Δ relative [%]	20.24	7.87	24.40	18.68	22.57	26.15
1B	L5167063-06319870202	1.48	2.95	2.17	20.31	9.64	4.16
1B	L71167063-06320010115	1.64	2.73	1.98	19.17	9.69	4.52
1B	L71167063-06320010131	1.53	2.65	1.72	19.97	9.66	4.25
1B	Δ absolute	0.16	0.30	0.45	1.14	0.05	0.36
1B	Δ relative [%]	10.81	11.32	26.16	5.95	0.52	8.65
1C	L5167063-06319870202	2.93	5.58	4.51	32.27	19.57	10.01
1C	L71167063-06320010115	3.71	5.85	5.73	27.90	21.82	13.33
1C	L71167063-06320010131	3.53	5.60	4.90	29.07	20.07	11.21
1C	Δ absolute	0.78	0.27	1.22	4.37	2.25	3.32
1C	Δ relative [%]	26.62	4.84	27.05	15.67	11.50	33.17

Location of the subregions in the composite surface reflectance images (bands 5,4,3).

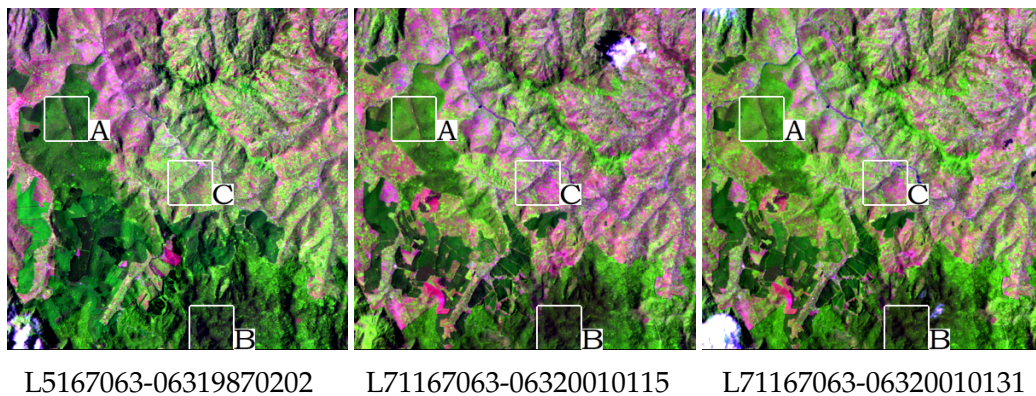


Table 3. Study Area 2: Summary scores for the median of the surface reflectance (in %) computed by LEDAPS for Landsat bands 1–5 and 7. Statistics are computed in the 50 × 50 pixel subregions labeled A in red, B in green, and C in blue color.

Subregion	Landsat image	B1	B2	B3	B4	B5	B7
2A	L5167063-06319870202	6.89	11.36	14.25	26.11	28.23	22.65
2A	L71167063-06320010115	6.30	10.79	13.49	29.03	28.10	21.69
2A	L71167063-06320010131	6.33	10.55	13.24	29.25	27.62	21.53
2A	Δ absolute	0.59	0.81	1.01	3.14	0.61	1.12
2A	Δ relative [%]	9.37	7.68	7.63	12.03	2.21	5.20
2B	L5167063-06319870202	1.20	3.85	2.41	2.74	2.17	1.66
2B	L71167063-06320010115	1.50	3.48	1.88	1.18	0.61	0.47
2B	L71167063-06320010131	1.37	3.64	1.80	1.06	0.34	0.45
2B	Δ absolute	0.30	0.37	0.61	1.68	1.83	1.21
2B	Δ relative [%]	25.00	10.63	33.89	158.49	538.24	268.89
2C	L5167063-06319870202	9.01	13.34	15.99	26.13	31.02	23.90
2C	L71167063-06320010115	7.71	11.41	12.77	27.82	27.41	19.53
2C	L71167063-06320010131	8.46	12.20	13.83	29.76	29.39	21.53
2C	Δ absolute	1.30	1.93	3.22	3.63	3.61	4.37
2C	Δ relative [%]	16.86	16.91	25.22	13.89	13.19	22.38

Location of the subregions in the composite surface reflectance images (bands 5,4,3).

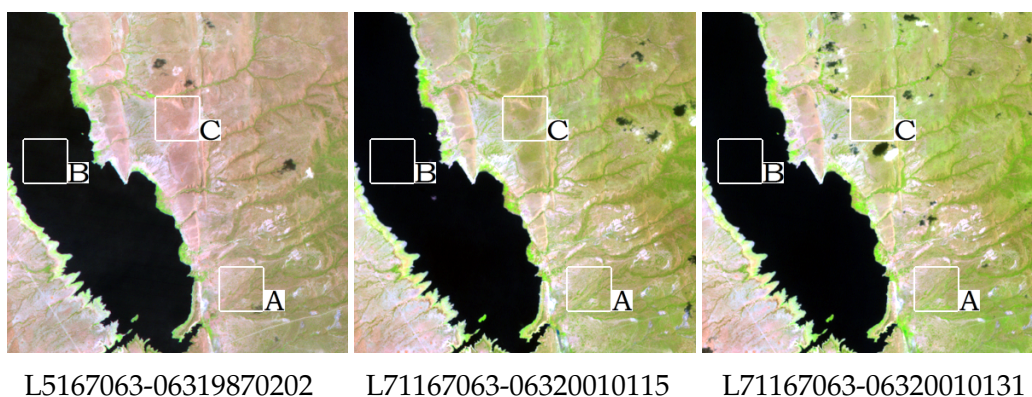


Table 4. Study Area 3: Summary scores for the median of the surface reflectance (in %) computed by LEDAPS for Landsat bands 1–5 and 7. Statistics are computed in the 50 × 50 pixel subregions labeled A in red, B in green, and C in blue color.

Subregion	Landsat image	B1	B2	B3	B4	B5	B7
3A	L5167063-06319841210	4.31	6.98	9.39	21.38	22.93	16.28
3A	L5167063-06319870101	5.89	9.82	14.48	26.74	31.73	25.46
3A	L71167063-06320011201	3.79	8.79	17.64	28.08	34.96	28.55
3A	Δ absolute	2.11	2.84	8.25	6.70	12.03	12.27
3A	Δ relative [%]	55.61	40.69	87.86	31.34	52.46	75.40
3B	L5167063-06319841210	5.56	8.87	10.55	22.15	23.48	18.11
3B	L5167063-06319870101	8.03	12.02	15.44	26.30	29.02	25.03
3B	L71167063-06320011201	6.09	10.65	16.58	25.86	30.95	25.50
3B	Δ absolute	2.47	3.15	6.03	4.15	7.47	7.39
3B	Δ relative [%]	44.42	35.51	57.16	18.74	31.81	40.81
3C	L5167063-06319841210	6.18	9.67	12.53	19.78	23.68	16.11
3C	L5167063-06319870101	10.51	15.99	20.50	29.66	36.09	29.92
3C	L71167063-06320011201	9.00	14.94	21.66	30.63	36.41	29.01
3C	Δ absolute	4.33	6.32	9.13	10.85	12.73	13.81
3C	Δ relative [%]	70.06	65.36	72.87	54.85	53.76	85.72

Location of the subregions in the composite surface reflectance images (bands 5,4,3).

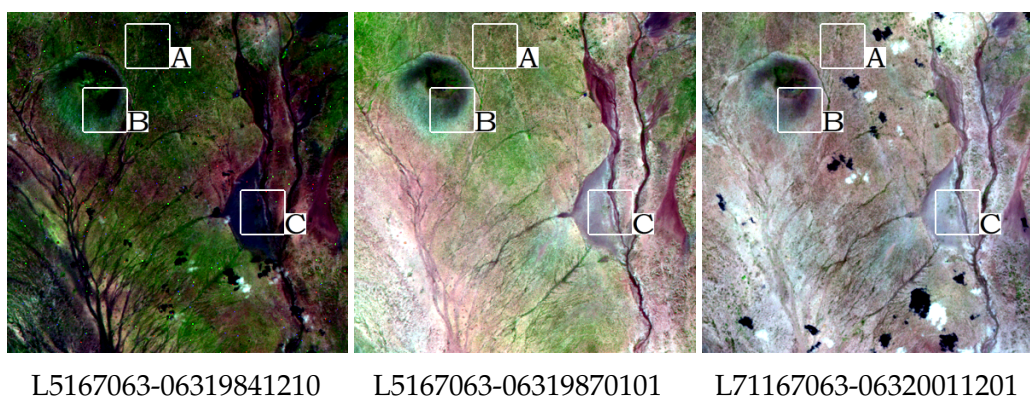
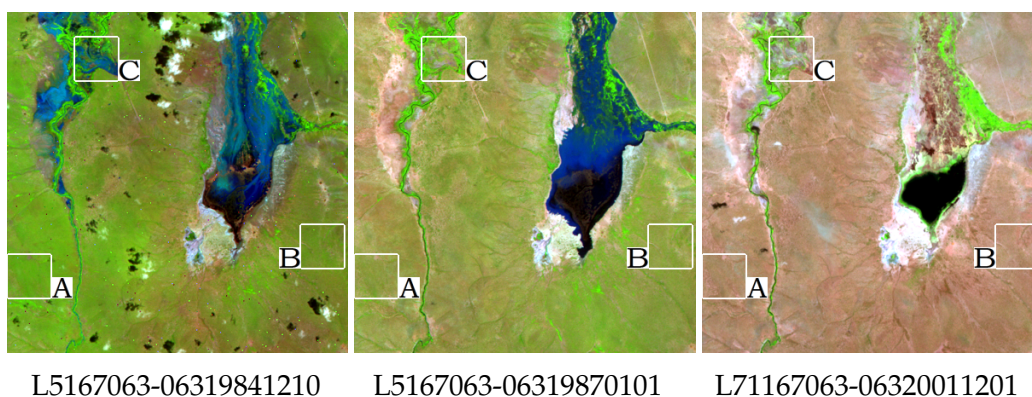


Table 5. Study Area 4: Summary scores for the median of the surface reflectance (in %) computed by LEDAPS for Landsat bands 1–5 and 7. Statistics are computed in the 50 × 50 pixel subregions labeled A in red, B in green, and C in blue color.

Subregion	Landsat image	B1	B2	B3	B4	B5	B7
4A	L5167063-06319841210	3.67	6.44	6.60	25.51	18.58	10.10
4A	L5167063-06319870101	4.62	7.82	9.92	24.33	24.79	17.07
4A	L71167063-06320011201	4.96	7.82	13.01	22.44	28.87	21.71
4A	Δ absolute	1.29	1.38	6.41	3.07	10.29	11.61
4A	Δ relative [%]	35.15	21.43	97.12	13.68	55.36	114.95
4B	L5167063-06319841210	3.97	6.90	7.34	22.44	19.50	11.89
4B	L5167063-06319870101	4.80	8.15	9.92	25.19	24.81	17.87
4B	L71167063-06320011201	4.81	8.29	14.08	23.38	31.12	24.89
4B	Δ absolute	0.84	1.39	6.74	2.75	11.62	13.00
4B	Δ relative [%]	21.16	20.14	91.83	12.25	59.59	109.34
4C	L5167063-06319841210	4.10	7.29	8.06	20.03	10.98	5.72
4C	L5167063-06319870101	4.92	8.54	9.80	26.59	23.24	16.08
4C	L71167063-06320011201	6.00	9.55	14.20	26.11	26.66	20.15
4C	Δ absolute	1.90	2.26	6.14	6.56	15.68	14.43
4C	Δ relative [%]	46.46	31.07	76.18	32.73	142.81	252.27

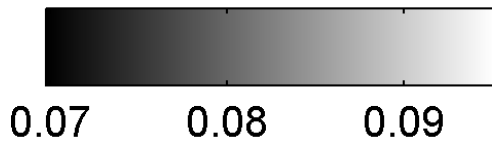
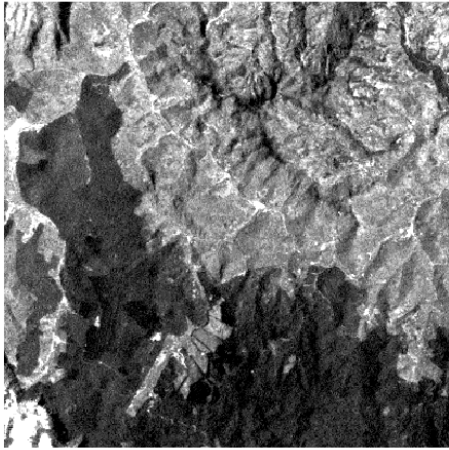
Location of the subregions in the composite surface reflectance images (bands 5,4,3).



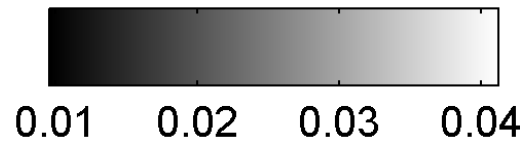
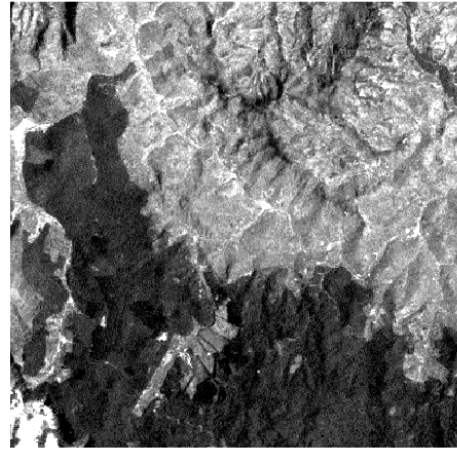
4.4 Comparison of top of atmosphere (TOA) with surface reflectance

To better understand the effect of the atmospheric correction done by LEDAS on the processed Landsat images, it appears interesting to compare the TOA reflectance with the estimated surface reflectance by LEDAPS. For this purpose, two different assessments are done. First we show side by side TOA and surface reflectance images, and compute the absolute and relative difference between both reflectance images (here the relative difference is calculated as the ratio between the TOA and the surface reflectance). Results for Landsat bands 1, 2 and 3 are shown in Fig. 18–Fig. 20. The correspondent scatter plots are shown in Fig. 21. We observe that the general spatial patterns of reflectance in both TOA and surface are preserved. Although the reflectance in the scatter plots shows a linear trend, the amount of correction introduced depends on the band and location of the pixel in the image.

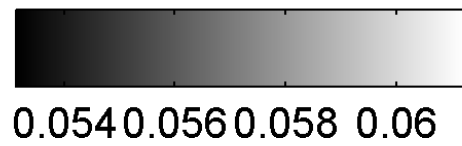
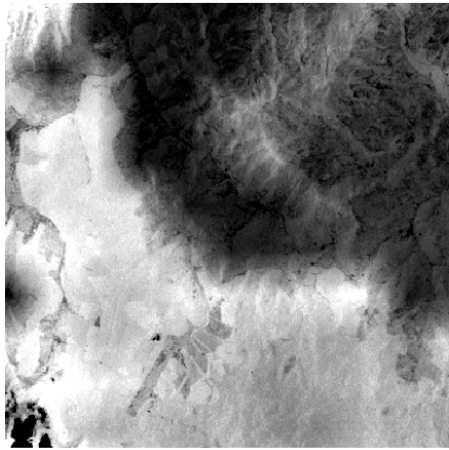
TOA reflectance (B1)



Surface reflectance (B1)



Absolute difference (B1)



Relative difference (B1)

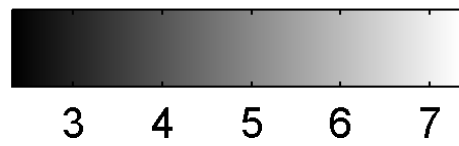
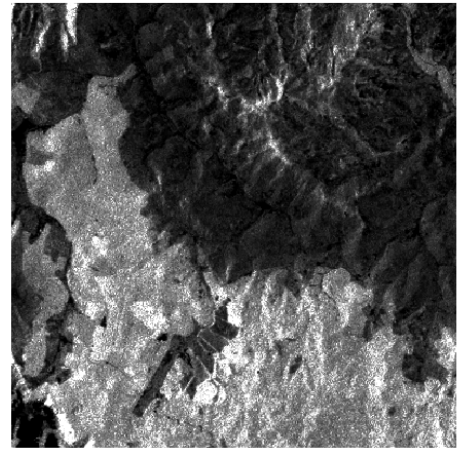
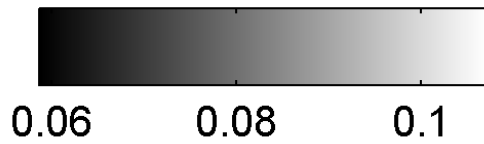
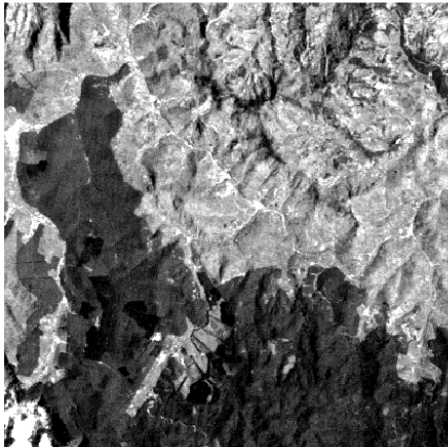
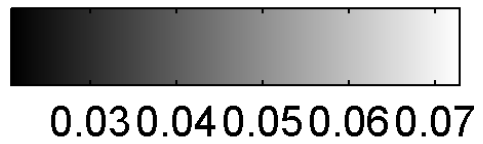
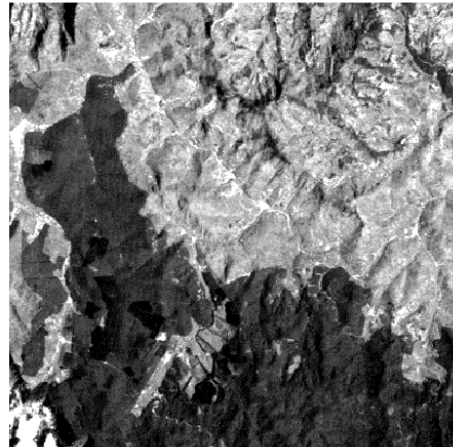


Figure 18. Top of atmosphere and surface reflectance estimated by LEDAPS for the band 1 of the Landsat image L5-167-063-063-1987-02-02. The absolute (TOA-SUR) and relative (TOA/SUR) difference maps are shown.

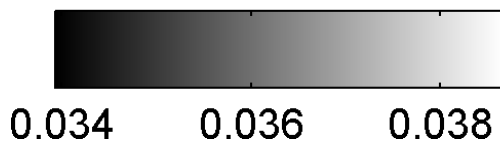
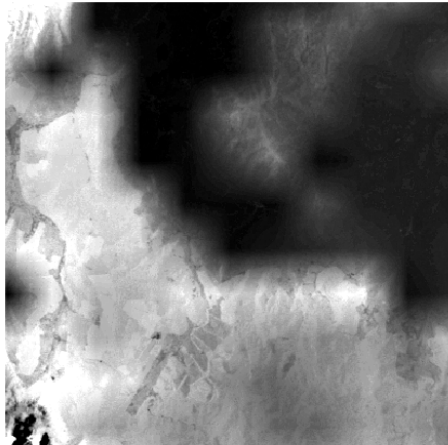
TOA reflectance (B2)



Surface reflectance (B2)



Absolute difference (B2)



Relative difference (B2)

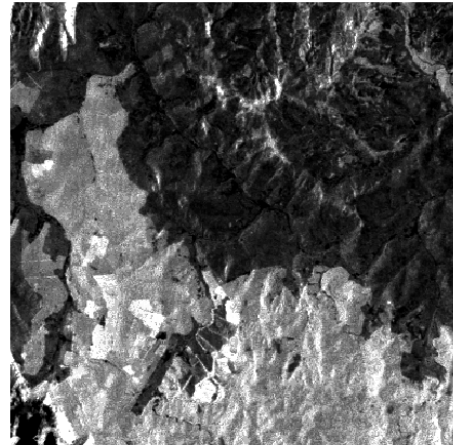
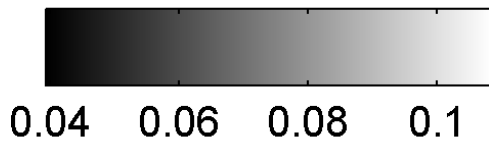
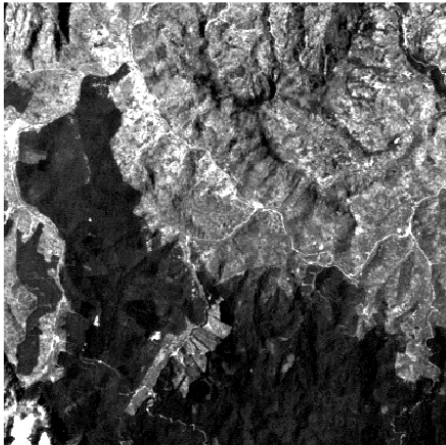
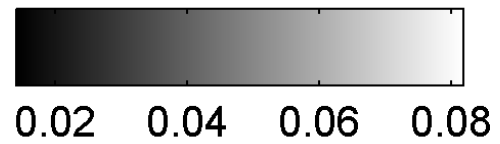
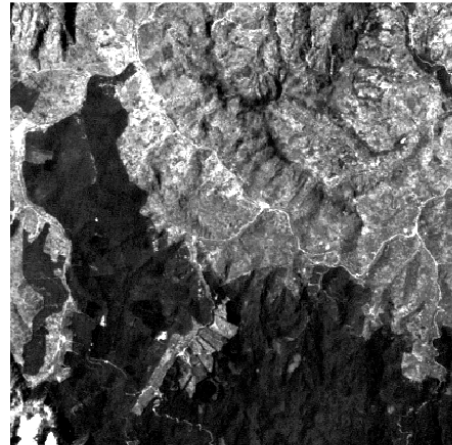


Figure 19. Top of atmosphere and surface reflectance estimated by LEDAPS for the band 2 of the Landsat image L5-167-063-063-1987-02-02. The absolute (TOA-SUR) and relative (TOA/SUR) difference maps are shown.

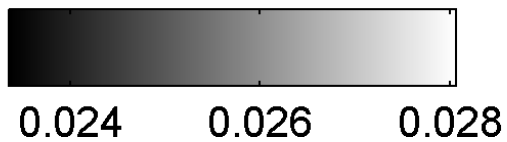
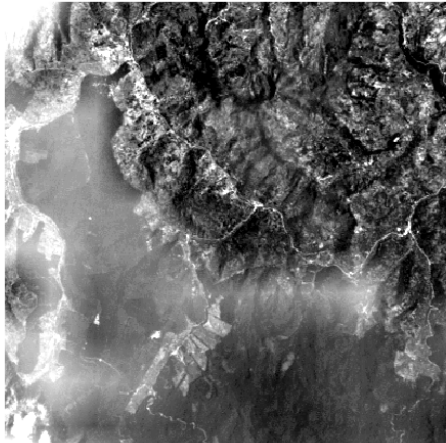
TOA reflectance (B3)



Surface reflectance (B3)



Absolute difference (B3)



Relative difference (B3)

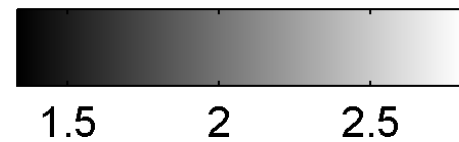
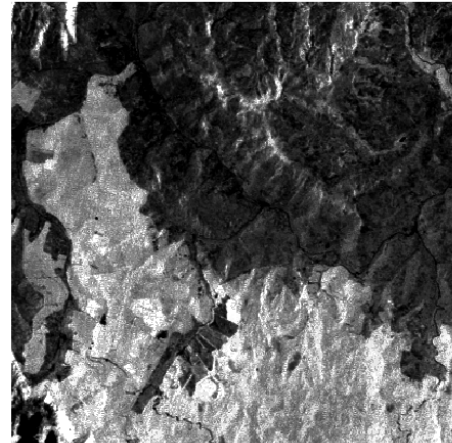


Figure 20. Top of atmosphere and surface reflectance estimated by LEDAPS for the band 3 of the Landsat image L5-167-063-063-1987-02-02. The absolute (TOA-SUR) and relative (TOA/SUR) difference maps are shown.

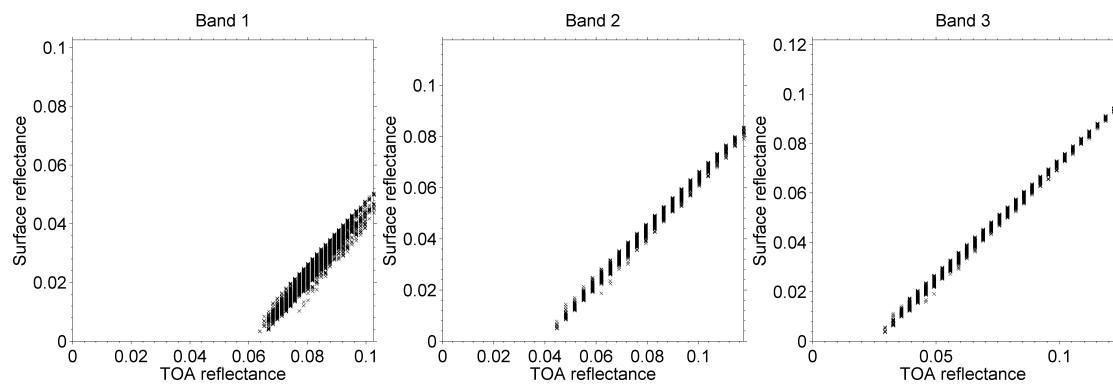


Figure 21. Top of atmosphere versus surface reflectance estimated by LEDAPS for the bands 1–3 of the Landsat image L5-167-063-063-1987-02-02.

4.5 Surface reflectance on regions under cloud shadows

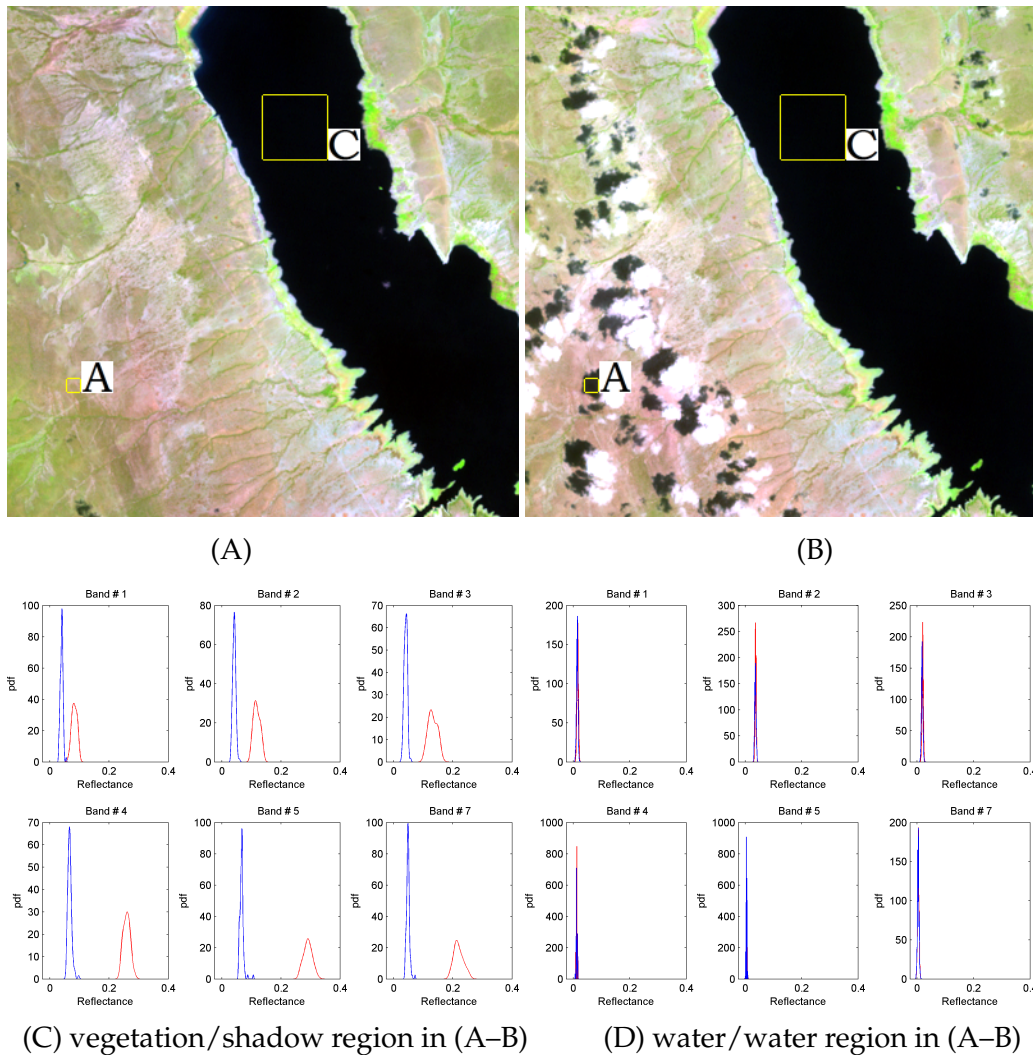


Figure 22. Study area 5. Surface reflectance composite (RGB bands 5,4,3) of a 1500×1500 m subregion from the Landsat images (A) L71-167-063-063-2001-01-15 and (B) L71-167-063-063-2001-01-31. The correspondent probability density estimates of the surface reflectance for the bands 1–5 and 7 of Landsat are depicted for both the blue and red patches corresponding to (C) vegetation covered by cloud shadow and (D) water region.

Image areas containing shadows due to cloud cover, if not properly taken in account, can negatively affect methodologies tailored for automatic classification of Landsat images based on the surface reflectance generated by LEDAPS.

To illustrate this effect, we compare the estimated probability density functions (pdf) of reflectance for two distinct image subregions acquired by Landsat 7 over the same geographic area. The images were acquired in January 2001 with a difference between acquisition times of only 16 days. A reasonable hypothesis is that the land cover is identical in both images, expecting the LEDAPS-estimated surface reflectances to be very similar in the regions not affected by shadows. This was previously confirmed in Figs. 2–5.

We focus the analyzes of the effect of shadows on the surface reflectance on a subwindow covered by vegetation, which was contaminated by cloud shadows in the second acquisition date. See Fig. 22 for details. The pdf of the surface reflectance samples was estimated and, for reference purposes, compared to the pdf of an area located inside a lake, which is not affected by clouds/shadows in both acquisition dates. As expected, the pdfs of the water samples, estimated from the reflectance images generated by LEDAPS in the different acquisition dates is very similar. When comparing the pdfs of the vegetation region, the pdf of the vegetation under cloud shadows resembles more the pdf of the water class than the vegetation class in the first acquisition. This is depicted in Fig. 22. We conclude that land cover/use classification of areas affected by cloud shadows using the surface reflectance estimated by LEDAPS would be very challenging, suggesting that an algorithm to mask the cloud shadows should be developed.

4.6 Surface reflectance on regions under thin clouds

LEDAPS uses the 6S radiative transfer code [Vermote et al. \(1997\)](#) to compute the transmission, intrinsic reflectance, and spherical albedo terms necessary to compute the surface reflectance. Clouds are masked using the ad hoc algorithm described in the user manual [Vermote and Saleous \(2007\)](#). Thick clouds are masked, but a remaining question is if the atmospheric correction module in LEDAPS can in general remove thin clouds or not.

To try to give a qualitative answer to this question, we selected data from a subregion of size 12×12 km from the the Landsat image L5-167-063-063-1984-1210, which contains both thick and and thin clouds. A color composite of the Landsat image is shown in Fig. 23. We compare the top of atmosphere reflectance, calculated using only sensor calibration parameters, with the surface reflectance estimated by LEDAPS. Visual analysis of both TOA and surface reflectance composites in Figs. 24–25 suggests that the thin clouds are not effectively removed with LEDAPS. This can be due the low spacial resolution of the ancillary data used to compute the necessary atmospheric parameters. We observe in Figs. 24–25 that the image (A) is brighter than (B), which is due the fact that TOA reflectance are greater then the surface reflectance. However, the difference of the alternative composite visualizations of the TOA in (C), and the corresponding surface reflectance by LEDAPS in (D) is almost unnoticeable when the thresholds used to generate the color composites are computed from each reflectance image individually. To give an idea of how similar are the images in (C) and (D), the RGB differences of the composite reflectance maps are on average lower than 8 digital counters when the reflectances are mapped to a [0-255] interval. However, whatever the chosen visualization is, the conclusion is that thin clouds are still present after the surface reflectance is computed using LEDAPS.

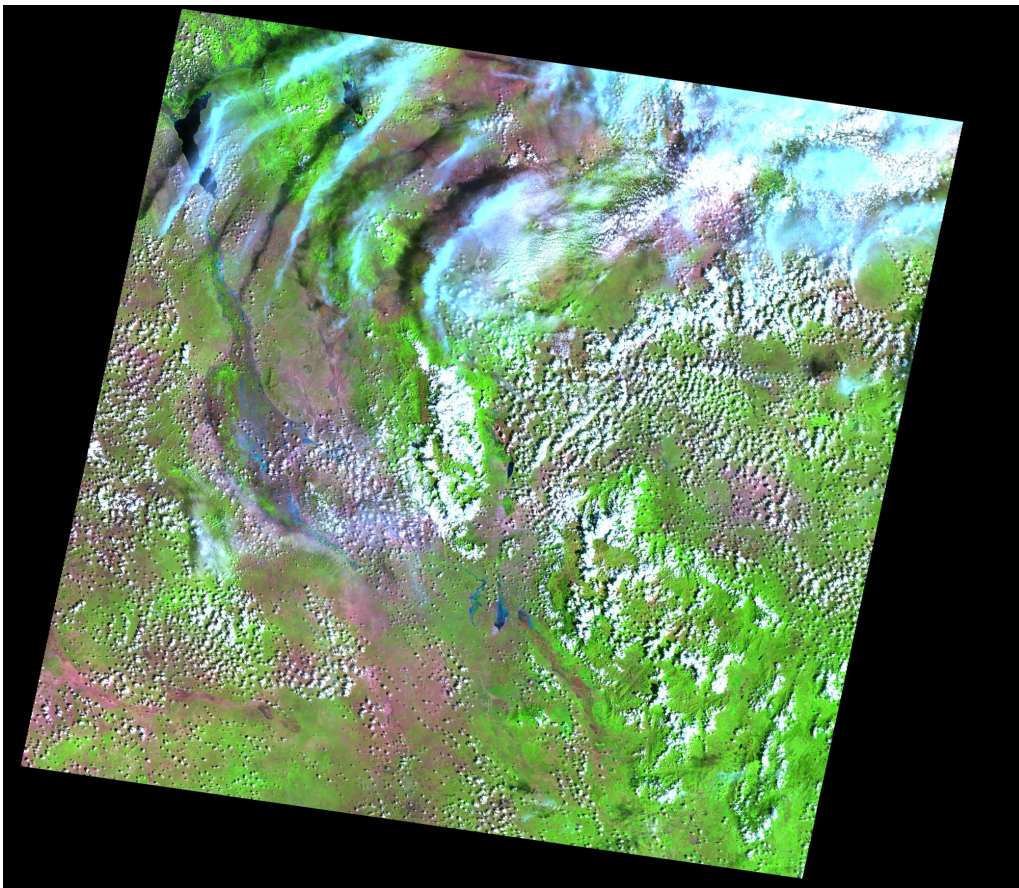
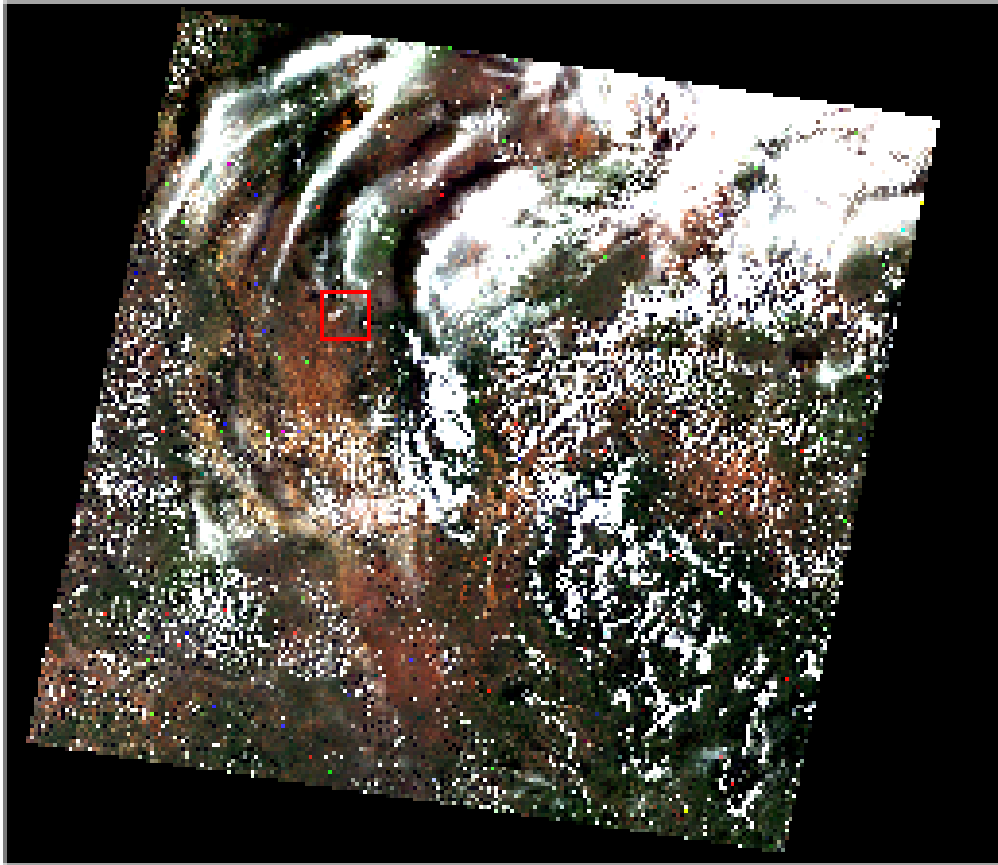


Figure 23. Landsat image L5-167-063-063-1984-1210 and the selected subregion of size 12×12 km indicated in red. RGB color composition with bands (top) (3,2,1), and bottom (5,4,3).

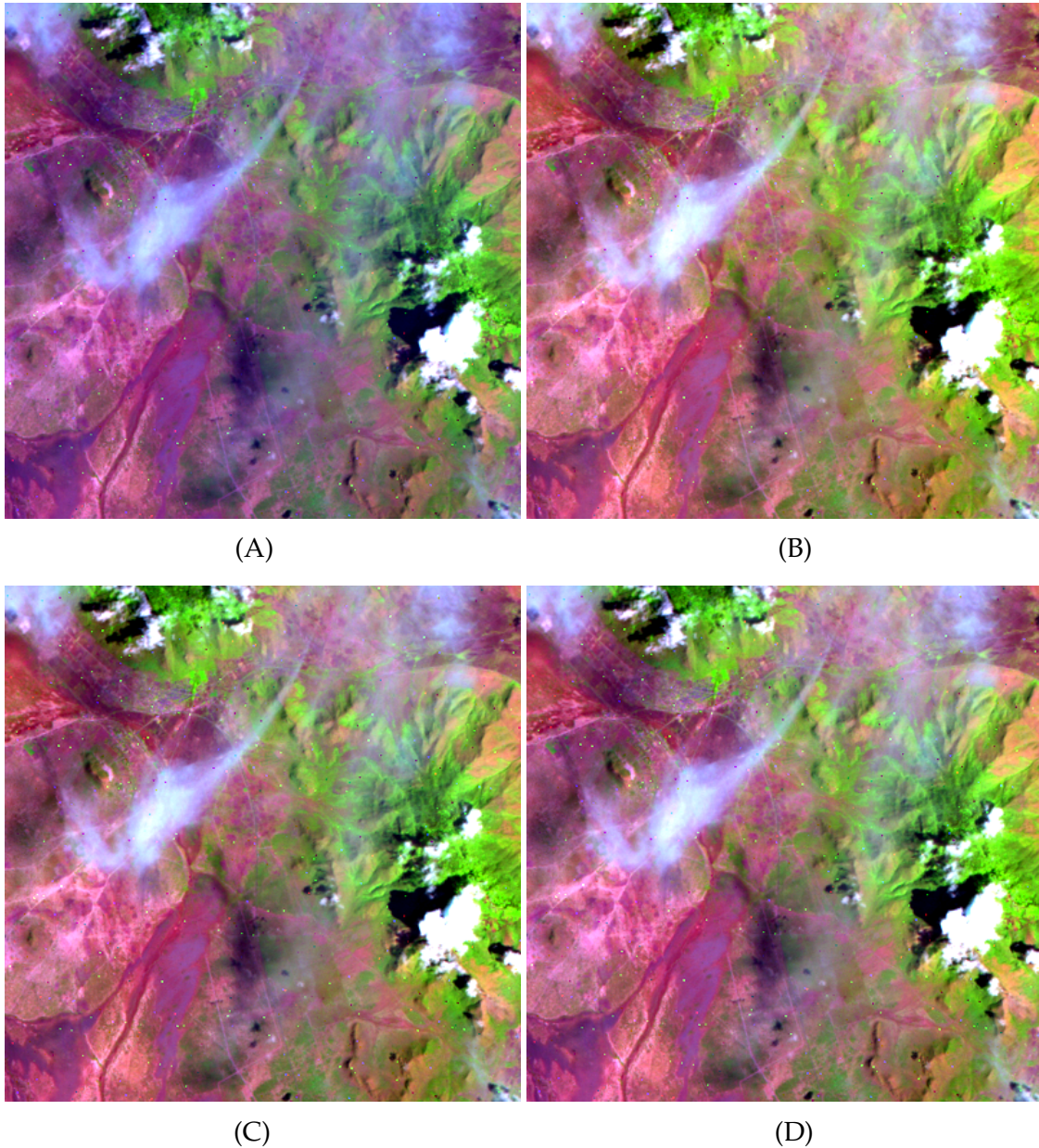
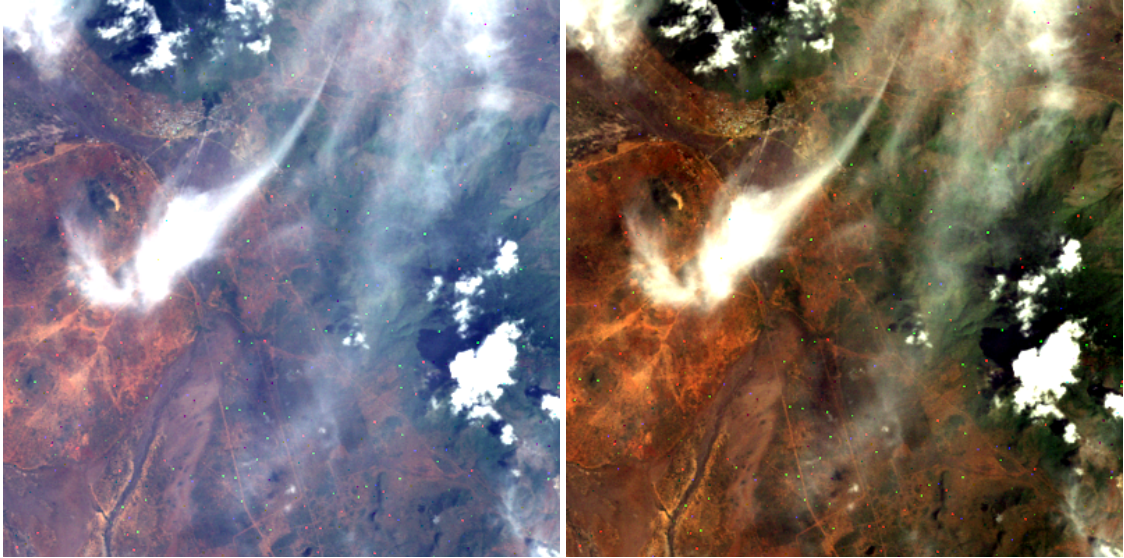
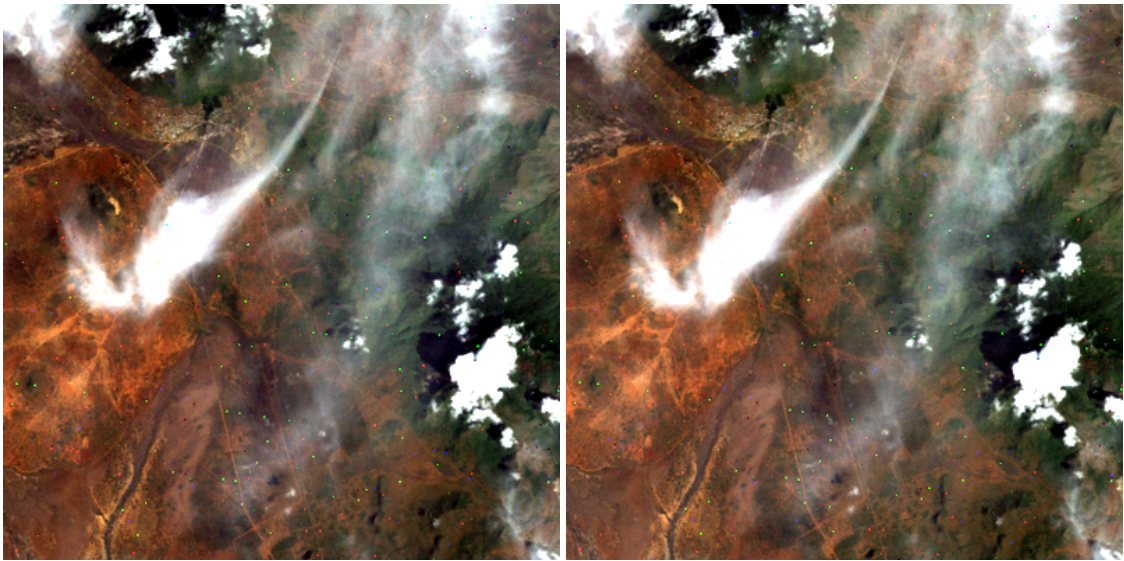


Figure 24. Study area 6. RGB composite images (bands 5,4,3) of the subregion of the Landsat image L5-167-063-063-1984-1210 indicated in Fig. 23. (A) is the TOA reflectance, and (B) is the surface reflectance estimated by LEDAPS. Both images “A” and “B” are generated using identical saturation thresholds during linear stretching. This is for visualization purposes only. (C) Visualization of the composite image of the TOA reflectance generate using linear stretching with the thresholds computed as the percentiles 1% and 99% of the TOA reflectance. (D) Visualization of the surface reflectance using linear stretching with the thresholds computed as the percentiles 1% and 99% of the surface reflectance.



(A)

(B)



(C)

(D)

Figure 25. Same as Figure 24, but for the RGB color composition using bands (3,2,1).

4.7 Short satellite revisit time: image set 1

In the first part of this report we focused on the analysis of images from a given area imaged at long revisit times.

In the second part of the report we present a sequence of comparisons of scenes acquired within the 16 days of temporal resolution of Landsat. The analysis of images acquired at very close time points should minimize the possible effect of long temporal changes accumulated in the area of interest.

In the first set considered (study areas 7–10), three images were jointly compared. These were acquired by Landsat 5 between November 6 and December 8, 2009.

In the second set of study areas considered (11–14), two images were jointly compared. These were acquired by Landsat 5 on May 30 and June 15, 2009.

The third set of study areas considered (15–17) also considered joint comparisons of two images. These were acquired by Landsat 5 on July 1 and July 17, 2009.

Note that the images 11–14 and 15–17, although close in time, were not compared together. This is due the fact that the land cover have changed in the period, specially between June 15 and July 1, 2009. We are uncertain what is the reason for it. We hypothesize that the successive observed visual changes may be due land cultivations or fires. See Fig. 26 for an illustration of a 24×24 km area centered at $9^{\circ}55'19''\text{S}$, $38^{\circ}8'49''\text{E}$ (close to Liwale). We note a high response of the red channel corresponding to the NIR reflectance of band 7 at an U-shaped region located at the center of the image acquired on July 17, 2009.

Due to the higher cloud coverage in the images used in this second part of the report, we decided to reduce the number of those small squared-window regions selected into each study area (to one each), increasing the number of different study areas, in order to keep a reasonable representativity for the analysis.

For the images in the study are 7–10, in addition to the surface reflectance, we show side-by-side color compositions of the TOA reflectance. In both cases we produce compositions using the RGB bands 5,4,3. To enhance visualization and the qualitative assessment, linear stretching with identical and conveniently chosen saturation thresholds were used in the three images of surface reflectance. Differently, in the case of the TOA images, the thresholds were not calculated but fixed at band5 [0–0.46], band 4 [0–0.44], and band 3 [0–0.23]. In this particular set of images, we note that even if the thresholds are kept constant, the TOA compositions at the different time points tested are already pretty similar. The surface reflectance given by LEDAPS is also very similar in the three images tested. Although the TOA values are higher than the surface reflectance, we found that if the appropriate thresholds are calculated also for the TOA images (instead of keeping them fixed), the resulting linearly scaled TOA compositions (not shown) would be also very similar to the surface reflectance color compositions. This finding is analogous to the outcome previously shown in Figs. 24–25 for another set of images.

A colored squared-window is located inside each of the surface reflectance images. It

indicates the subregion used for the quantitative assessment of the surface reflectance, where the pdf, and the median of the surface reflectance is calculated in each Landsat band.

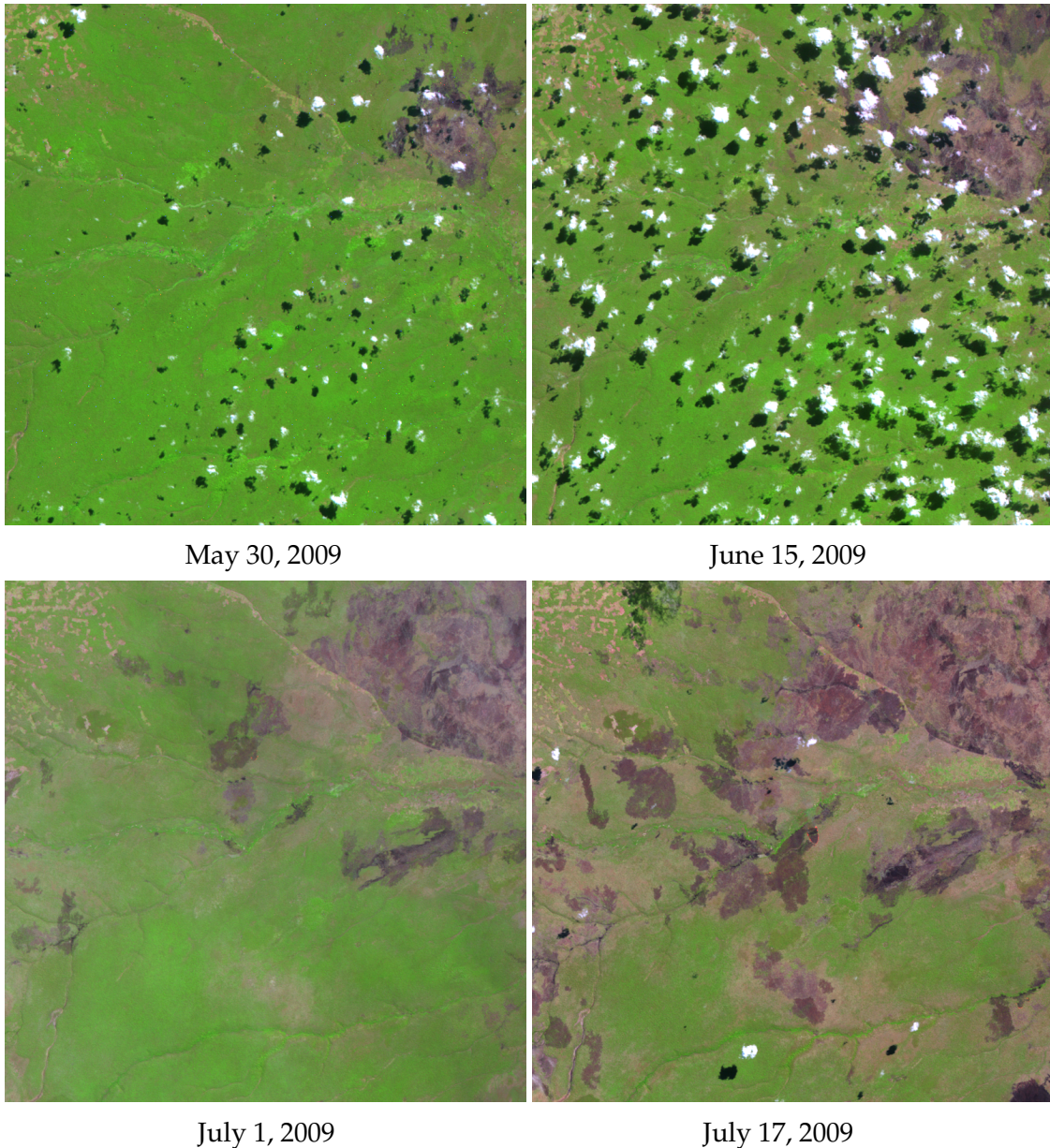


Figure 26. Surface reflectance composite (RGB bands 5,4,3) of a 24×24 km area centered at $9^{\circ}55'19''$ S, $38^{\circ}8'49''$ E (close to Liwale). The four images were acquired by Landsat 5 (166/67) over an area subject to land cover changes in this particular year. We hypothesize that the changes may be due cultivations or fires (note the high response of the red channel corresponding to the NIR reflectance of band 5 at the U-shaped region located at the center of the image acquired on July 17, 2009).

4.7.1 Inter-image surface reflectance comparison, study area 7

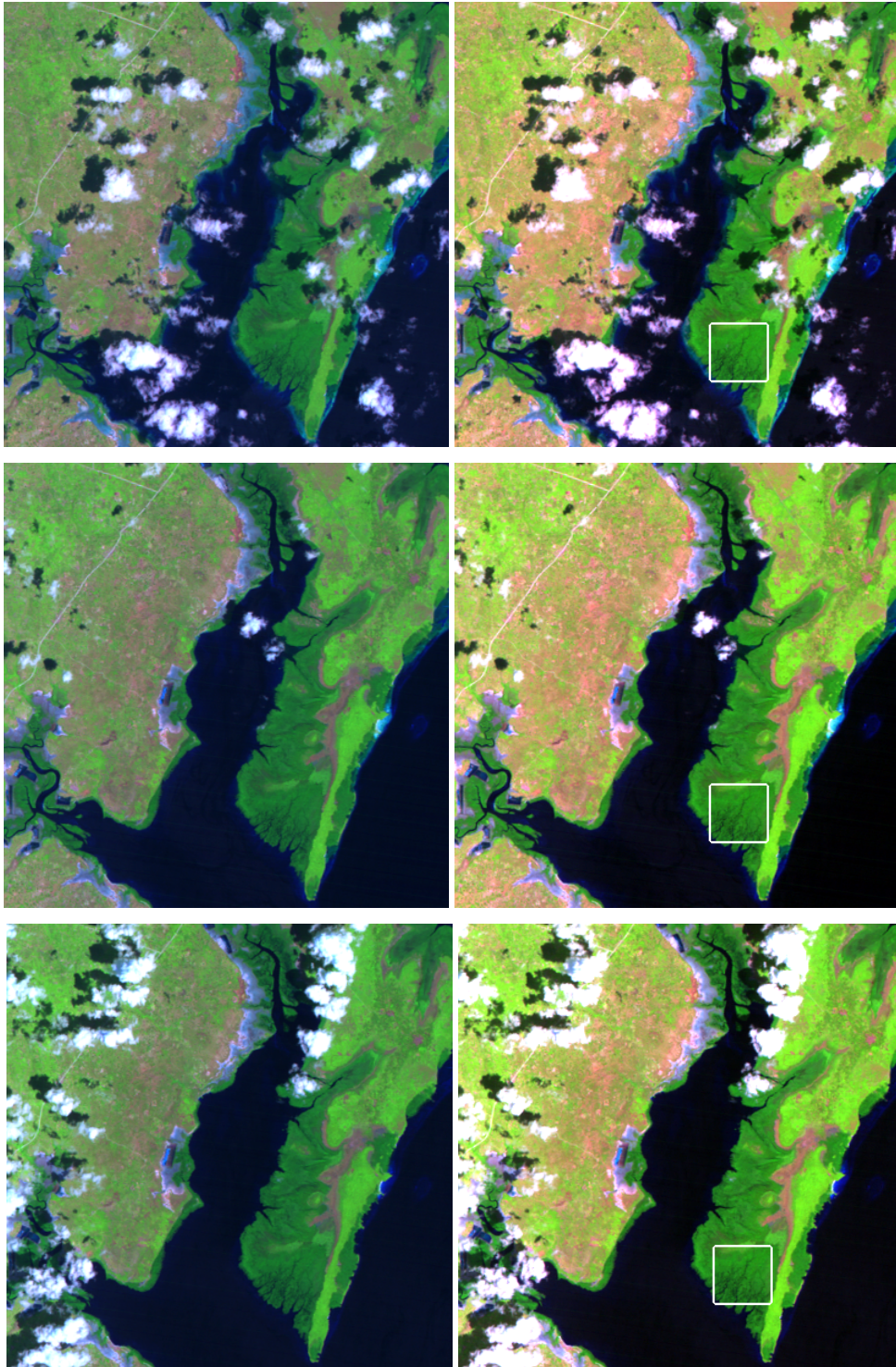


Figure 27. Study area 7. (left) TOA reflectance, and (right) surface reflectance composite (RGB bands 5,4,3) of a 12×12 km area from the Landsat images L5166063-06320091106 (top), L5166063-06320091122 (middle), and L5166063-06320091208 (bottom). To enhance visualization for a qualitative assessment, linear stretching with identical and conveniently chosen saturation thresholds were used in the three images of surface reflectance. Differently, in the case of the TOA images, the thresholds were not calculated but fixed at band 5 [0–0.46], band 4 [0–0.44], and band 3 [0–0.23].

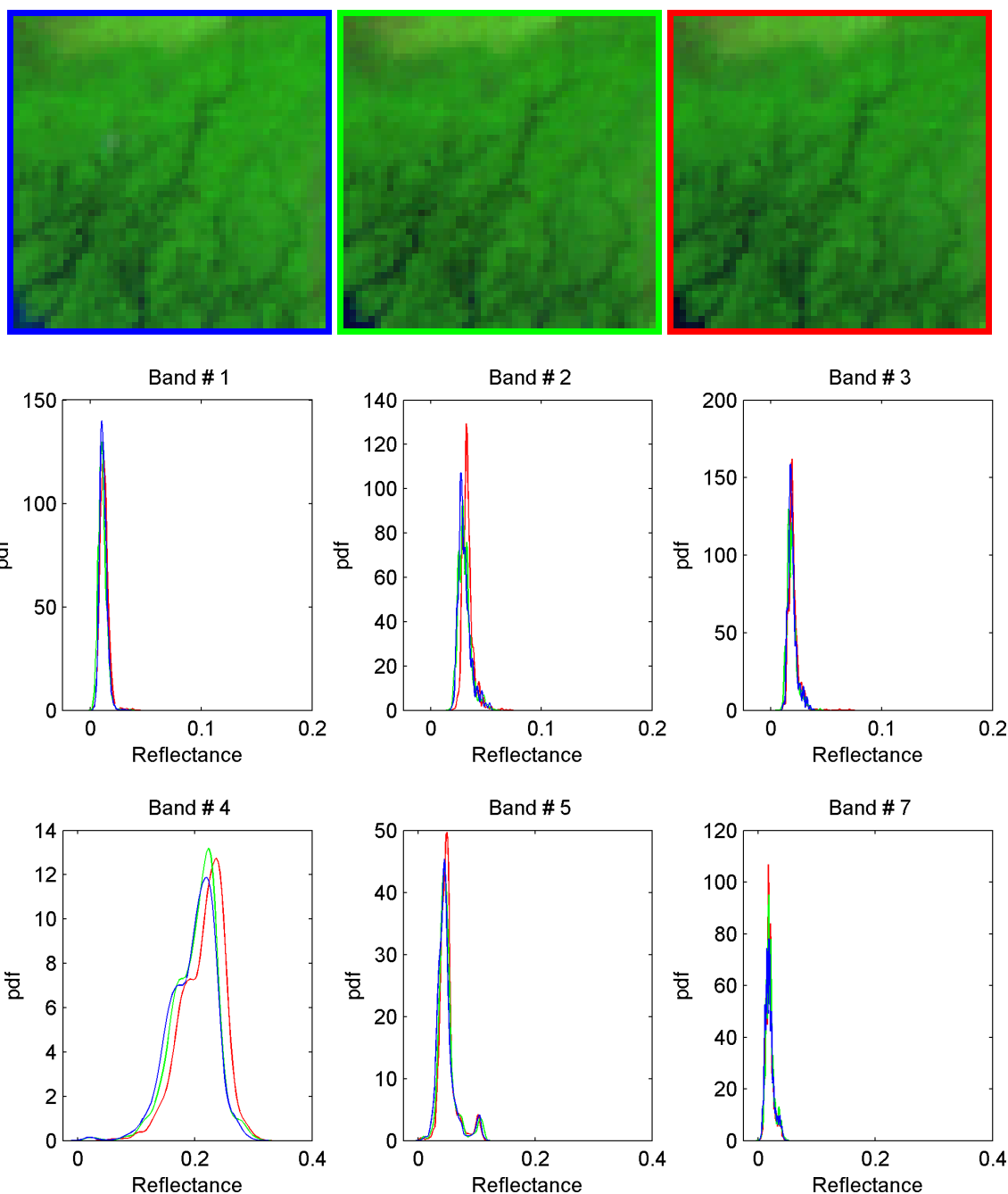


Figure 28. Study area 7. (Top) Closer look at the surface reflectance composite (RGB bands 5,4,3) of the 1500×1500 m subregion in Fig. 27. The patches are from the Landsat images L5166063-06320091106 (red color), L5166063-06320091122 (green color), and L5166063-06320091208 (blue). (Bottom) The correspondent probability density estimates of the surface reflectance for the bands 1–5 and 7 of Landsat are depicted. A total of 2500 reflectance samples (pixels) are available in each patch.

4.7.2 Inter-image surface reflectance comparison, study area 8

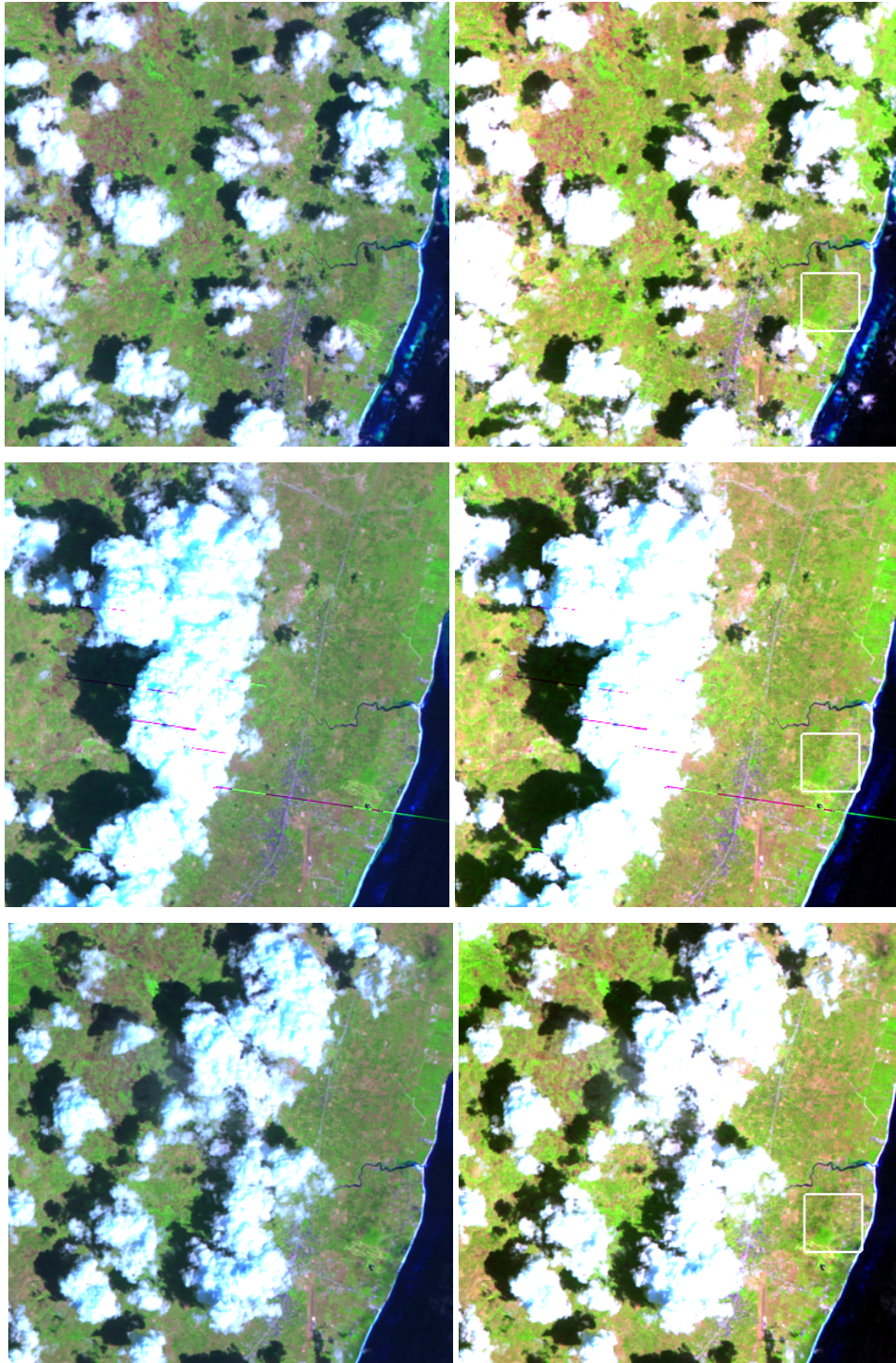


Figure 29. Study area 8. (left) TOA reflectance, and (right) surface reflectance composite (RGB bands 5,4,3) of a 12×12 km area from the Landsat images L5166063-06320091106 (top), L5166063-06320091122 (middle), and L5166063-06320091208 (bottom). To enhance visualization for a qualitative assessment, linear stretching with identical and conveniently chosen saturation thresholds were used in the three images of surface reflectance. Differently, in the case of the TOA images, the thresholds were not calculated but fixed at band 5 [0–0.46], band 4 [0–0.44], and band 3 [0–0.23].

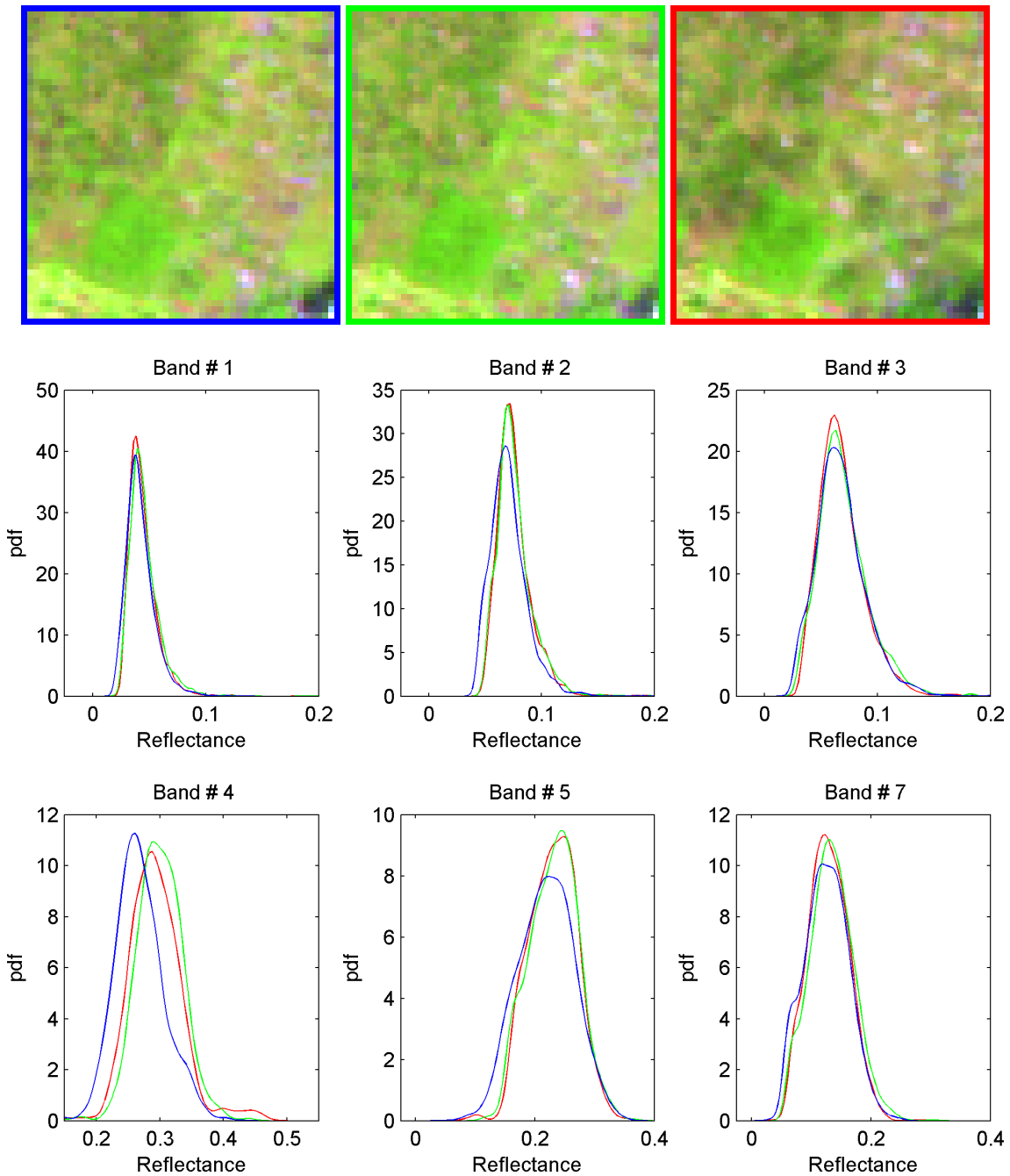


Figure 30. Study area 8. (Top) Closer look at the surface reflectance composite (RGB bands 5,4,3) of the 1500×1500 m subregion in Fig. 29. The patches are from the Landsat images L5166063-06320091106 (red color), L5166063-06320091122 (green color), and L5166063-06320091208 (blue). (Bottom) The correspondent probability density estimates of the surface reflectance for the bands 1–5 and 7 of Landsat are depicted. A total of 2500 reflectance samples (pixels) are available in each patch.

4.7.3 Inter-image surface reflectance comparison, study area 9

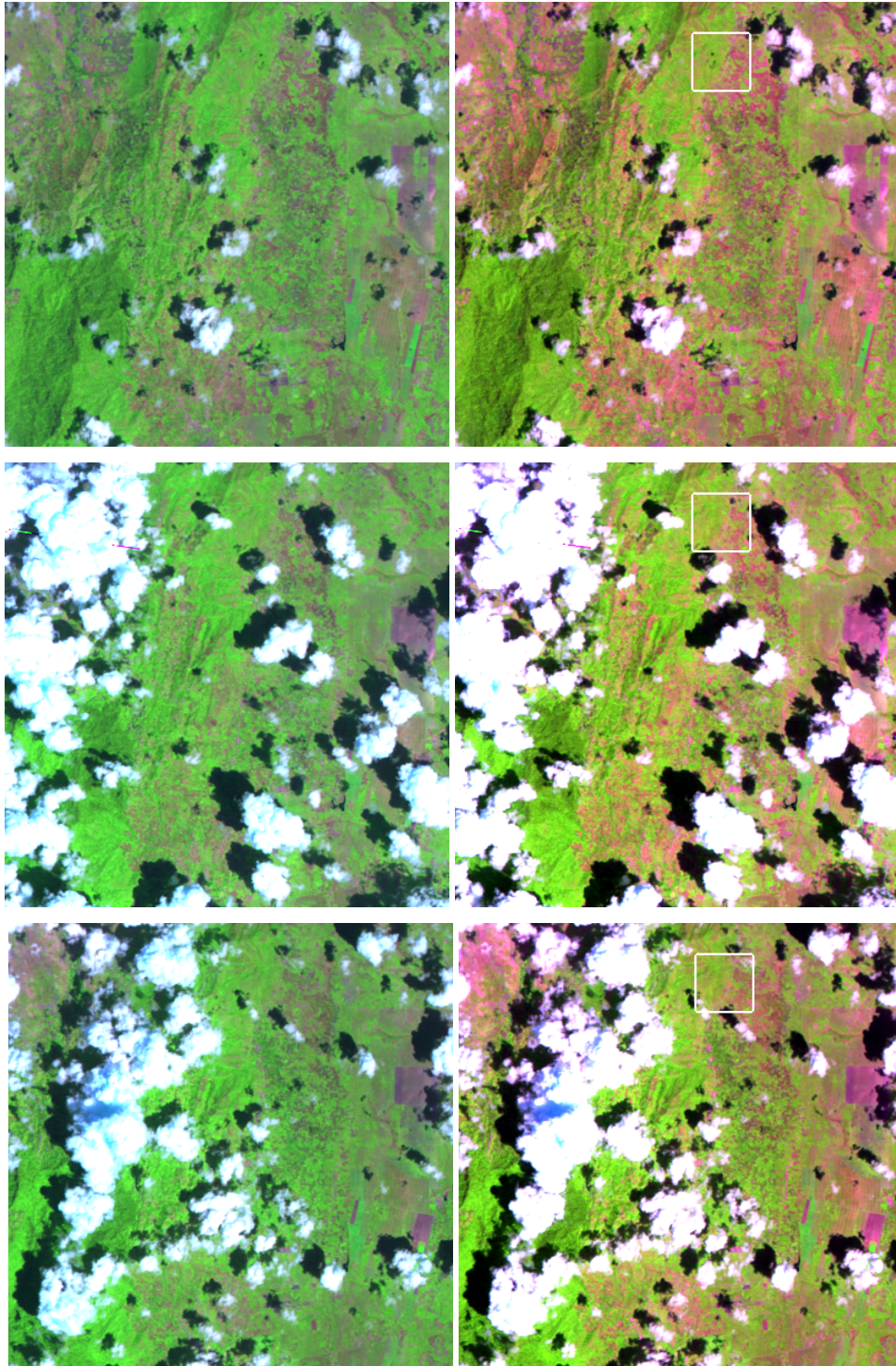


Figure 31. Study area 9. (left) TOA reflectance, and (right) surface reflectance composite (RGB bands 5,4,3) of a 12×12 km area from the Landsat images L5166063-06320091106 (top), L5166063-06320091122 (middle), and L5166063-06320091208 (bottom). To enhance visualization for a qualitative assessment, linear stretching with identical and conveniently chosen saturation thresholds were used in the three images of surface reflectance. Differently, in the case of the TOA images, the thresholds were not calculated but fixed at band 5 [0–0.46], band 4 [0–0.44], and band 3 [0–0.23].

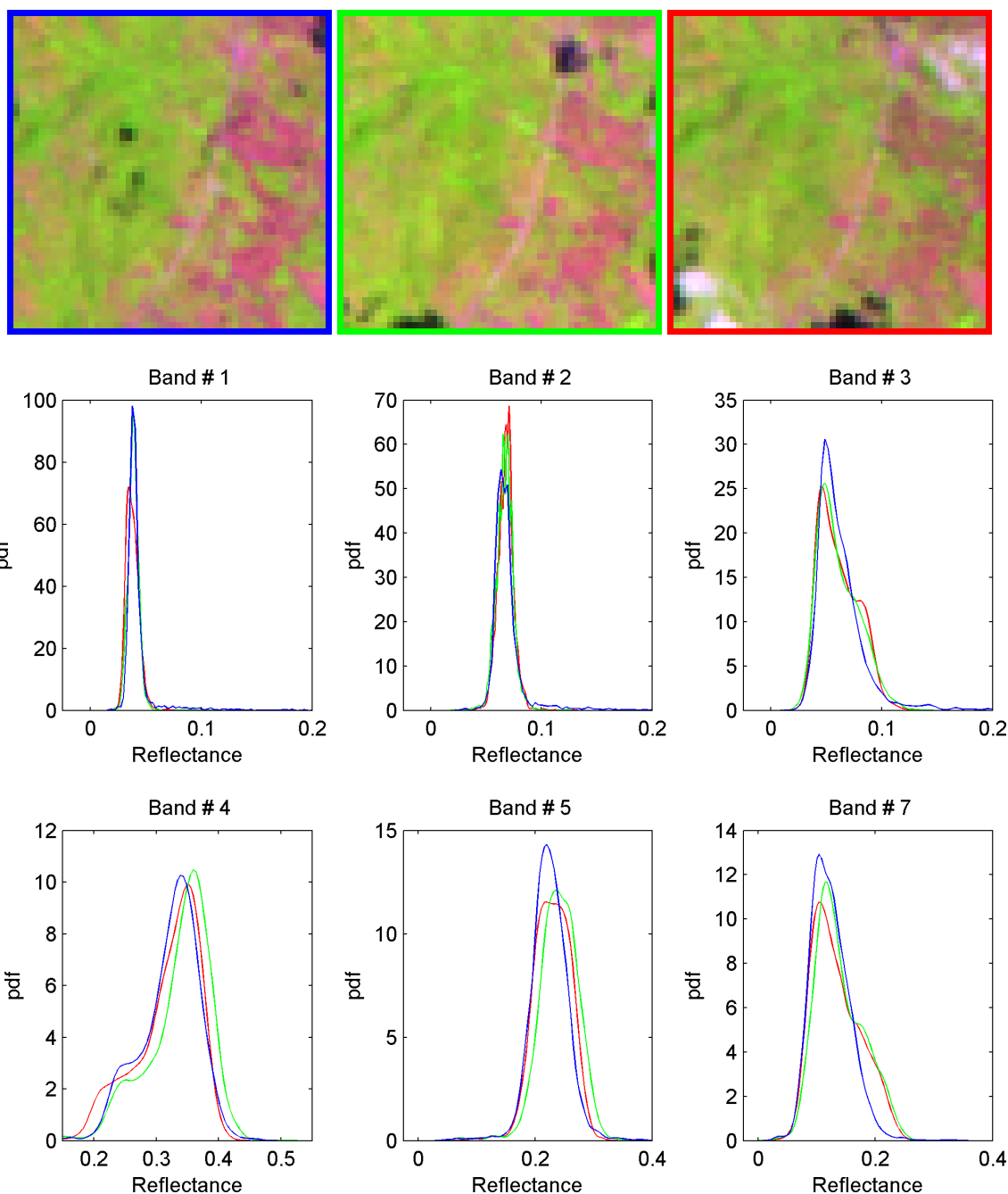


Figure 32. Study area 9. (Top) Closer look at the surface reflectance composite (RGB bands 5,4,3) of the 1500×1500 m subregion in Fig. 31. The patches are from the Landsat images L5166063-06320091106 (red color), L5166063-06320091122 (green color), and L5166063-06320091208 (blue). (Bottom) The correspondent probability density estimates of the surface reflectance for the bands 1–5 and 7 of Landsat are depicted. A total of 2500 reflectance samples (pixels) are available in each patch.

4.7.4 Inter-image surface reflectance comparison, study area 10

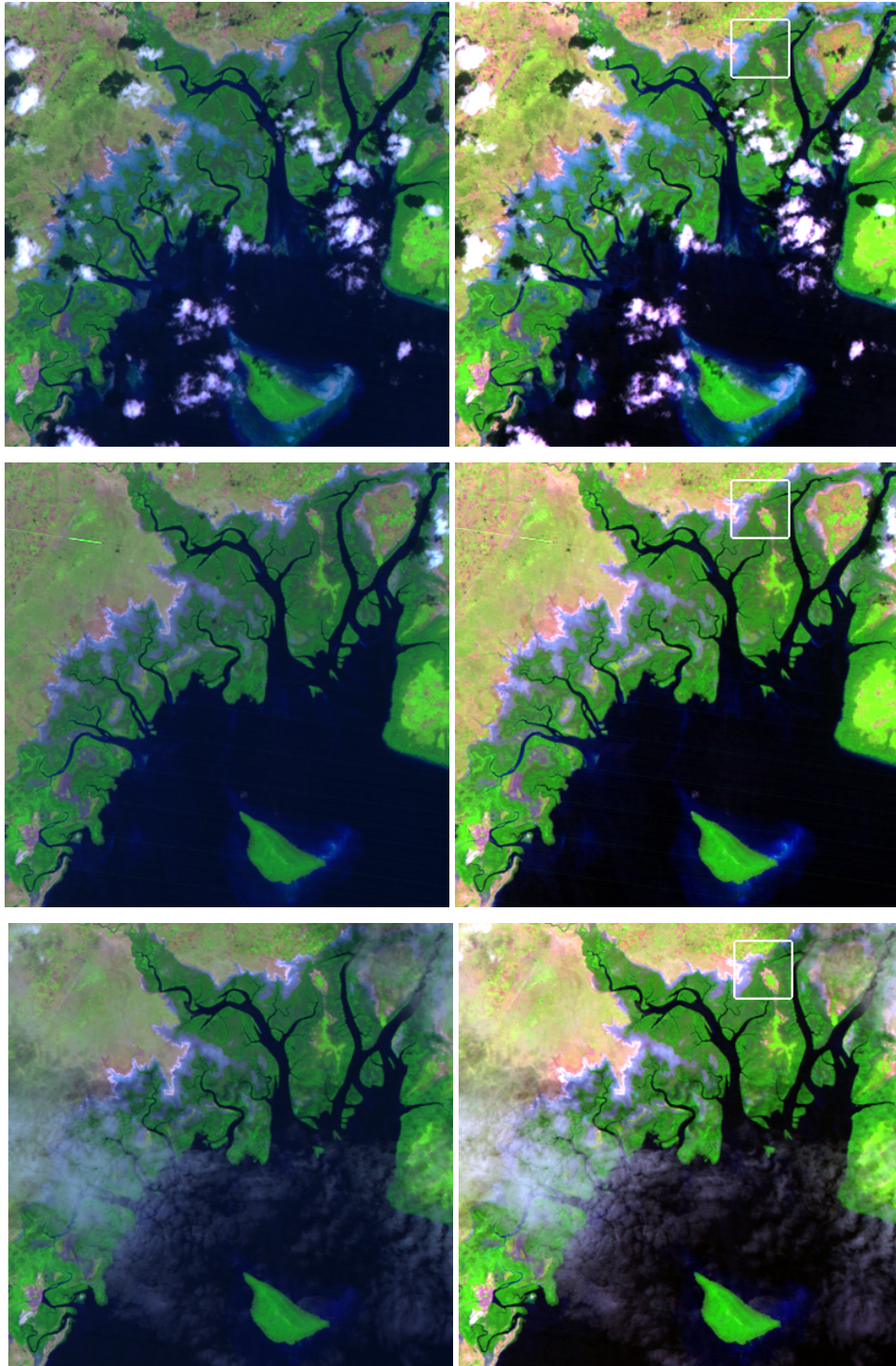


Figure 33. Study area 10. (left) TOA reflectance, and (right) surface reflectance composite (RGB bands 5,4,3) of a 12×12 km area from the Landsat images L5166063-06320091106 (top), L5166063-06320091122 (middle), and L5166063-06320091208 (bottom). To enhance visualization for a qualitative assessment, linear stretching with identical and conveniently chosen saturation thresholds were used in the three images of surface reflectance. Differently, in the case of the TOA images, the thresholds were not calculated but fixed at band 5 [0–0.46], band 4 [0–0.44], and band 3 [0–0.23].

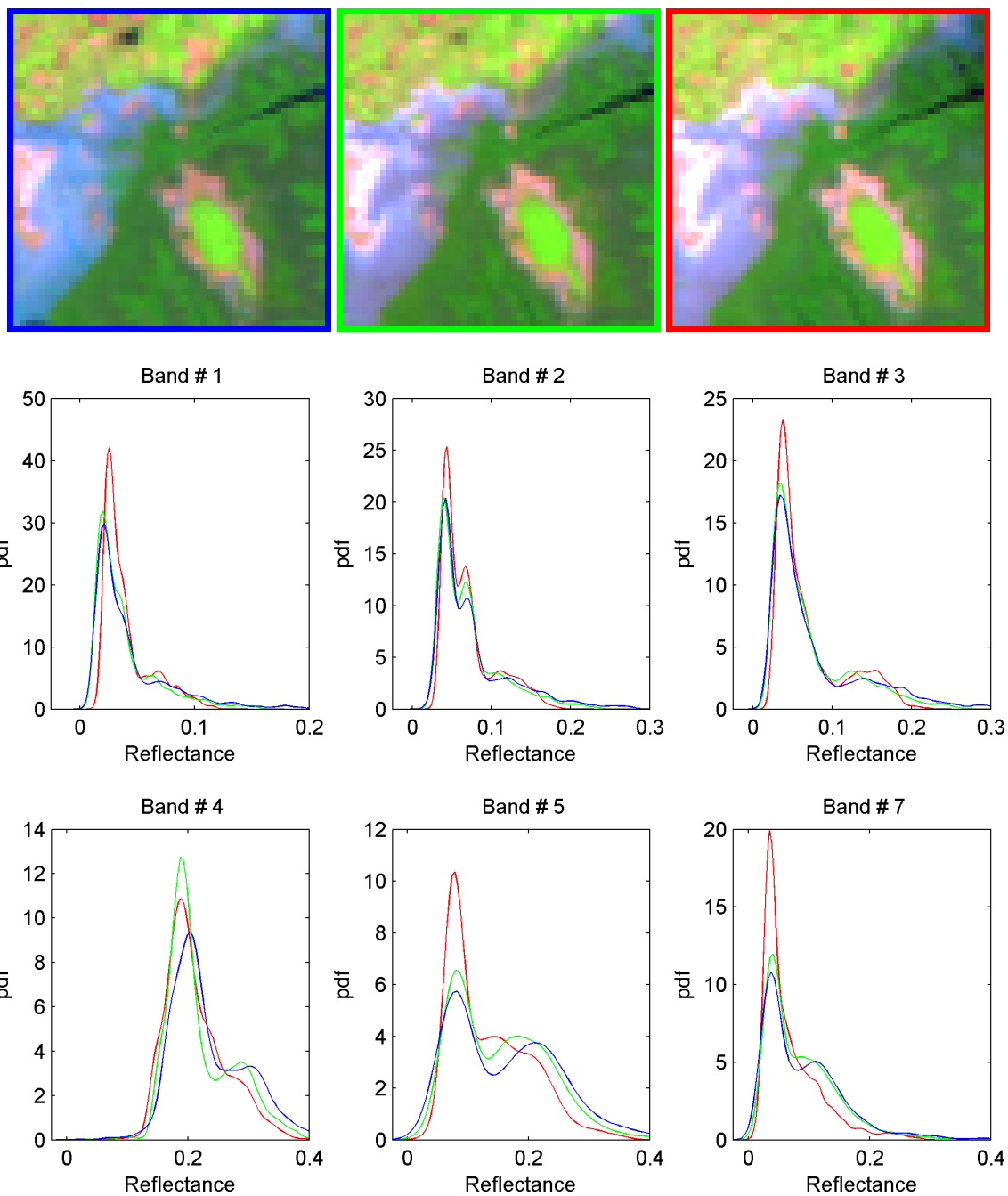


Figure 34. Study area 10. (Top) Closer look at the surface reflectance composite (RGB bands 5,4,3) of the 1500×1500 m subregion in Fig. 33. The patches are from the Landsat images L5166063-06320091106 (red color), L5166063-06320091122 (green color), and L5166063-06320091208 (blue). (Bottom) The correspondent probability density estimates of the surface reflectance for the bands 1–5 and 7 of Landsat are depicted. A total of 2500 reflectance samples (pixels) are available in each patch.

4.8 Short satellite revisit time: image set 2

4.8.1 Inter-image surface reflectance comparison, study area 11

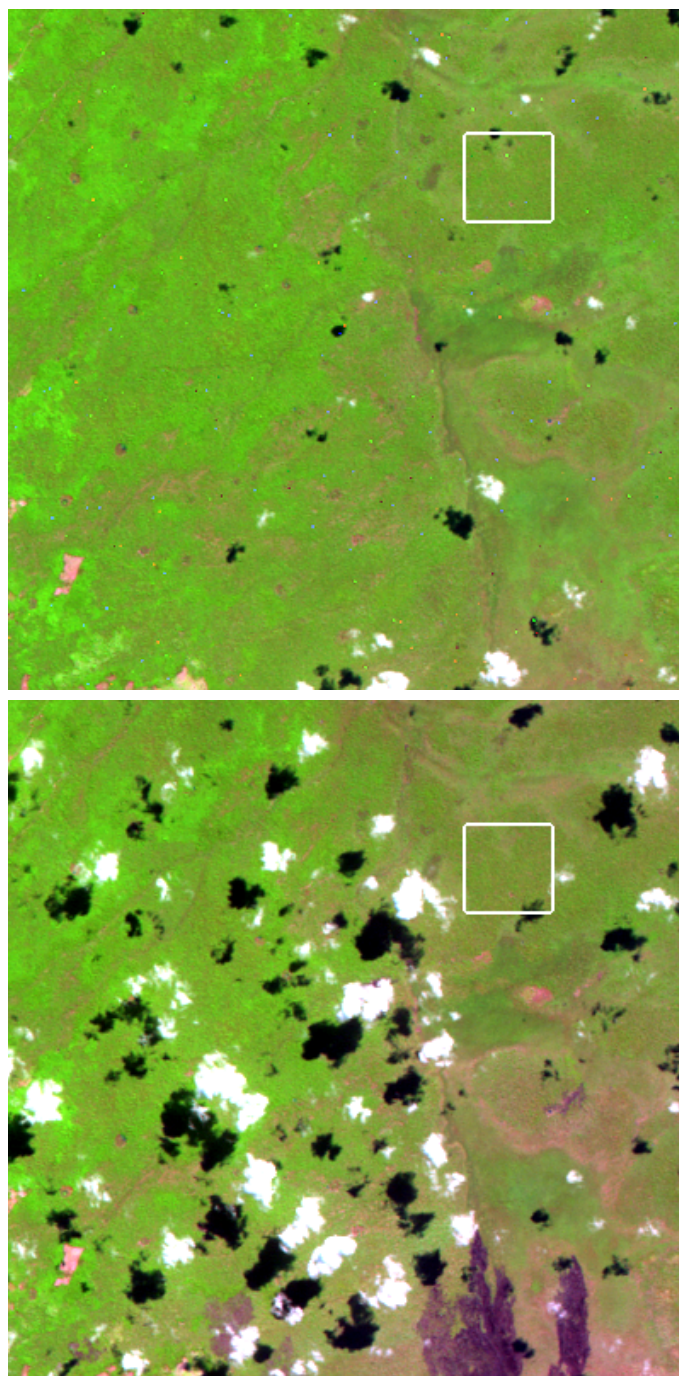


Figure 35. Study area 11. Surface reflectance composite (RGB bands 5,4,3) of a 12×12 km area from the Landsat images L5166067-06720090530 (top) and L5166067-06720090615 (bottom). To enhance visualization for a qualitative assessment, linear stretching with identical and conveniently chosen saturation thresholds were used in both images. The colored squared-window is used for the quantitative assessment of the surface reflectance, by computing the pdf, and the median, of the surface reflectance in each Landsat band.

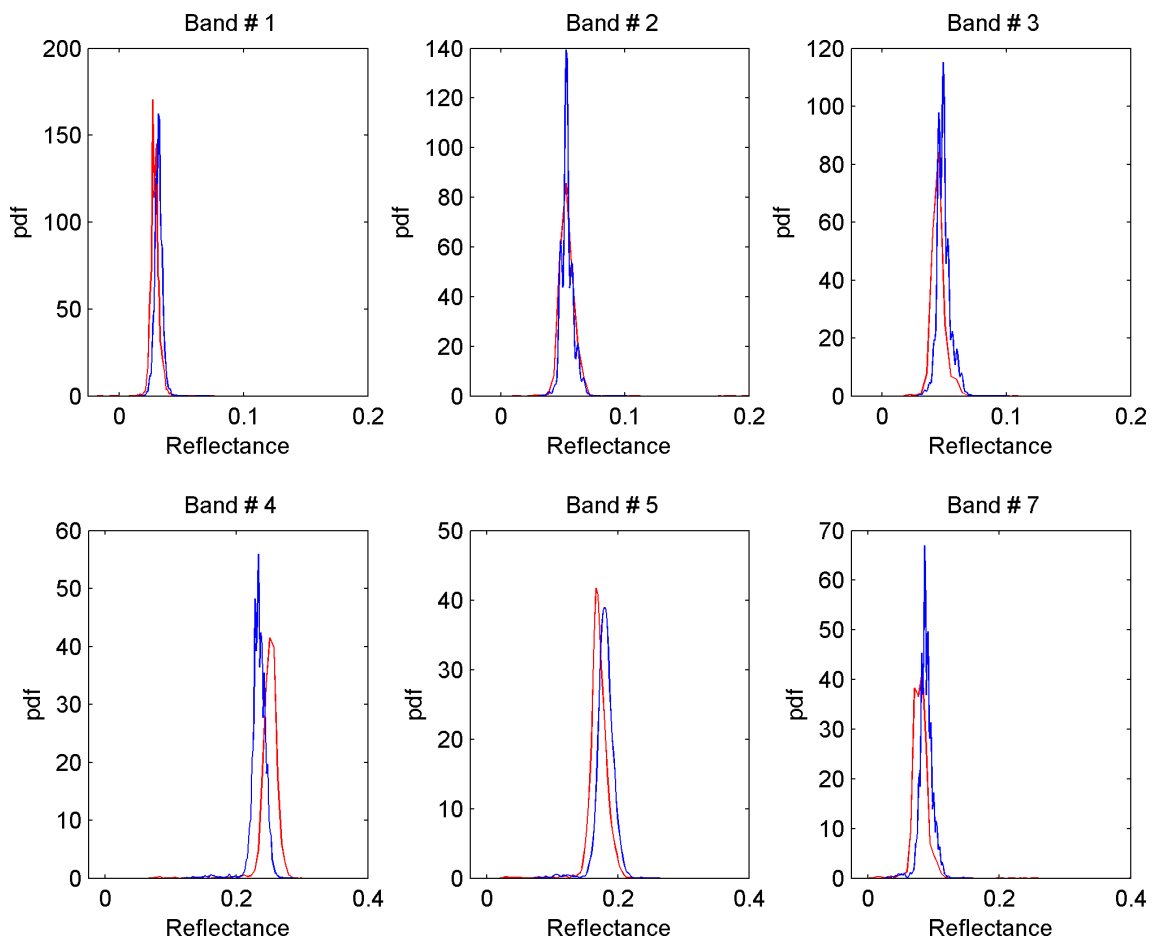
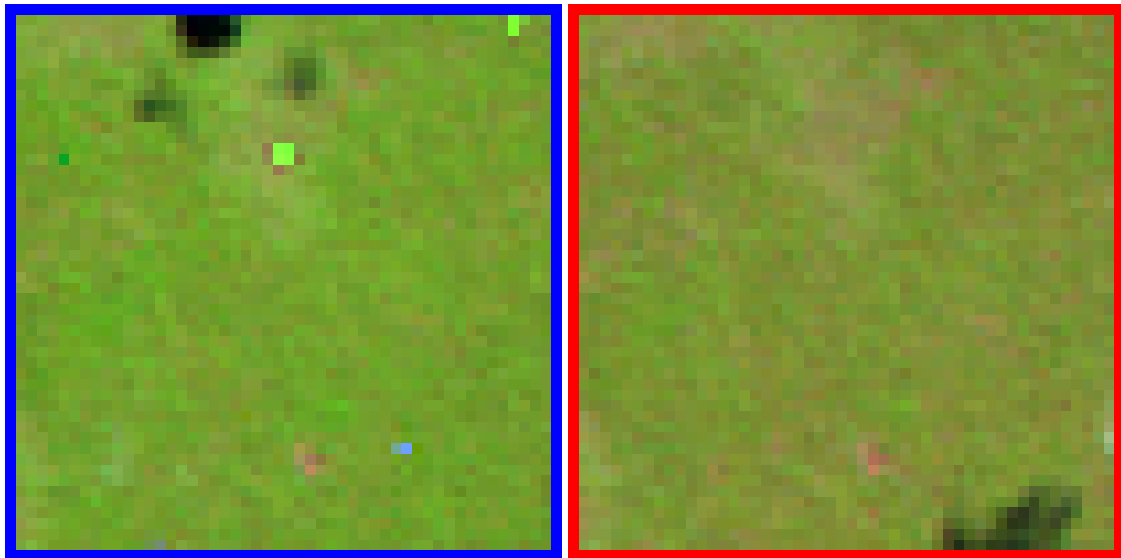


Figure 36. Study area 11. (Top) Closer look at the surface reflectance composite (RGB bands 5,4,3) of the 1500×1500 m subregion in Fig. 35. The patches are from the Landsat images L5166067-06720090530 (blue color), and L5166067-06720090615 (red color). (Bottom) The correspondent probability density estimates of the surface reflectance for the bands 1–5 and 7 of Landsat are depicted. A total of 2500 reflectance samples (pixels) are available in each patch.

4.8.2 Inter-image surface reflectance comparison, study area 12

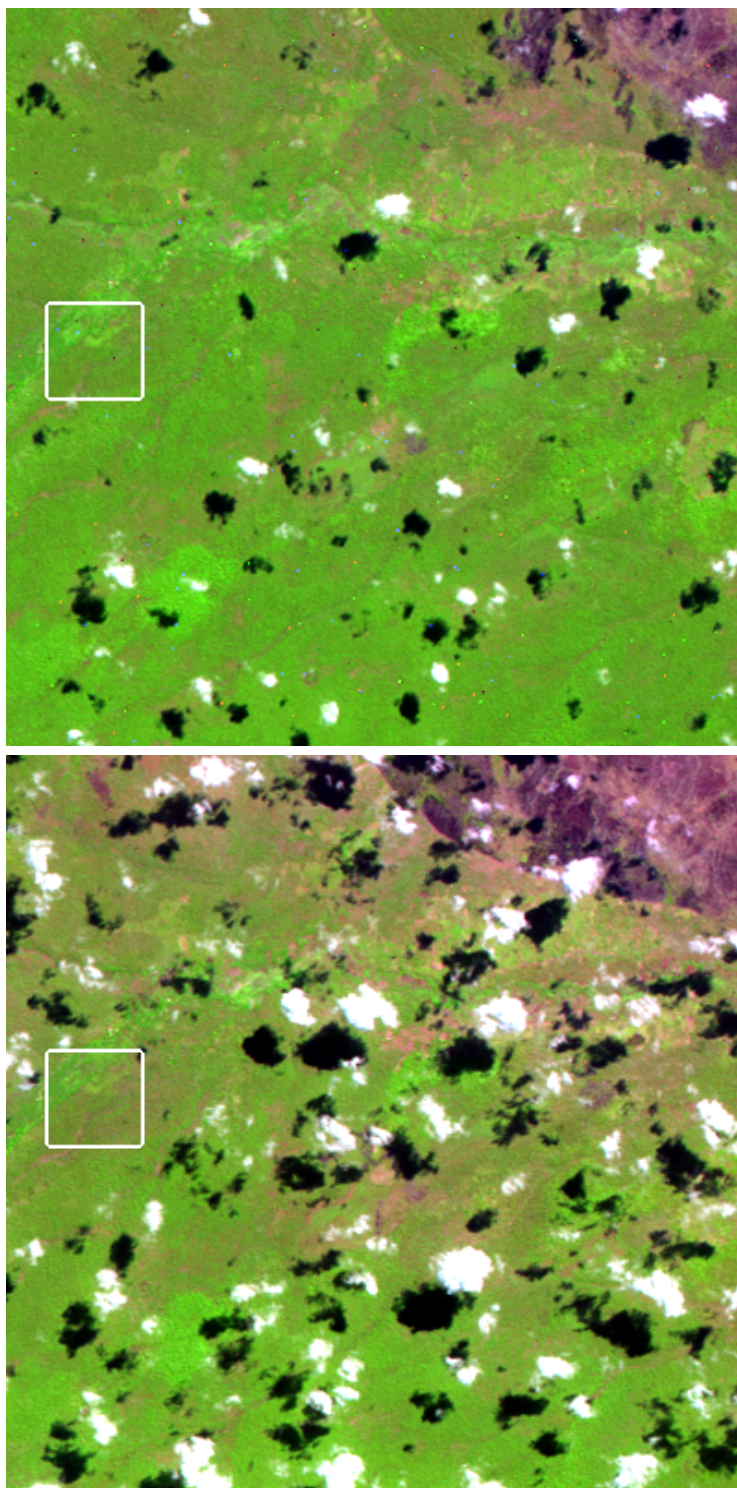


Figure 37. Study area 12. Surface reflectance composite (RGB bands 5,4,3) of a 12×12 km area from the Landsat images L5166067-06720090530 (top) and L5166067-06720090615 (bottom). To enhance visualization for a qualitative assessment, linear stretching with identical and conveniently chosen saturation thresholds were used in both images. The colored squared-window is used for the quantitative assessment of the surface reflectance, by computing the pdf, and the median, of the surface reflectance in each Landsat band.

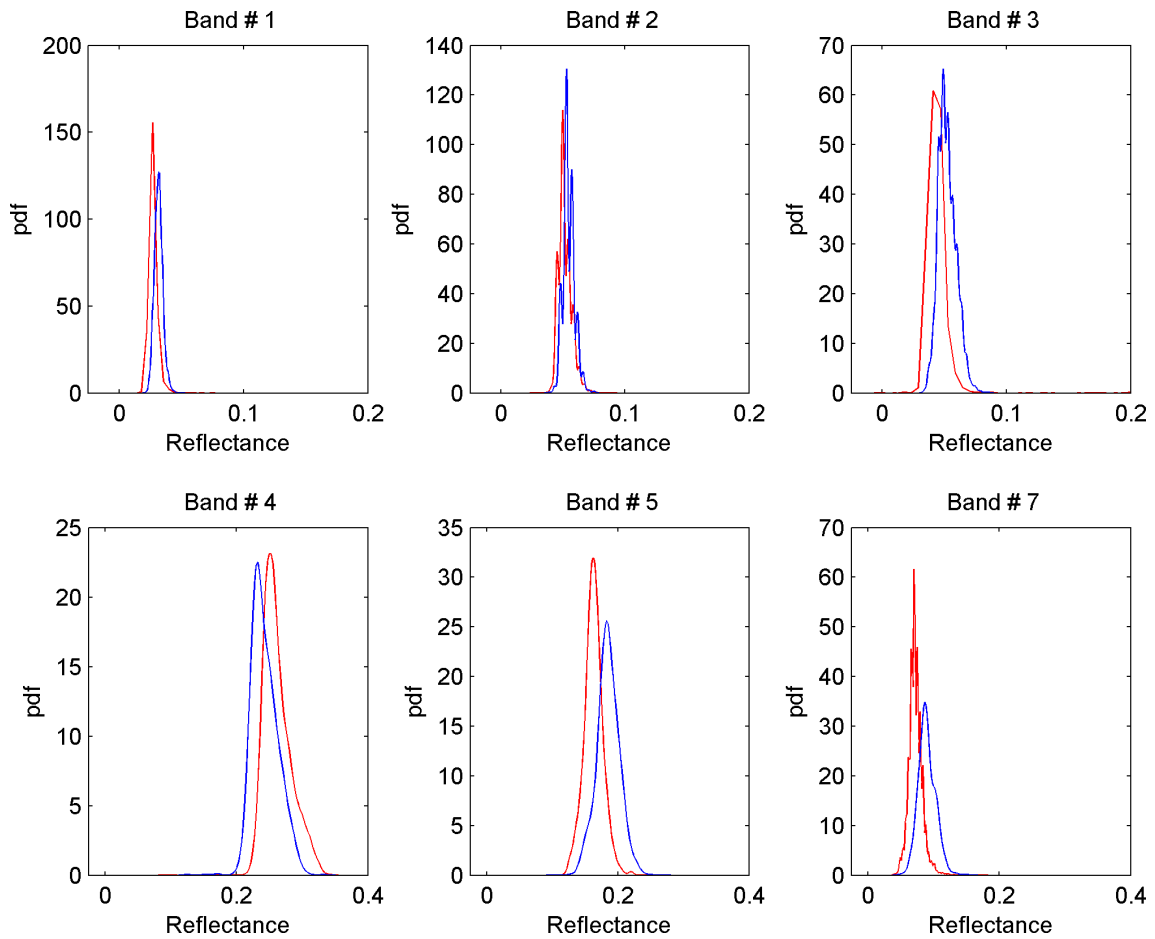
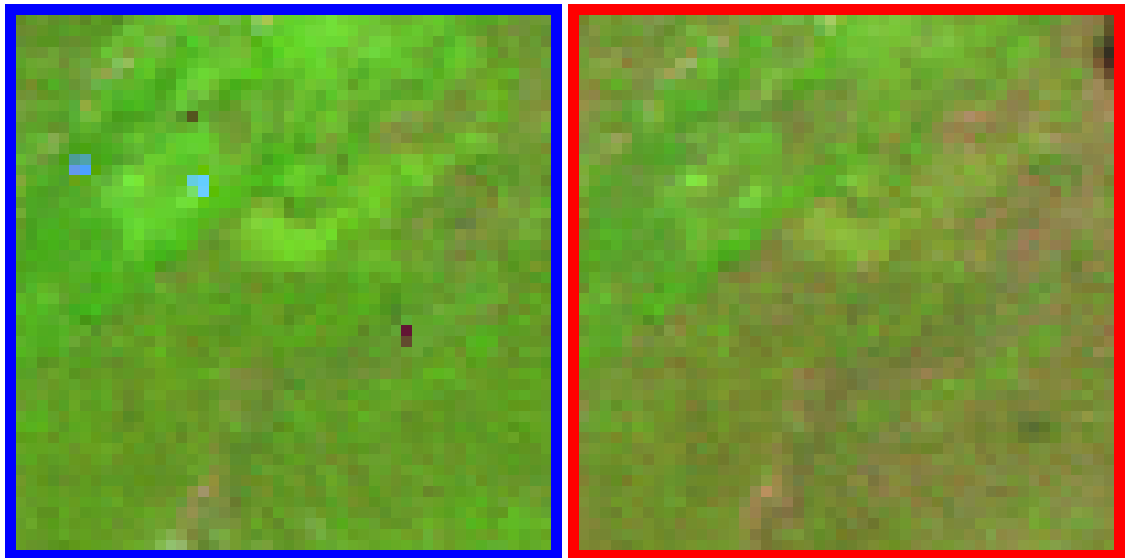


Figure 38. Study area 12. (Top) Closer look at the surface reflectance composite (RGB bands 5,4,3) of the 1500×1500 m subregion in Fig. 37. The patches are from the Landsat images L5166067-06720090530 (blue color), and L5166067-06720090615 (red color). (Bottom) The correspondent probability density estimates of the surface reflectance for the bands 1–5 and 7 of Landsat are depicted. A total of 2500 reflectance samples (pixels) are available in each patch.

4.8.3 Inter-image surface reflectance comparison, study area 13

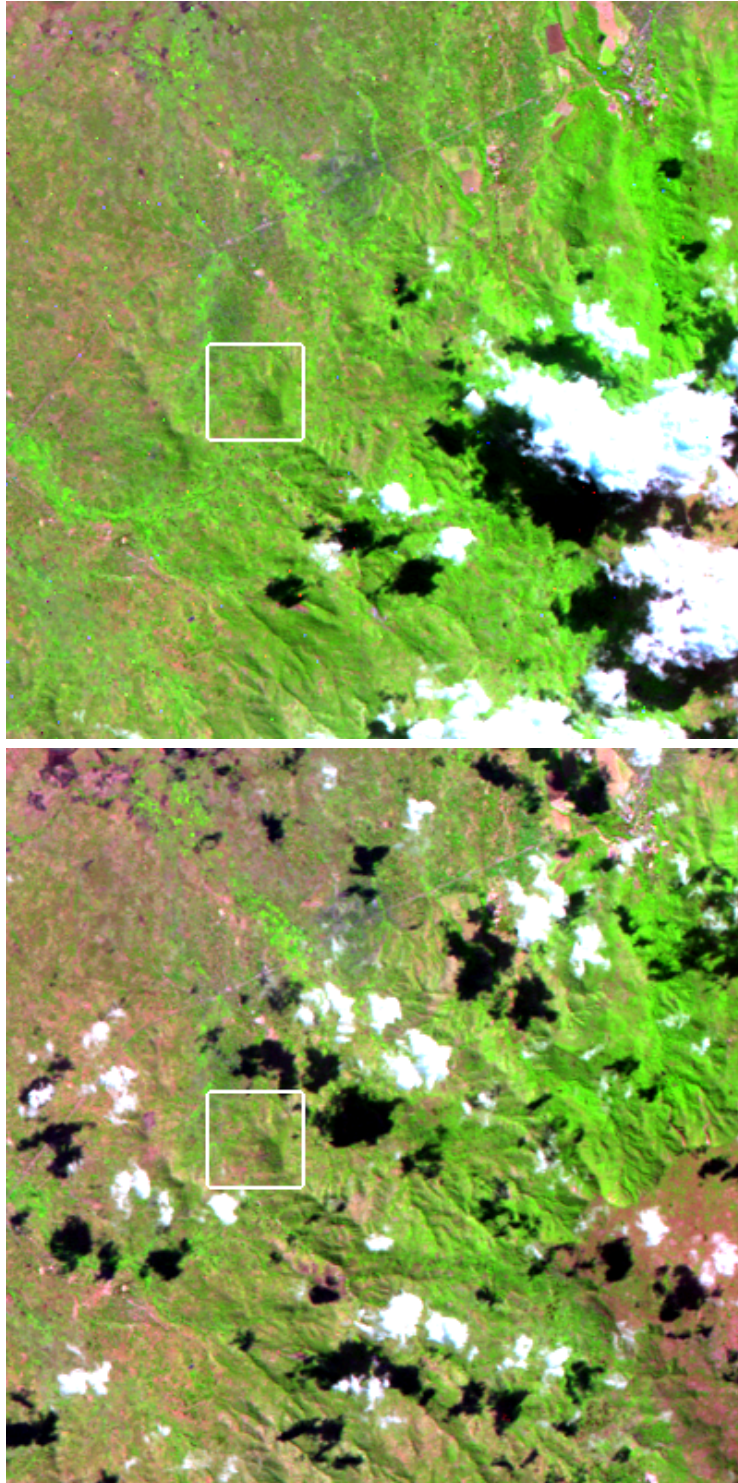


Figure 39. Study area 13. Surface reflectance composite (RGB bands 5,4,3) of a 12×12 km area from the Landsat images L5166067-06720090530 (top) and L5166067-06720090615 (bottom). To enhance visualization for a qualitative assessment, linear stretching with identical and conveniently chosen saturation thresholds were used in both images. The colored squared-window is used for the quantitative assessment of the surface reflectance, by computing the pdf, and the median, of the surface reflectance in each Landsat band.

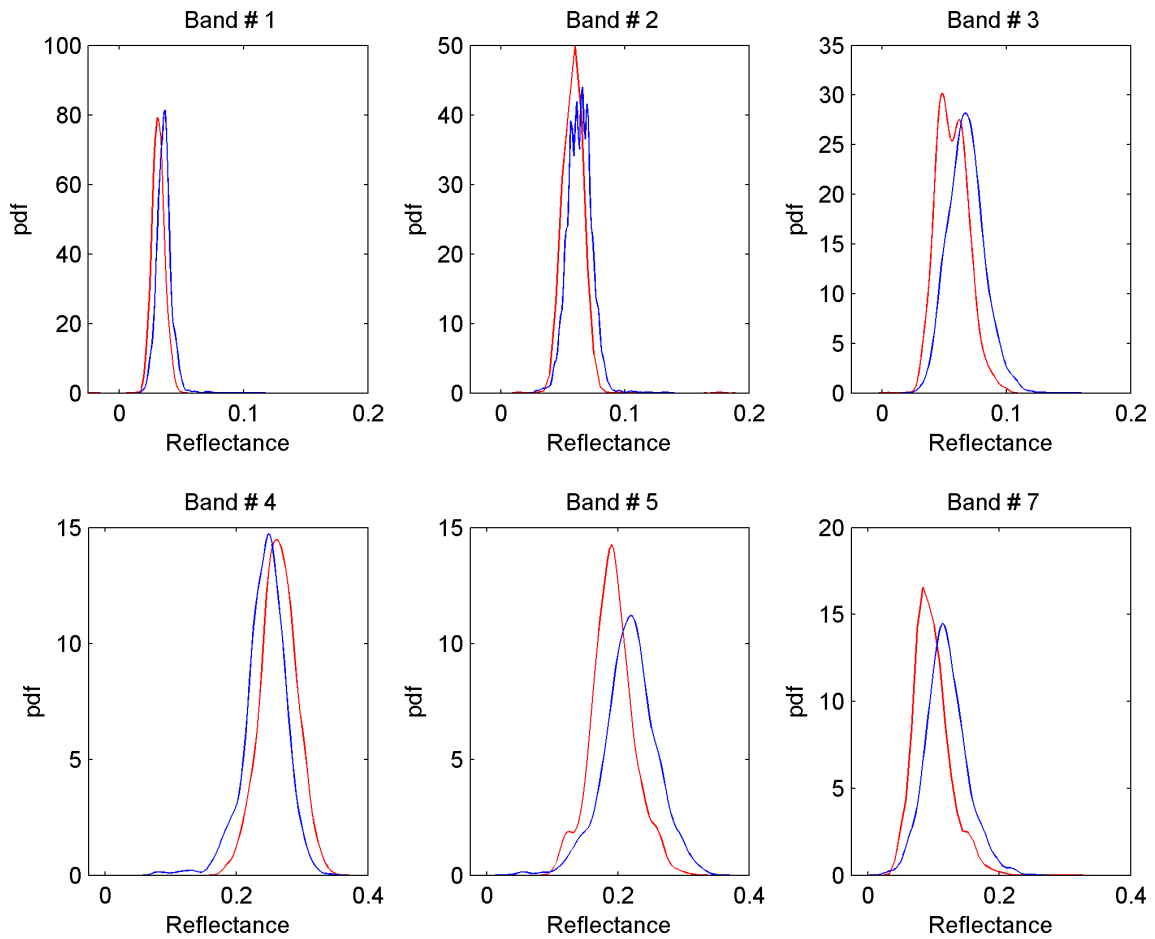
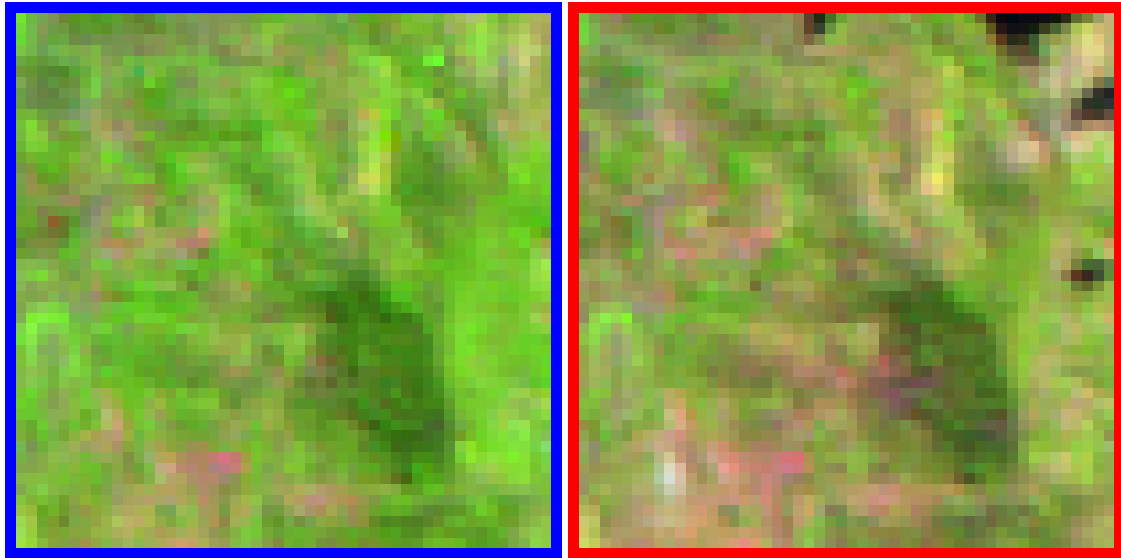


Figure 40. Study area 13. (Top) Closer look at the surface reflectance composite (RGB bands 5,4,3) of the 1500×1500 m subregion in Fig. 39. The patches are from the Landsat images L5166067-06720090530 (blue color), and L5166067-06720090615 (red color). (Bottom) The correspondent probability density estimates of the surface reflectance for the bands 1–5 and 7 of Landsat are depicted. A total of 2500 reflectance samples (pixels) are available in each patch.

4.8.4 Inter-image surface reflectance comparison, study area 14

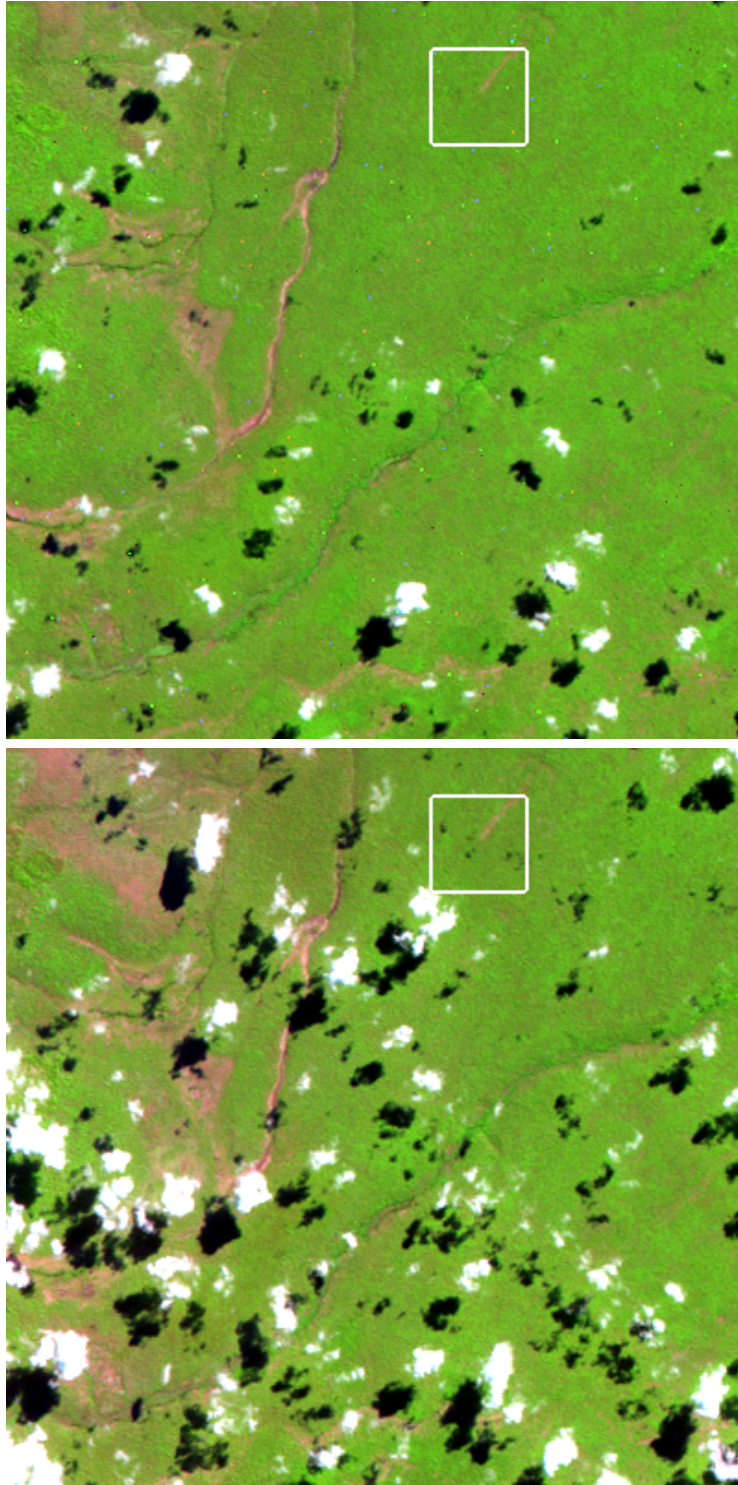


Figure 41. Study area 14. Surface reflectance composite (RGB bands 5,4,3) of a 12×12 km area from the Landsat images L5166067-06720090530 (top) and L5166067-06720090615 (bottom). To enhance visualization for a qualitative assessment, linear stretching with identical and conveniently chosen saturation thresholds were used in both images. The colored squared-window is used for the quantitative assessment of the surface reflectance, by computing the pdf, and the median, of the surface reflectance in each Landsat band.

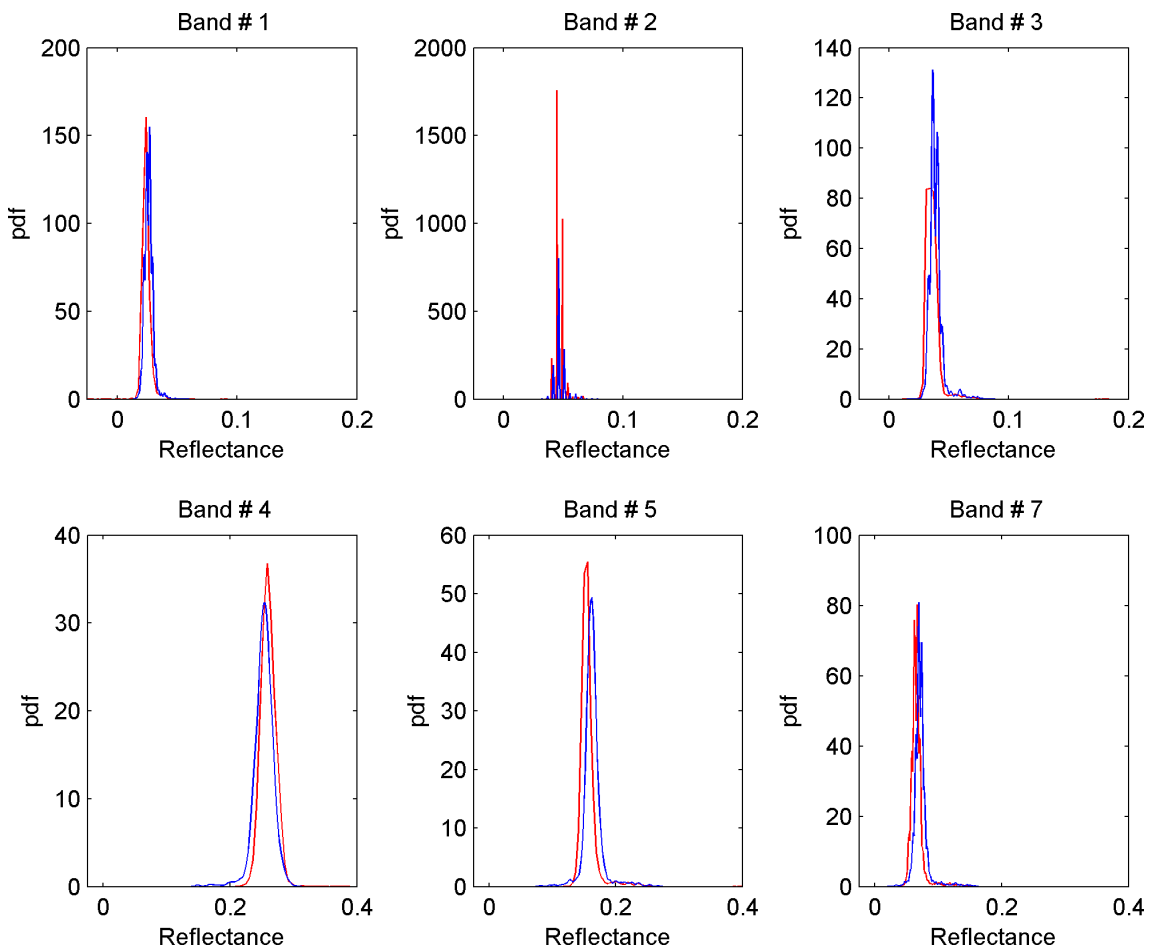
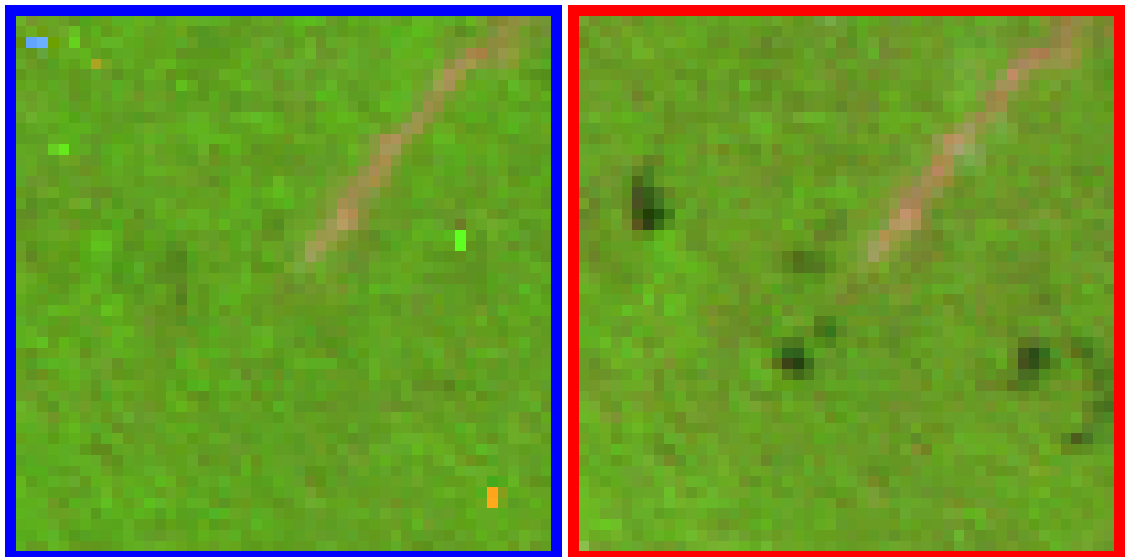


Figure 42. Study area 14. (Top) Closer look at the surface reflectance composite (RGB bands 5,4,3) of the 1500 × 1500 m subregion in Fig. 41. The patches are from the Landsat images L5166067-06720090530 (blue color), and L5166067-06720090615 (red color). (Bottom) The correspondent probability density estimates of the surface reflectance for the bands 1–5 and 7 of Landsat are depicted. A total of 2500 reflectance samples (pixels) are available in each patch.

4.9 Short satellite revisit time: image set 3

4.9.1 Inter-image surface reflectance comparison, study area 15

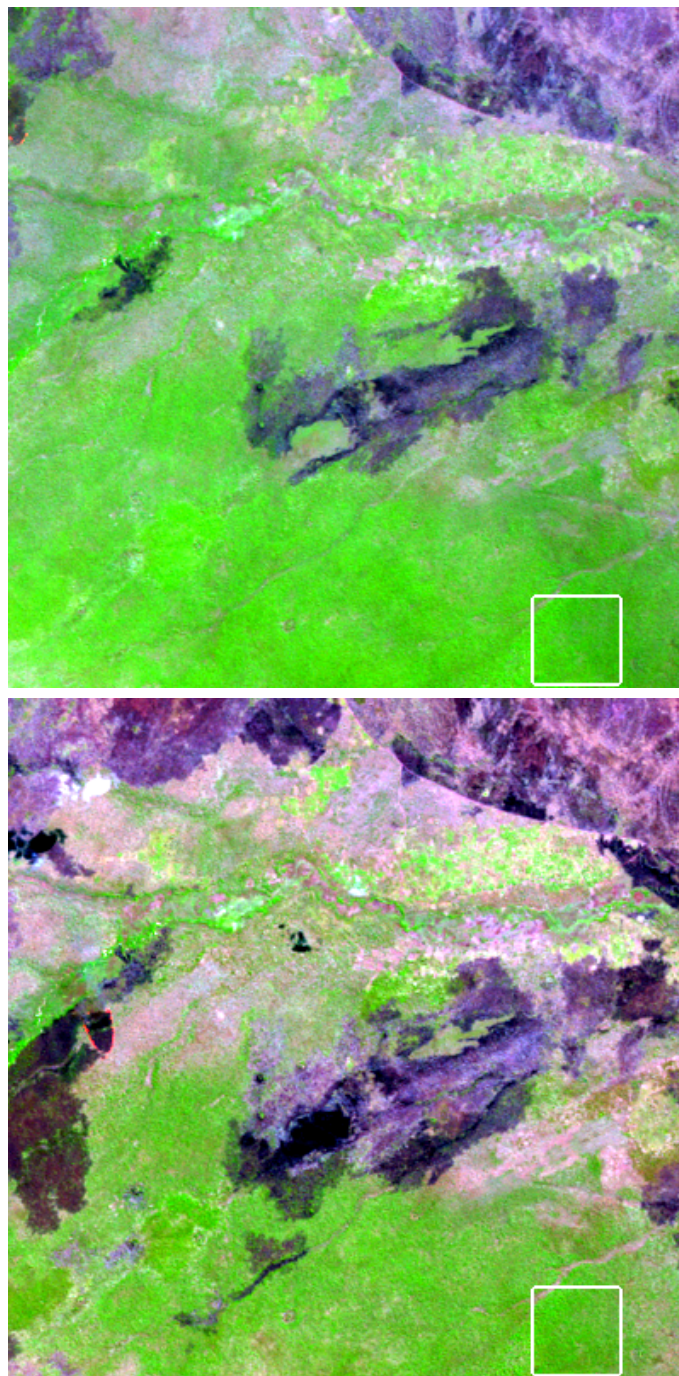


Figure 43. Study area 15. Surface reflectance composite (RGB bands 5,4,3) of a 12×12 km area from the Landsat images L5166067-06720090701 (top) and L5166067-06720090717 (bottom). To enhance visualization for a qualitative assessment, linear stretching with identical and conveniently chosen saturation thresholds were used in both images. The colored squared-window is used for the quantitative assessment of the surface reflectance, by computing the pdf, and the median, of the surface reflectance in each Landsat band.

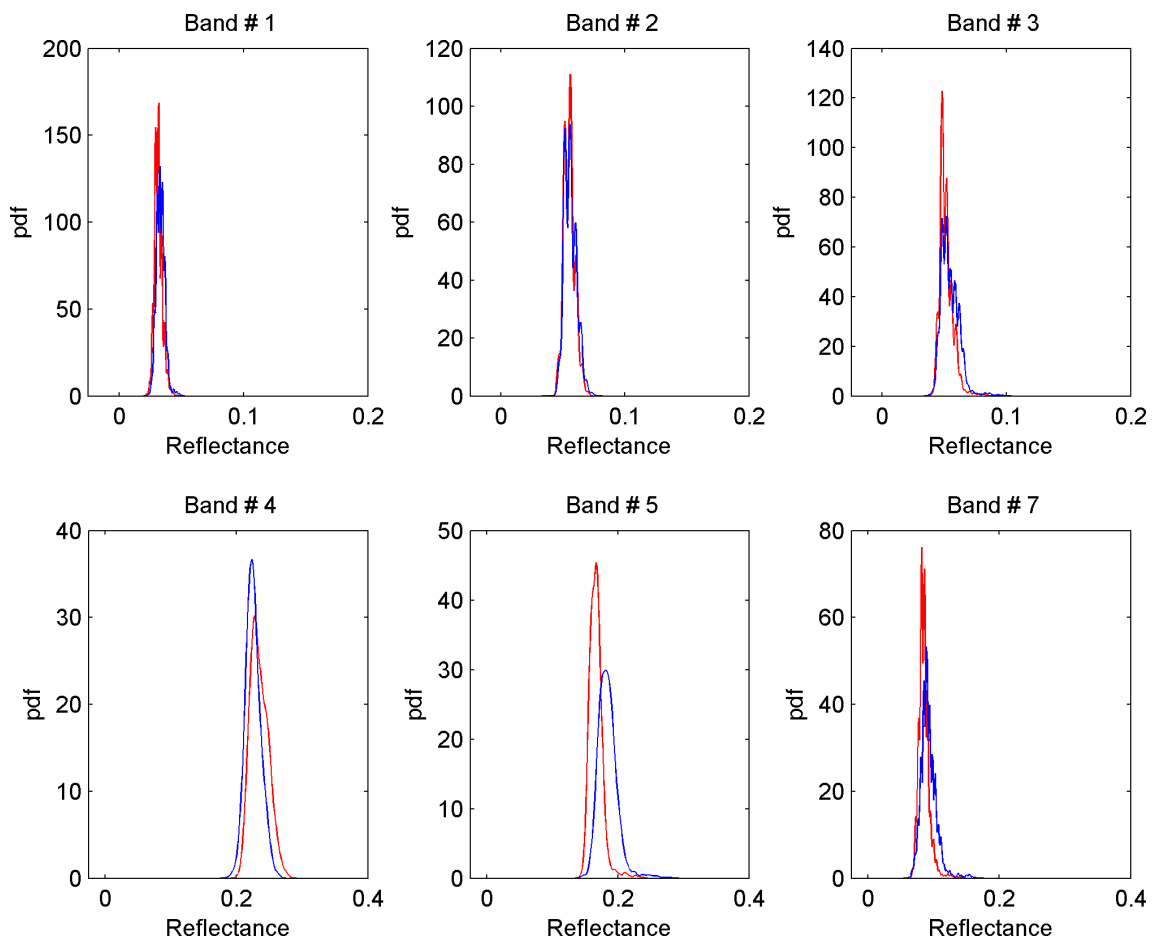
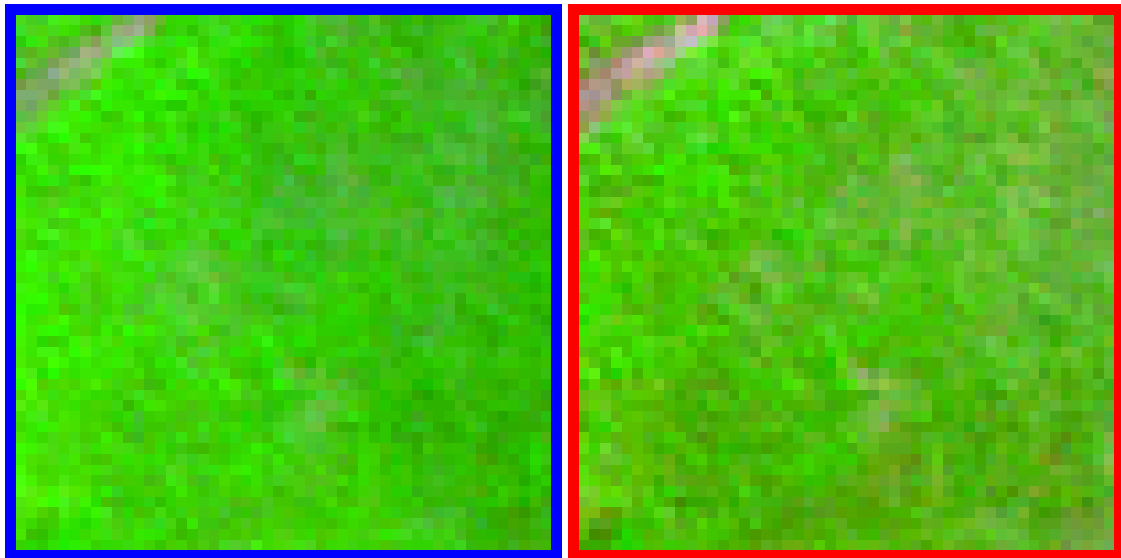


Figure 44. Study area 15. (Top) Closer look at the surface reflectance composite (RGB bands 5,4,3) of the 1500×1500 m subregion in Fig. 43. The patches are from the Landsat images L5166067-06720090701 (blue color), and L5166067-06720090717 (red color). (Bottom) The correspondent probability density estimates of the surface reflectance for the bands 1–5 and 7 of Landsat are depicted. A total of 2500 reflectance samples (pixels) are available in each patch.

4.9.2 Inter-image surface reflectance comparison, study area 16

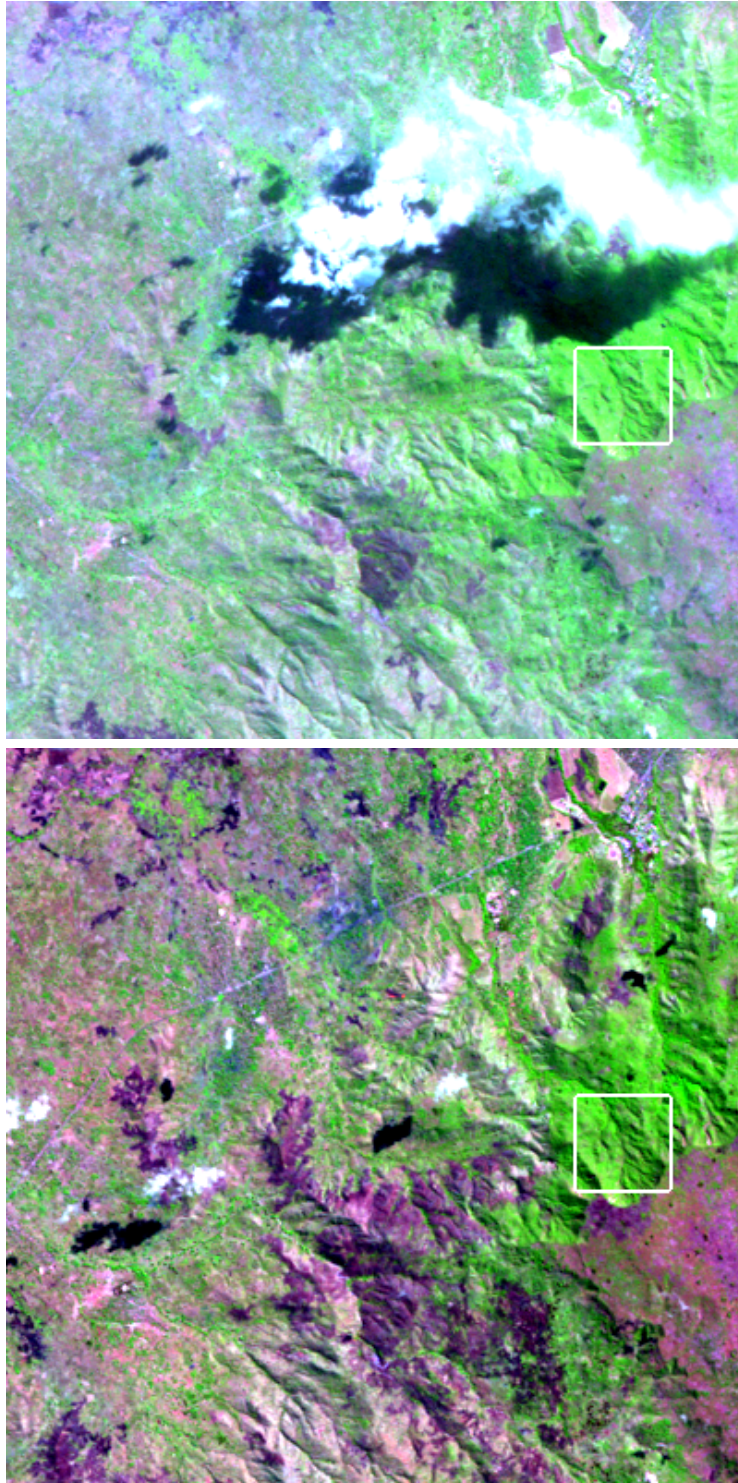


Figure 45. Study area 16. Surface reflectance composite (RGB bands 5,4,3) of a 12×12 km area from the Landsat images L5166067-06720090701 (top) and L5166067-06720090717 (bottom). To enhance visualization for a qualitative assessment, linear stretching with identical and conveniently chosen saturation thresholds were used in both images. The colored squared-window is used for the quantitative assessment of the surface reflectance, by computing the pdf, and the median, of the surface reflectance in each Landsat band.

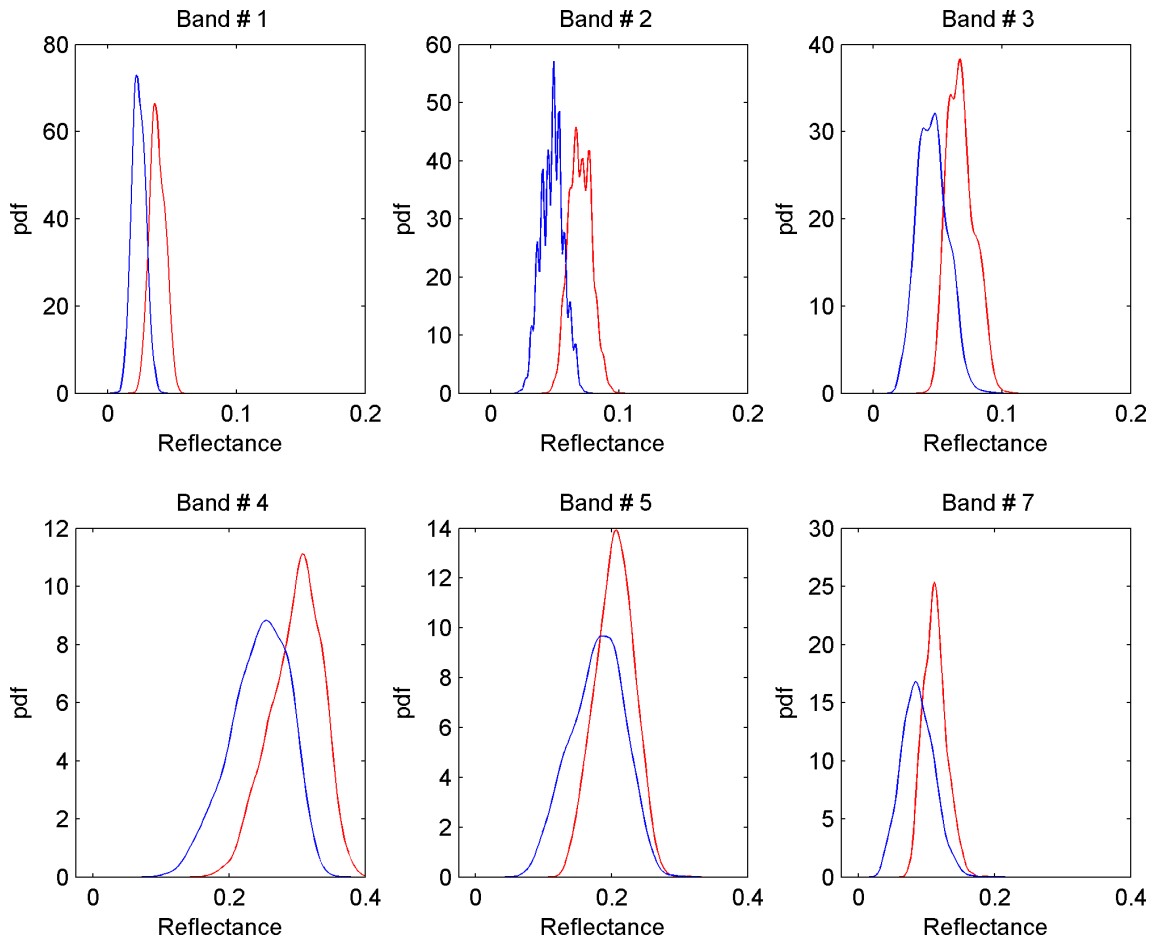
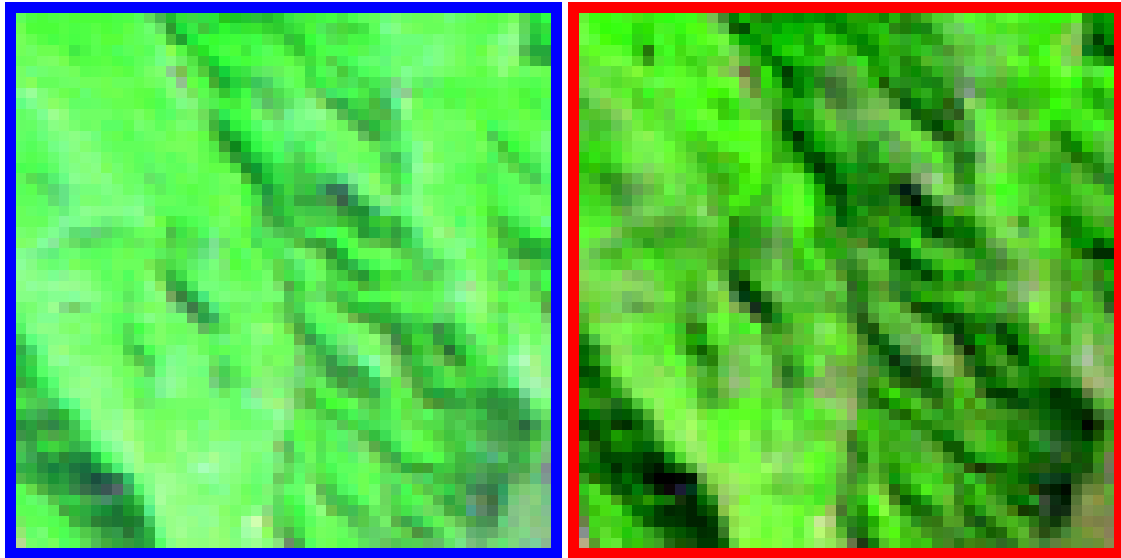


Figure 46. Study area 16. (Top) Closer look at the surface reflectance composite (RGB bands 5,4,3) of the 1500×1500 m subregion in Fig. 45. The patches are from the Landsat images L5166067-06720090701 (blue color), and L5166067-06720090717 (red color). (Bottom) The correspondent probability density estimates of the surface reflectance for the bands 1–5 and 7 of Landsat are depicted. A total of 2500 reflectance samples (pixels) are available in each patch.

4.9.3 Inter-image surface reflectance comparison, study area 17

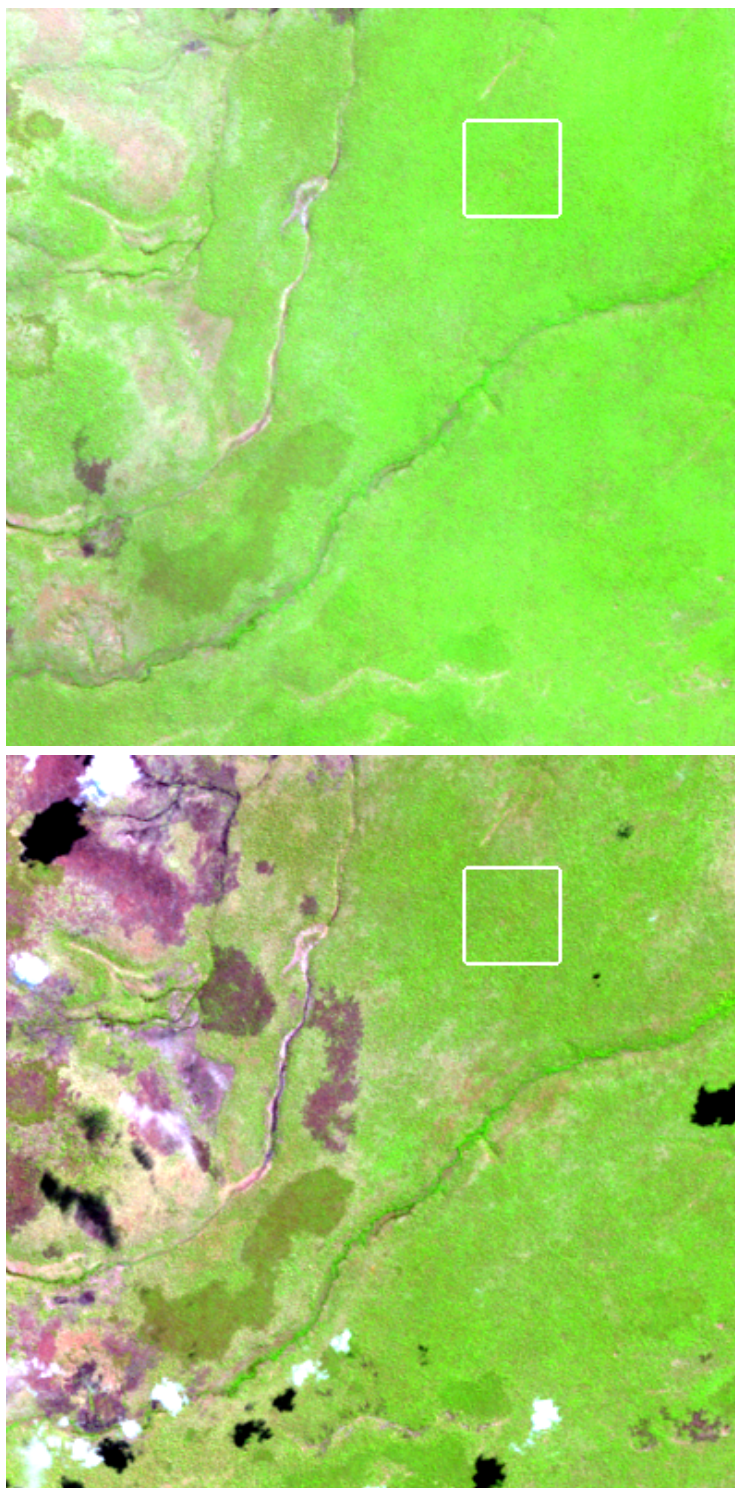


Figure 47. Study area 17. Surface reflectance composite (RGB bands 5,4,3) of a 12×12 km area from the Landsat images L5166067-06720090701 (top) and L5166067-06720090717 (bottom). To enhance visualization for a qualitative assessment, linear stretching with identical and conveniently chosen saturation thresholds were used both images. The colored squared-window is used for the quantitative assessment of the surface reflectance, by computing the pdf, and the median, of the surface reflectance in each Landsat band.

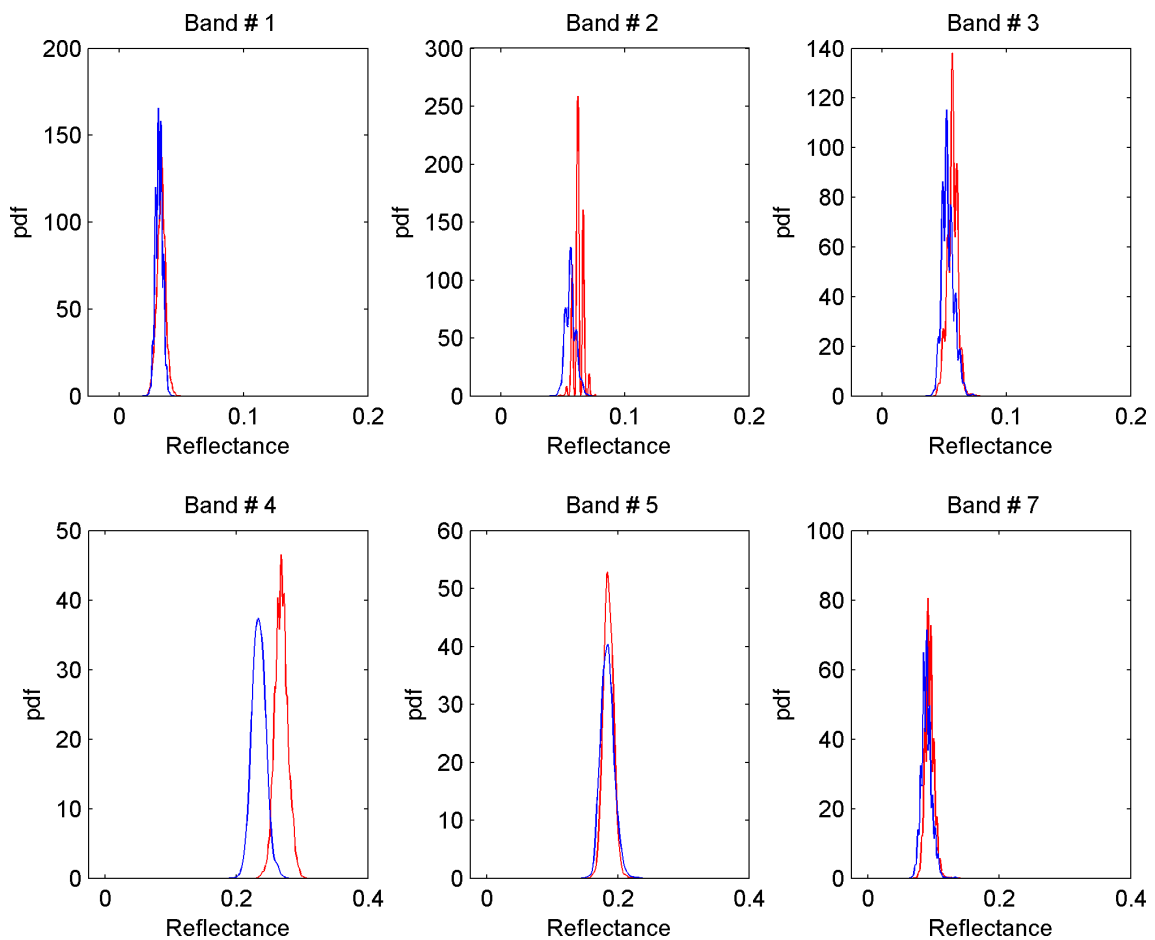
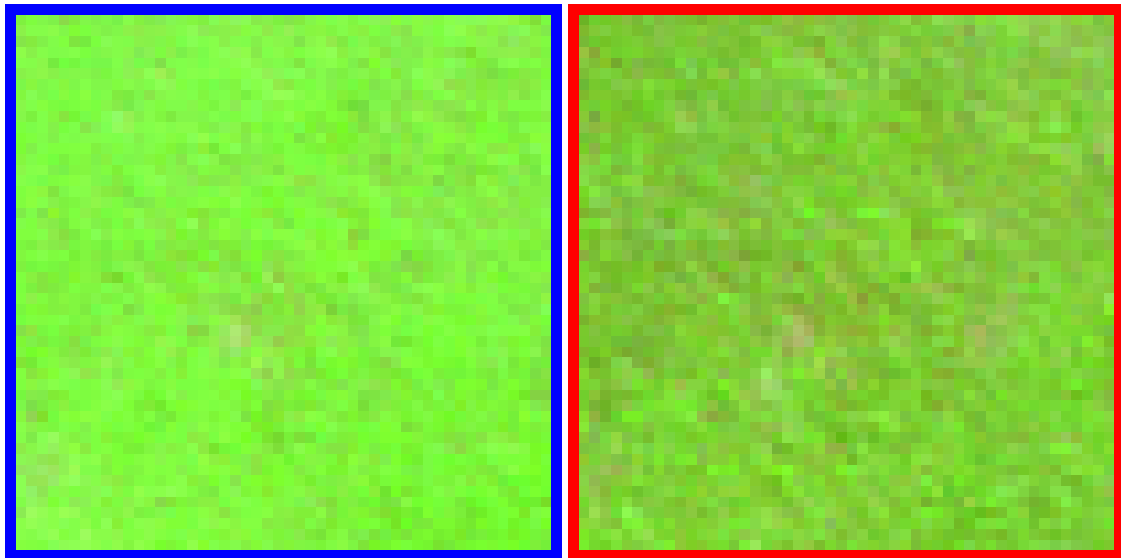


Figure 48. Study area 17. (Top) Closer look at the surface reflectance composite (RGB bands 5,4,3) of the 1500×1500 m subregion in Fig. 47. The patches are from the Landsat images L5166067-06720090701 (blue color), and L5166067-06720090717 (red color). (Bottom) The correspondent probability density estimates of the surface reflectance for the bands 1–5 and 7 of Landsat are depicted. A total of 2500 reflectance samples (pixels) are available in each patch.

Table 6. Study Areas 7–10: Summary scores for the median of the surface reflectance (in %) computed by LEDAPS for Landsat bands 1–5 and 7. Statistics are computed in the 50 × 50 pixel subregions

Subregion	Landsat image	B1	B2	B3	B4	B5	B7
7	L5166063-06320091106	1.17	3.23	1.90	22.11	4.86	1.78
7	L5166063-06320091122	1.03	2.90	1.84	20.58	4.73	1.81
7	L5166063-06320091208	1.09	2.88	1.82	20.38	4.45	1.90
7	Δ absolute	0.14	0.35	0.08	1.72	0.41	0.12
7	Δ relative [%]	13.59	12.15	4.40	8.46	9.21	6.74
8	L5166063-06320091106	4.20	7.38	6.41	28.92	23.17	12.78
8	L5166063-06320091122	4.29	7.26	6.58	30.00	23.28	13.30
8	L5166063-06320091208	3.98	6.81	6.48	26.42	21.92	12.55
8	Δ absolute	0.31	0.57	0.17	3.58	1.36	0.75
8	Δ relative [%]	7.65	8.37	2.65	13.55	6.20	5.98
9	L5166063-06320091106	3.72	6.75	5.82	33.13	23.01	12.67
9	L5166063-06320091122	3.85	6.59	5.71	34.72	24.22	12.98
9	L5166063-06320091208	3.92	6.60	5.69	33.01	22.34	12.13
9	Δ absolute	0.20	0.16	0.13	1.71	1.88	0.85
9	Δ relative [%]	5.52	2.43	2.28	5.18	8.42	7.01
10	L5166063-06320091106	3.23	6.12	5.12	20.05	11.64	5.23
10	L5166063-06320091122	2.91	6.12	5.17	20.17	15.17	7.09
10	L5166063-06320091208	3.09	6.16	5.27	21.45	15.98	7.29
10	Δ absolute	0.32	0.04	0.15	1.40	4.34	2.07
10	Δ relative [%]	11.00	0.65	2.93	6.98	37.34	39.48

4.10 Summary tables of short revisit time for the study areas 7–17

Summary scores of the inter comparison of surface reflectance images generated by LEDAPS for areas studied with short Landsat revisit time are shown in Tables 6–7. As mentioned earlier in this report, the scores are based on the median of the 50 × 50 pixel subregions. In addition to the median, the absolute difference (computed as the maximum minus the minimum value) and the relative (maximum divided by the minimum) of the median of the surface reflectance for each of the three images is included.

In general we notice that the agreement of the surface reflectance for scenes acquired between short revisit time is better than for long revisit time. This suggests that LEDAPS was able to estimate similar ground reflectance for regions where the phenological change, between sequentially acquired scenes, is expected to be smaller.

In detail, for areas 7–10, the median of the absolute reflectance difference is 0.0038, with a relative difference of 7% of the estimated reflectance value (Tab. 6). For areas 11–14 the correspondent figures is 0.0073 and 9%, where for the areas 15–17 they are 0.0072 and 10%. (Tab. 7). The scores for the study areas 11–17 are based on multiple comparisons of sets of two images. In the case of the study areas 7–10, three images were analyzed.

Table 7. The same as Tab. 6, but for the study areas 11–17. Here only two Landsat images are compared simultaneously (instead of three as done before). Apparently there is some (phenological) change between the images acquired between May 30 and July 17. The images 0530, 0615 are visually different from those acquired in 0701 and 0717, but 0701 is still similar to 0717. Thus, we compare the first two, and the latter two images separately.

Subregion	Landsat image	B1	B2	B3	B4	B5	B7
11	L5166067-06720090530	2.87	5.31	4.26	25.21	16.89	7.96
11	L5166067-06720090615	3.14	5.27	4.90	23.37	18.03	8.68
11	Δ absolute	0.27	0.04	0.64	1.84	1.14	0.72
11	Δ relative [%]	9.41	0.76	15.02	7.87	6.75	9.05
12	L5166067-06720090530	2.63	4.98	4.32	25.59	16.26	7.09
12	L5166067-06720090615	3.13	5.30	5.23	23.85	18.58	8.69
12	Δ absolute	0.50	0.32	0.91	1.74	2.32	1.60
12	Δ relative [%]	19.01	6.43	21.06	7.30	14.27	22.50
13	L5166067-06720090530	3.11	5.90	5.51	26.37	19.10	9.25
13	L5166067-06720090615	3.59	6.48	6.63	24.77	21.96	11.69
13	Δ absolute	0.48	0.58	1.12	1.59	2.86	2.44
13	Δ relative [%]	15.43	9.83	20.33	6.44	14.97	26.38
14	L5166067-06720090530	2.37	4.48	3.58	26.06	15.41	6.66
14	L5166067-06720090615	2.64	4.64	3.69	25.32	16.28	6.92
14	Δ absolute	0.27	0.16	0.11	0.74	0.87	0.26
14	Δ relative [%]	11.39	3.57	3.07	2.92	5.65	3.90
15	L5166067-06720090701	3.12	5.57	5.16	23.23	16.47	8.62
15	L5166067-06720090717	3.25	5.55	5.17	22.37	18.26	8.96
15	Δ absolute	0.13	0.02	0.01	0.86	1.79	0.34
15	Δ relative [%]	4.17	0.36	0.19	3.84	10.87	3.94
16	L5166067-06720090701	3.81	7.04	6.74	30.29	20.56	11.12
16	L5166067-06720090717	2.34	4.88	4.57	24.96	18.24	8.52
16	Δ absolute	1.47	2.16	2.17	5.33	2.32	2.60
16	Δ relative [%]	62.82	44.26	47.48	21.35	12.72	30.52
17	L5166067-06720090701	3.37	6.19	5.65	26.80	18.46	9.16
17	L5166067-06720090717	3.12	5.61	5.18	23.21	18.53	8.95
17	Δ absolute	0.25	0.58	0.47	3.59	0.07	0.21
17	Δ relative [%]	8.01	10.34	9.07	15.47	0.38	2.35

4.11 An example of reflectance comparison on deforested areas

Changes in the land cover, as those due deforestation, produces a change in the reflectance measured by space-borne sensors. This is a key factor analyzed by automatic algorithms attempting to spot changes in the natural landscape, at a given temporal scale.

Here we examine two examples that appears to be a case of deforestation occurred between 1987 and 2001 at the West Usambaras Lushoto Mountain Reserve in Tanzania ($4^{\circ}39'S$, $38^{\circ}14'E$), shown in Fig. 49. In particular, we analyze how the surface reflectance, estimated by LEDAPS, changed in a sequence of three Landsat images in two spots of interests. Visual analysis of each spot, of size 1500×1500 m, reveals a substantial change of the land cover, close to 50%. The first image, acquired on February 2, 1987 is compared with two consecutive images acquired on January 15 and 31, 2001.

Visual inspection of the surface reflectance composite in Fig. 49 suggests a deforestation pattern, which alters the estimated probability density of the reflectance measurements shown in Figs. 50– 51. The probability density analysis suggests that the differences in the reflectance distribution, due to deforestation, is much higher than the differences due to the natural variability expected in the two consecutive images from 2001. Differences are more remarkable at bands 5 and 7. We conjecture that such difference in the estimated pdf densities could be used for the development of a change detection algorithm.

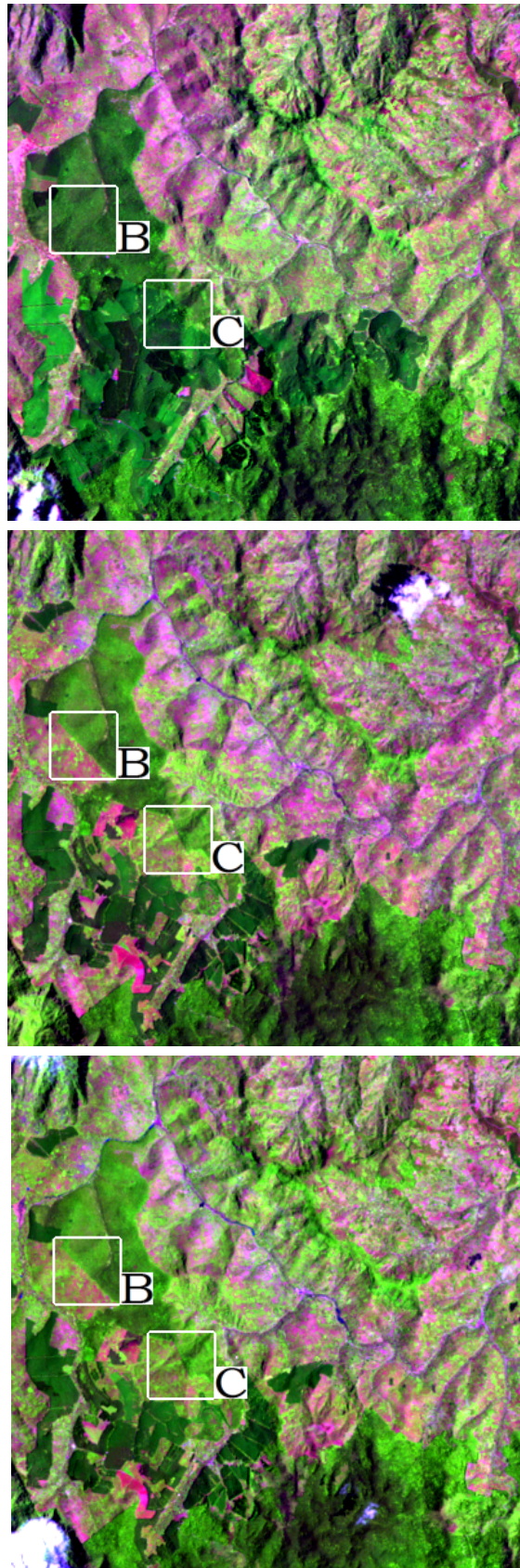


Figure 49. Study area 18 (same location as 2). Surface reflectance composite (RGB bands 5,4,3) of a 12×12 km area from the Landsat images L5167063-0631987-02-02 (top), L71167063-0632001-01-15 (middle), and L71167063-0632001-01-31 (bottom).

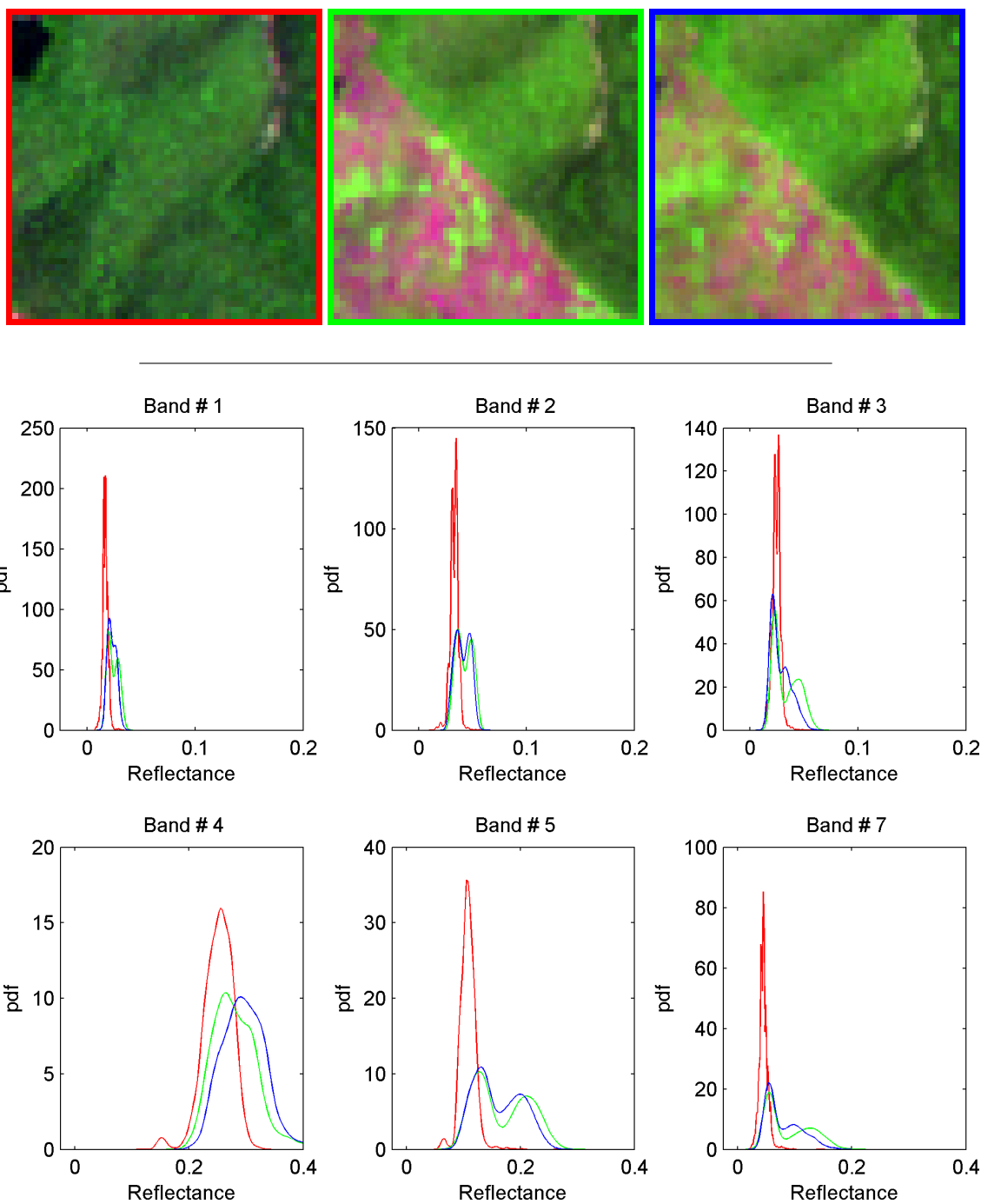


Figure 50. Study area 18 (same location as 2). (Top) Closer look at the surface reflectance composite (RGB bands 5,4,3) of the 1500×1500 m subregion "B" in Fig. 49. The patches are from the Landsat images L5167063-06319870202 (red color), L71167063-06320010115 (green color), and L71167063-06320010131 (blue color). (Bottom) The correspondent probability density estimates of the surface reflectance for the bands 1–5 and 7 of Landsat are depicted. A total of 2500 reflectance samples (pixels) are available in each patch.

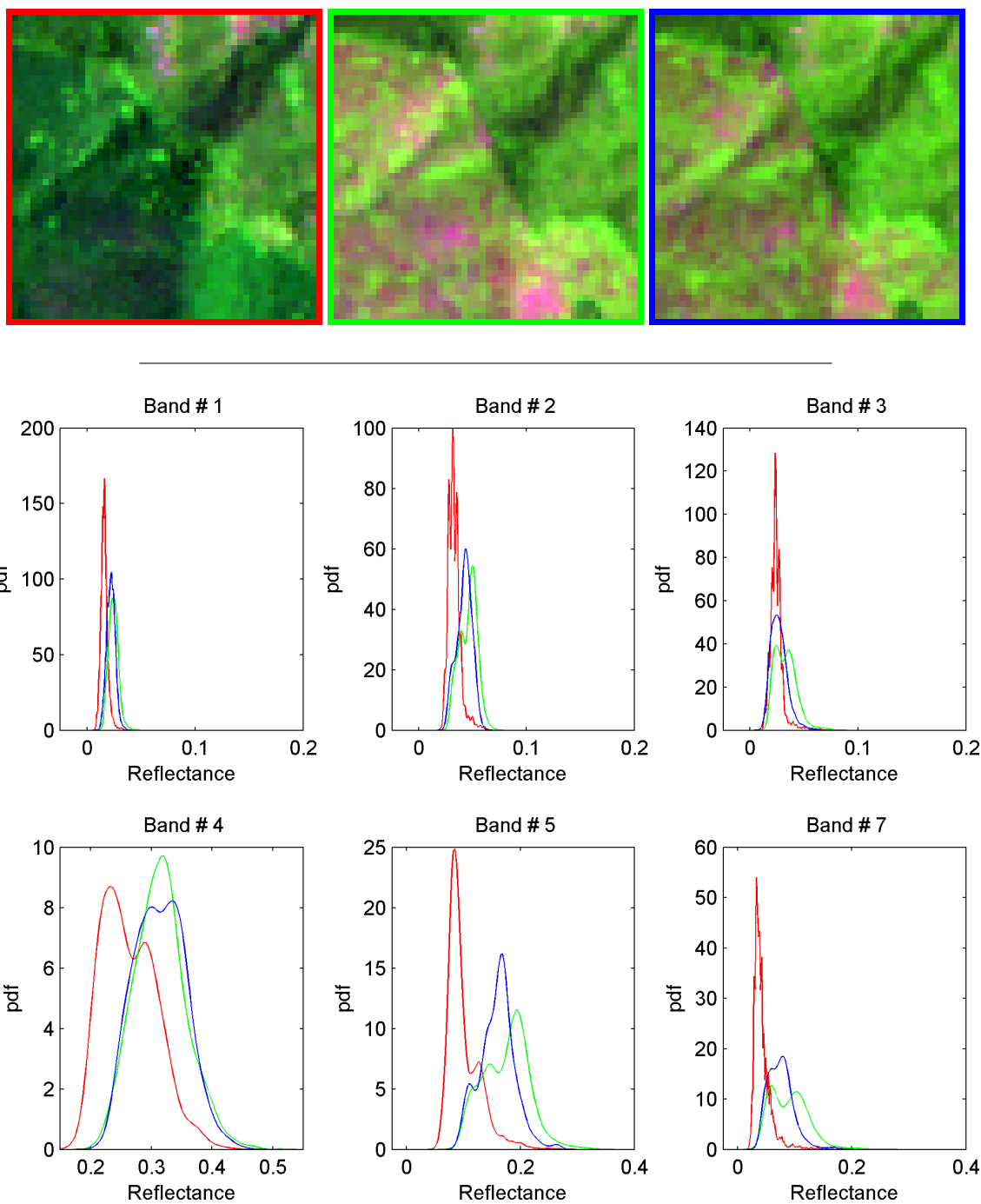


Figure 51. Study area 18 (same location as 2). (Top) Closer look at the surface reflectance composite (RGB bands 5,4,3) of the 1500×1500 m subregion "C" in Fig. 49. The patches are from the Landsat images L5167063-06319870202 (red color), L71167063-06320010115 (green color), and L71167063-06320010131 (blue color). (Bottom) The correspondent probability density estimates of the surface reflectance for the bands 1–5 and 7 of Landsat are depicted. A total of 2500 reflectance samples (pixels) are available in each patch.

4.12 An example of reflectance comparison in adjacent Landsat images

We conclude the experiments analyzing the surface reflectance estimated by LEDAPS on a set of three subregions located at the border of adjacent images. The images were acquired by Landsat 5 when passing at successive orbits. In particular, we focus on a set of three images from:

- November 22, 2009 (path/row 166/063)
- November 29, 2009 (path/row 167/063)
- December 08, 2009 (path/row 166/063)

Visual analysis of selected color compositions (shown in Fig. 52), the estimated pdf of the surface reflectance in Figs. 53–55, and the median scores summarized in Tab. 8, suggests in general a good agreement of the surface reflectance, for this particular set of images tested. We also observe that the selected subregions in Figs. 53–55 are not perfectly co-registered (there is a shift of about 2 pixels). This is due the different viewing geometries during the acquisition of the Landsat scenes. In any event, the resulting impact on our current analysis should be limited, because the quantitative assessment relies on the median values for each band in the selected areas, rather than computing pixel-wise differences between the scenes.

It is worth noting that in our current experimental setting, the current estimated differences on surface reflectance are also partially due to the effect of the bidirectional reflectance distribution function (BRDF) of the target regions, which is a function of the illumination and viewing geometry of Landsat for the adjacent orbits.

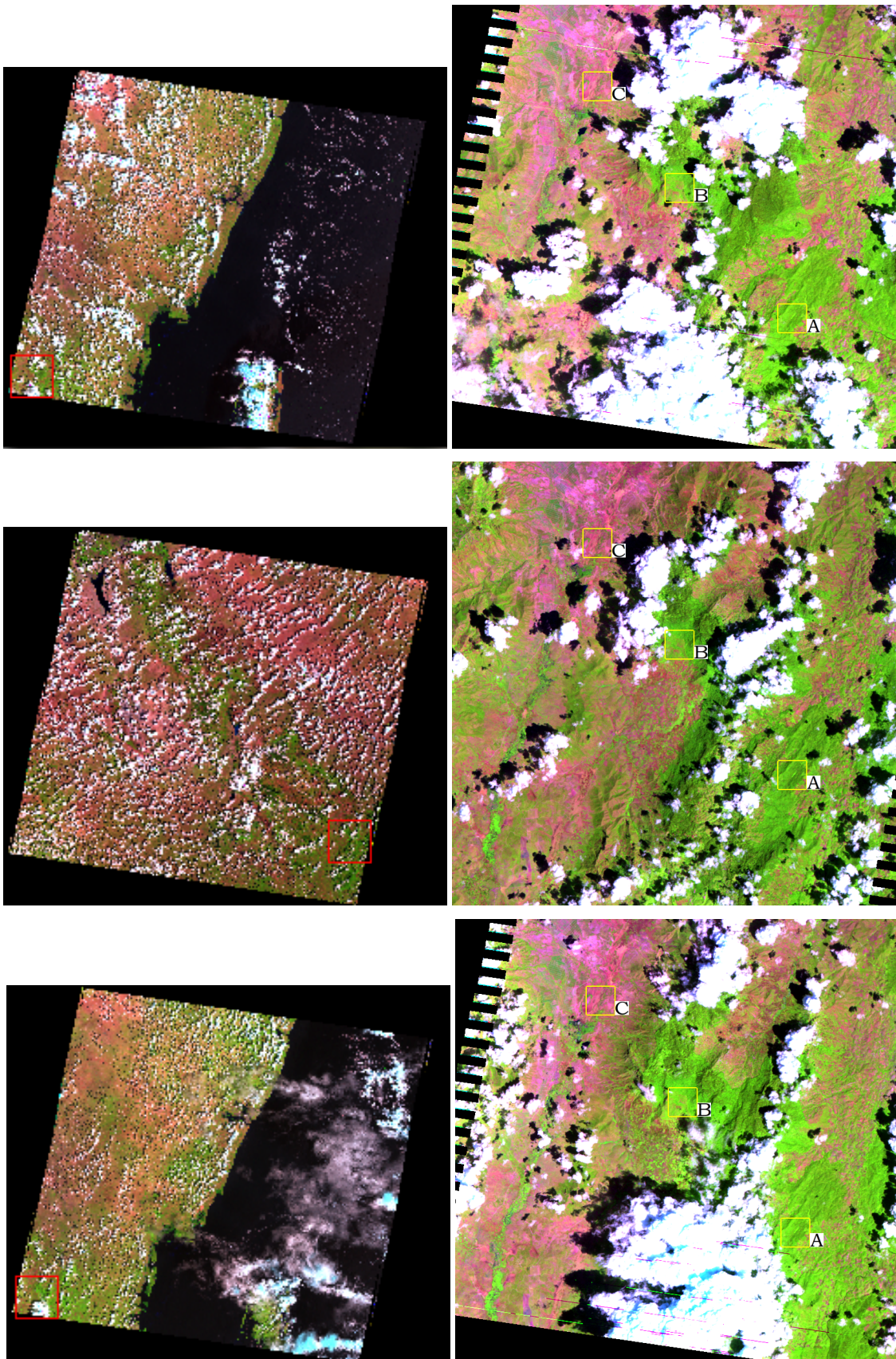


Figure 52. Study area 19. (Left) Color composition showing the location of the selected areas in the (right) side: surface reflectance composite (RGB bands 5,4,3) of a 24×24 km area from the Landsat images L5-166-063-0632009-1122 (top), L5-167-063-0632009-1129 (middle), and L5-166-063-0632009-1208 (bottom). To enhance visualization for a qualitative assessment, linear stretching with identical and conveniently chosen saturation thresholds were used in the three images. Note the three small subregions "A", "B", and "C".

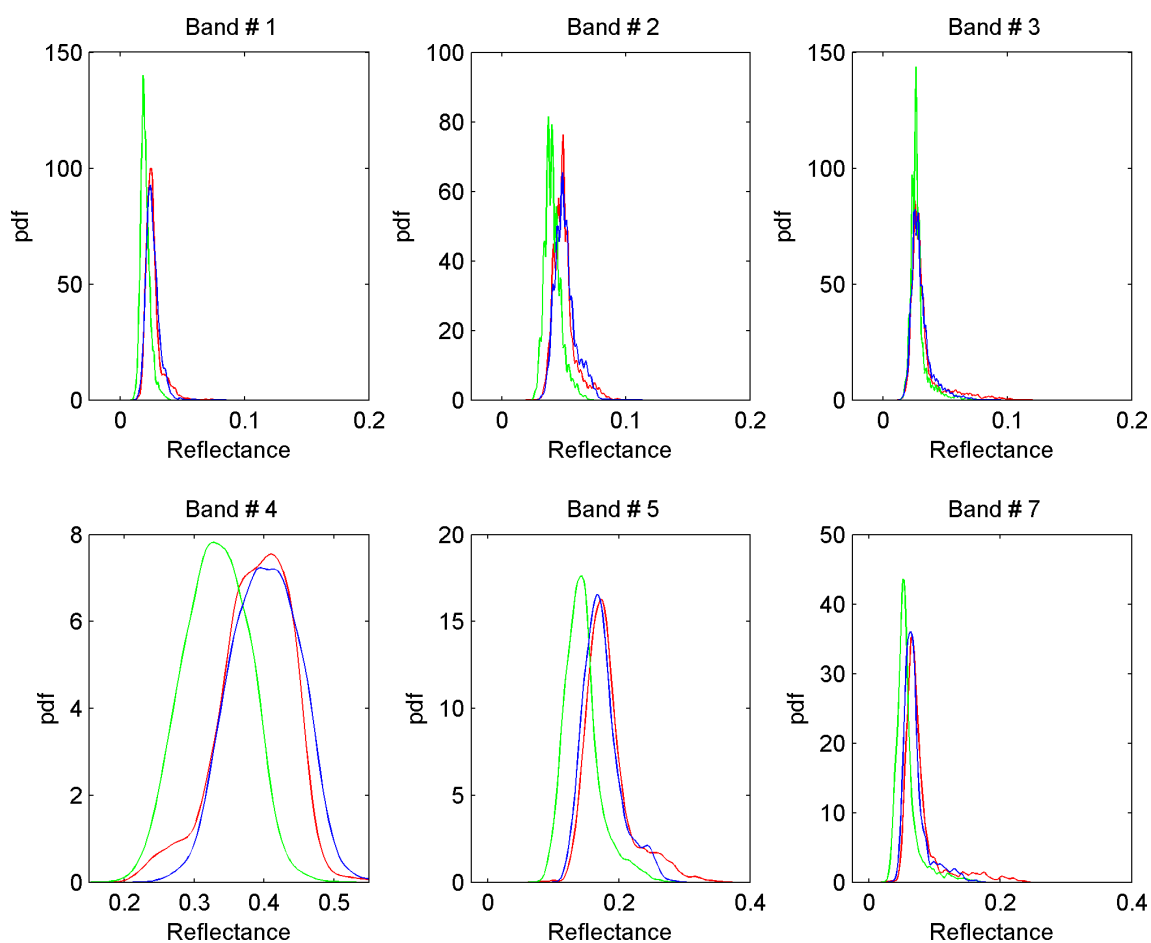
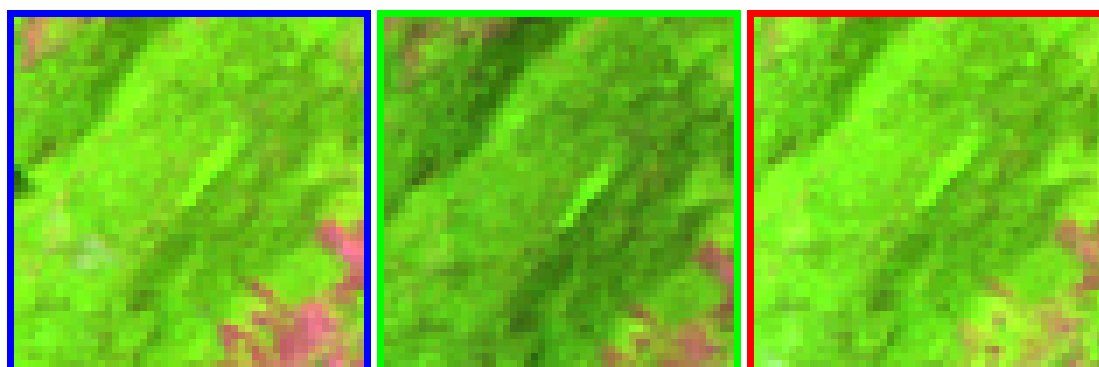


Figure 53. Study area 19. (Top) Closer look at the surface reflectance composite (RGB bands 5,4,3) of the 1500×1500 m subregion "A" in Fig. 52. The patches are from the Landsat images L5166063-0632009-1122 (blue color), L5167063-0632009-1129 (green color), and L5166063-0632009-1208 (red color). (Bottom) The correspondent probability density estimates of the surface reflectance for the bands 1–5 and 7 of Landsat are depicted. A total of 2500 reflectance samples (pixels) are available in each patch.

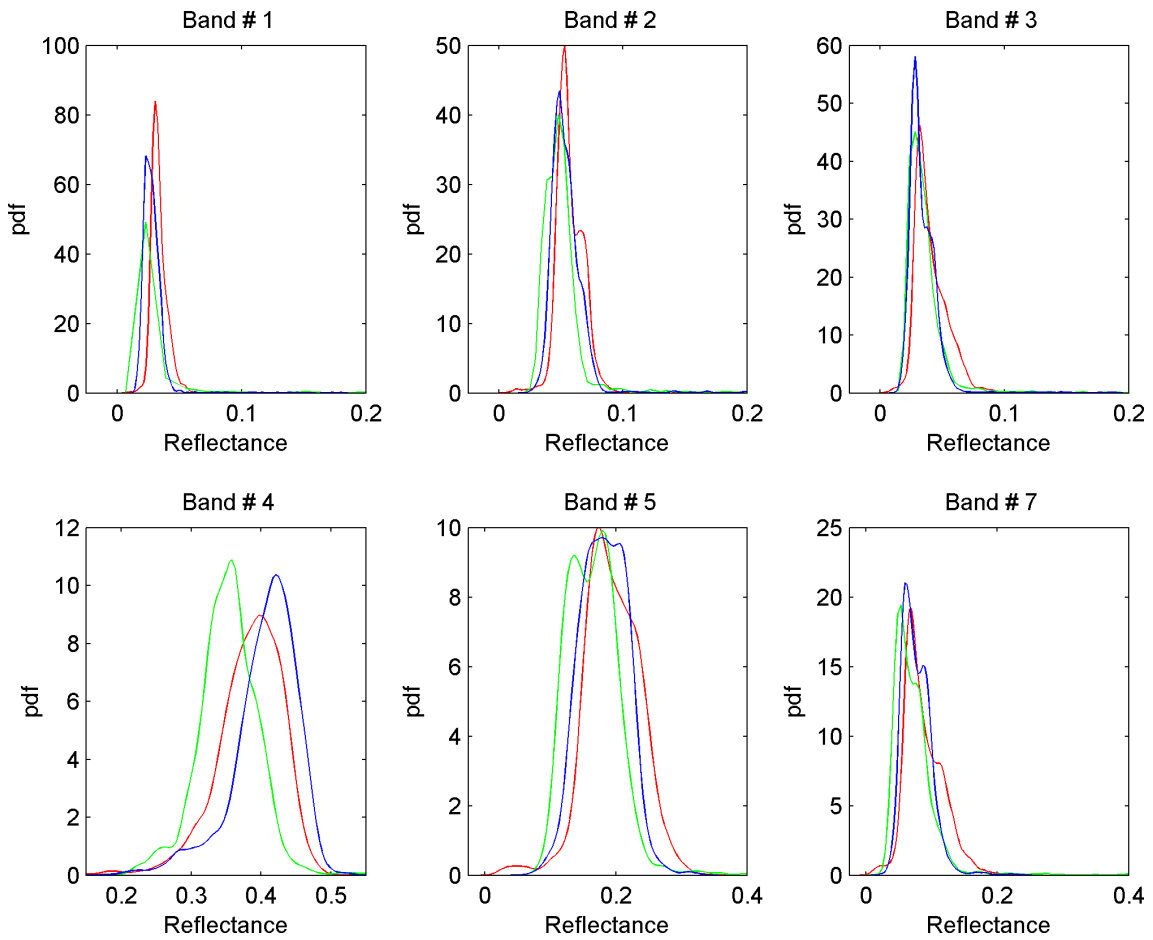
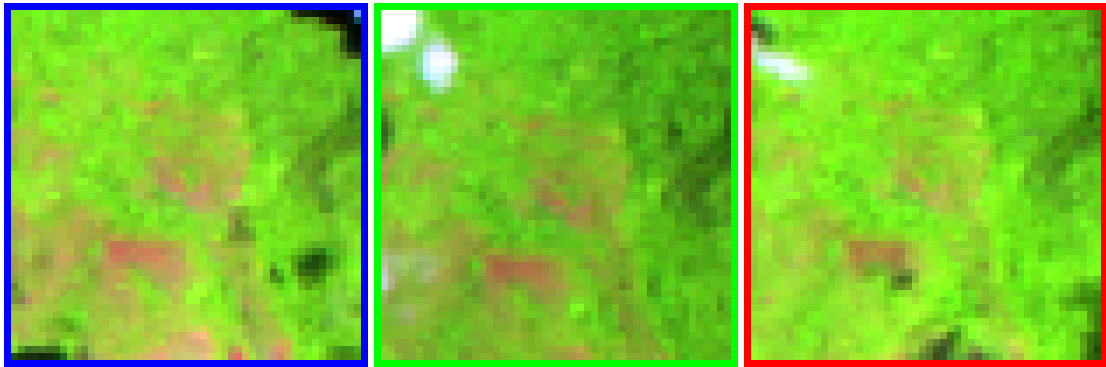


Figure 54. Study area 19. (Top) Closer look at the surface reflectance composite (RGB bands 5,4,3) of the 1500×1500 m subregion "B" in Fig. 52. The patches are from the Landsat images L5166063-0632009-1122 (blue color), L5167063-0632009-1129 (green color), and L5166063-0632009-1208 (red color). (Bottom) The correspondent probability density estimates of the surface reflectance for the bands 1–5 and 7 of Landsat are depicted. A total of 2500 reflectance samples (pixels) are available in each patch.

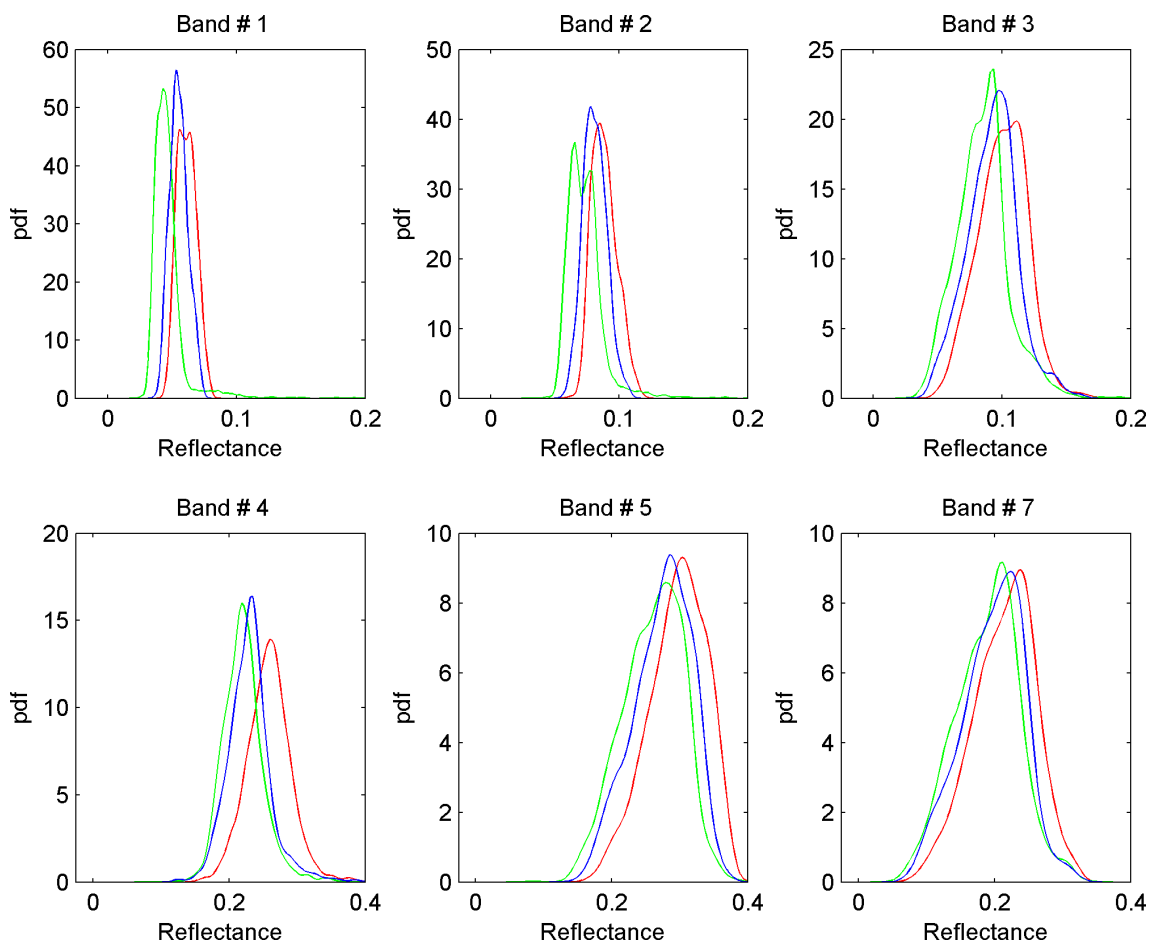
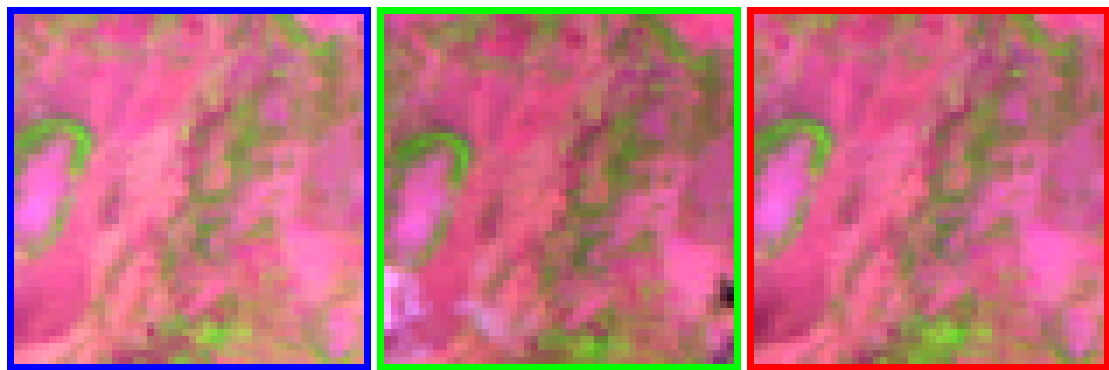
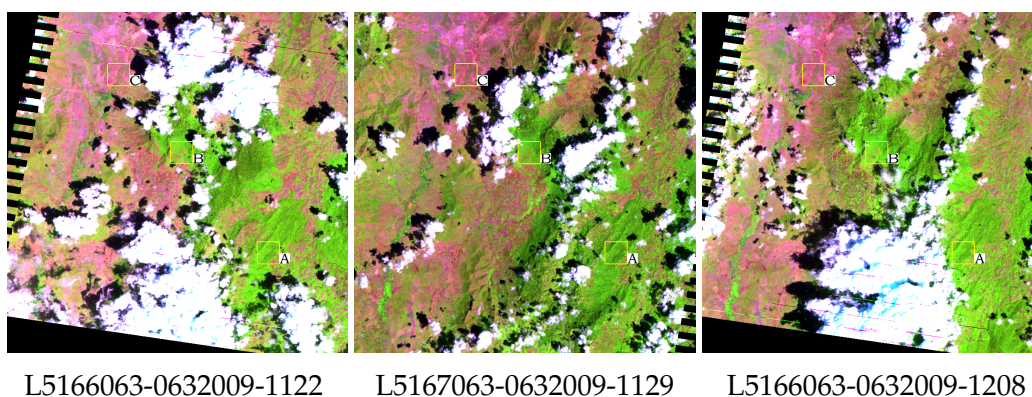


Figure 55. Study area 19. (Top) Closer look at the surface reflectance composite (RGB bands 5,4,3) of the 1500×1500 m subregion "C" in Fig. 52. The patches are from the Landsat images L5166063-0632009-1122 (blue color), L5167063-0632009-1129 (green color), and L5166063-0632009-1208 (red color). (Bottom) The correspondent probability density estimates of the surface reflectance for the bands 1–5 and 7 of Landsat are depicted. A total of 2500 reflectance samples (pixels) are available in each patch.

Table 8. Study Area 19: Summary scores for the median of the surface reflectance (in %) computed by LEDAPS for Landsat bands 1–5 and 7. Statistics are computed in the 50 × 50 pixel subregions labeled A in red, B in green, and C in blue color.

Subregion	Landsat image	B1	B2	B3	B4	B5	B7
19A	L5166063-06320091122	2.49	4.88	2.86	39.20	17.53	7.08
19A	L5167063-06320091129	1.96	4.04	2.62	33.24	14.12	5.22
19A	L5166063-06320091208	2.47	4.88	2.79	40.18	17.05	6.58
19A	Δ absolute	0.53	0.84	0.24	6.95	3.41	1.86
19A	Δ relative [%]	27.04	20.79	9.16	20.89	24.15	35.63
19B	L5166063-06320091122	3.22	5.38	3.74	38.89	19.32	8.10
19B	L5167063-06320091129	2.48	4.79	3.20	35.31	16.42	6.58
19B	L5166063-06320091208	2.70	5.23	3.08	41.33	18.23	7.29
19B	Δ absolute	0.74	0.59	0.66	6.02	2.90	1.52
19B	Δ relative [%]	29.84	12.32	21.43	17.05	17.66	23.10
19C	L5166063-06320091122	6.09	8.79	10.21	25.79	30.09	21.88
19C	L5167063-06320091129	4.46	7.31	8.39	21.90	26.50	19.45
19C	L5166063-06320091208	5.47	8.09	9.42	22.93	27.92	20.33
19C	Δ absolute	1.63	1.48	1.82	3.89	3.59	2.43
19C	Δ relative [%]	36.55	20.25	21.69	17.76	13.57	12.49

Location of the subregions in the composite surface reflectance images (bands 5,4,3).



5 Discussion and conclusions

The intercomparison evaluation of the surface reflectance estimated by LEDAPS indicates a reasonable agreement between the reflectance values estimated using different Landsat images of the same geographic area. The assumption was that the selected areas for this study presented similar phenological conditions for the different time period analyzed.

The agreement between the estimated surface reflectance was found dependent of the band and image sets tested. Experimental evidence suggests a higher agreement of the surface reflectance for scenes acquired between short instead of long revisit time. This suggests that LEDAPS was able to estimate similar ground reflectance for regions where the phenological change, within the temporal resolution of Landsat (16 days), was expected to be smaller.

As indicative figures for the selected cases of long revisit time (up to 17 years in some of the image test tested), the study areas 1 and 2 were found to be more stable, with an agreement of surface reflectance, quantified by the median of different scenes, below 0.013 and 17% of the absolute and relative values, respectively. These median figures increased to 0.070 and 54% in the study areas 3 and 4. The reason may be that the land cover was assumed to be unchanged over more than a decade between the acquisition of some of the Landsat images used in this study (1984–2001). Despite the careful selection, changes may have occurred in some of the subregions considered, adding to the error scores. This is likely to be the case of two of the study areas considered (study areas 3 and 4). Also, Tanzania is experiencing less rainfall nowadays than 20–30 years ago, which may explain why some areas appears drier in recent images. Again, the changes that can be observed seem to follow natural trends. There is a long rain period in February–April, resulting in a peak in greenness in May, with a gradual reduction of greenness through June and July. This appears to be the case for the series of images from 30 May 2009, 15 June 2009, 1 July 2009, and 17 July 2009. In other words, the changes observed in the surface reflectance follow the expected natural trends.

For visual interpretation, we have demonstrated (Figs. 24–25) that a linear scaling of the intensity values of each band can produce a result similar to the surface reflectance as produced by LEDAPS. However, such linear scaling is difficult in automatic processing of satellite images, which is why there is a need for the LEDAPS preprocessing to obtain surface reflectance values, which in turn can be monitored through a growing season to study annual cycles, and over several years, to study land use/land cover changes and forest cover changes.

For the case of short revisit time (in the order of the temporal resolution of Landsat, 16 days), the median of the absolute reflectance difference was bellow 0.0073, with a relative difference bellow 10% of the estimated reflectance value.

On the matter of thin clouds and haze removal, our preliminary analysis suggests that these are not effectively removed by the current atmospheric correction incorporated in LEDAPS. This may be due to the low spatial resolution of the ancillary data used to com-

pute the necessary parameters for atmospheric correction. For instance, the water vapor is taken from the National Centers for Environmental Prediction (NCEP) re-analysis database, which has a coarse spatial resolution of 2.5 degrees.

Another point that deserves attention is image regions affected by cloud shadows. Inspection of the probability density function of the reflectance estimated by LEDAPS in such areas suggests that the land cover/use classification would be very challenging if shadows are not properly taken in account. As for the challenging problem of cloud detection, we recommend the development of an specific algorithm to mask those areas affected by cloud shadows.

The surface reflectance estimated by LEDAPS on a small set of subregions located at the border of adjacent images, acquired by Landsat when passing at successive orbits, at close acquisition times, showed good agreement. In such experimental setting, the current estimated differences on surface reflectance are also partially due to the effect of the bidirectional reflectance distribution function (BRDF) of the target regions, which is a function of the illumination and viewing geometry of Landsat.

References

- Masek, J., Vermote, E., Saleous, N., Wolfe, R., Hall, F., Huemmrich, K., Gao, F., Kutler, J., and Lim, T. (2006). A landsat surface reflectance dataset for north america, 1990-2000. *Geoscience and Remote Sensing Letters, IEEE*, 3(1):68–72. 5
- Vermote, E. and Saleous, N. (2007). *LEDAPS surface reflectance product description*. On-line, http://ledaps.nascom.nasa.gov/docs/pdf/SR_productdescript_dec06.pdf. 5, 6, 42
- Vermote, E., Tanré, D., Deuze, J., Herman, M., and Morcette, J. (1997). Second simulation of the satellite signal in the solar spectrum, 6s: An overview. *Geoscience and Remote Sensing, IEEE Transactions on*, 35(3):675–686. 42